1991-92 ANNUAL REPORT

Reactions of Toxic Pollutants in Soil Systems

KEARNEY FOUNDATION OF SOIL SCIENCE
DIVISION OF AGRICULTURE AND NATURAL RESOURCES
UNIVERSITY OF CALIFORNIA

1991-92 ANNUAL REPORT

Reactions of Toxic Pollutants in Soil Systems

EDITED BY DEBORAH SILVA

DR. ANDREW C. CHANG, DIRECTOR
KEARNEY FOUNDATION OF SOIL SCIENCE
DIVISION OF AGRICULTURE AND NATURAL RESOURCES
UNIVERSITY OF CALIFORNIA

Contents

Annual Progress Reports

Appendix

Kearney Foundation of Soil Science: A Brief Overview

Mitigating the impacts of soil pollution is one of the major challenges facing California in the 1990s. Events that occur in soil have profound effects on surface and ground water quality, but the dynamics of the relationship between soil quality and water quality are not understood fully. At present, scientists lack sufficient data from field situations on the movement, transformation, and fate of soil contaminants that influence water quality. Whether soil contamination arises from seepage of solvents used to clean aircraft at military bases, from leaking petroleum storage tanks at industrial sites, from normal application of fertilizers and pesticides in farming operations, from waste disposal, or from buildup of toxic levels of metals due to trace element-laden agricultural drainage water, University of California soil scientists are the experts who must develop the knowledge base to predict the fate of toxics, provide leadership in remediation strategies, and recommend scientifically sound techniques to prevent future degradation of soil and water quality in the state.

Pesticides provide a good example of soil contaminants requiring further study. Half of the pesticides used in the United States are applied in California, which ranks fifth worldwide in terms of agricultural revenue. The state accounts for 25% of the world's annual pesticide usage. The pressing need for additional scientific research about the transport and fate of toxic chemicals as they travel down the soil profile becomes unequivocal when such consumption of xenobiotic compounds is coupled with the state's dependence on irrigation agriculture and its public health mandate to sustain groundwater quality for domestic use.

For more than 50 years, the M. Theodore Kearney Foundation of Soil Science at the University of California has established an impressive record in addressing critical research needs in the state and providing an intellectual forum for international leadership in soil science research. The Foundation has an endowment fund that supports, through a competitive grants process, fundamental and applied research by University faculty and Cooperative Extension personnel in the fields of soils, plant nutrition, and water science.

Mission for 1991-96: Reactions of Toxic Pollutants in Soil Systems

The Foundation's 1991-96 mission, Reactions of Toxic Pollutants in Soil Systems, represents the first time the Foundation has focused on examination of soil pollution problems rather than production of agricultural products. Environmental problems, such as soil pollution, are characterized by an intimate intertwining of physical, chemical, and biological processes that require multidisciplinary research approaches. Many chemical sources of contamination are not miscible in water, but they can be transported, degraded, and transformed in soil. These soil processes need to be studied and managed for the protection of the state's natural resources and the public health of its citizens. The reactions, mechanisms, and interactions that occur in the soil's

vadose region above the water table and in ground water under saturation conditions are not understood fully. The current five-year Kearney mission focuses only on soil pollution problems in the vadose zone as stated in the outline below:

I. Investigate soil mechanisms, processes, and interactions that control transport, degradation, transformation, and crop uptake of toxic pollutants

- Quantify and model soil processes that determine mobility and reactivity of pollutants in soil and the vadose zone, resulting in groundwater pollution
- Investigate interactions of soil, water, rhizosphere, and pollutants
- For multi-phase and/or multi-pollutant systems, investigate physical, chemical, and biological reactions and porous media transport involved

II. Develop methodology for scaling up microscopic soil mechanisms and reactions to field-scale processes that apply to agricultural and urban soils

- Investigate spatial variation of physical, chemical, and biological reactions in soil and the vadose zone
- Improve predictive accuracy, including mathematical models' descriptions of soil reactions
- Develop management strategies, including application of the Geographical Information System, to prevent soil and water pollution by toxic environmental pollutants

The fundamental knowledge base, including remediation and management strategies, developed by this mission on toxics during the next five years will be applicable throughout the state and will serve as a basis for developing application-related programs in agricultural and urban environments. Many soil science issues, such as the fate of toxics, know few boundaries between agricultural and urban soil.

History

The Kearney Foundation of Soil Science was established by the Regents of the University of California in 1954 to conduct research in soil science, plant nutrition and water science. Mr. M. Theodore Kearney, a prominent Fresno area farmer and founding member of the California Raisin Growers Association, died in 1906 and bequeathed his entire Fruit Vale Estate, worth close to $1.1 million, to the Regents of the University of California for agricultural research purposes. Over the years, Mr. Kearney had developed a fruitful working relationship with UC soil scientists whose advice regarding problems with drainage, salinity, and sodium had been essential to his ranch's success. Approximately 1,500 acres of Mr. Kearney's 5,000 acre estate had been planted to grapes for raisin production and the remainder was planted to alfalfa.

It was on Mr. Kearney's farm that University of California Professor W.P. Kelley conducted his classical experiments on alkali soil reclamation. UC Professor E.J. Wickson conducted field research on viticulture there. W.W. Mackie of the United States Department of Agriculture was the first to investigate land reclamation using a tile drainage system at the Kearney property in 1905. Mr. Kearney admired UC Professor E. Hilgard, widely regarded as the "father" of the California Agricultural Experiment Station. Dr. Hilgard began alkali soil studies in the San Joaquin Valley on horseback in 1877.

In 1908, the University took over management of the Kearney estate, located 10 miles west of Fresno, and operated it as a commercial farm until 1948, when the Regents authorized its sale. Income and proceeds from the sale of the farm resulted in the establishment of the Kearney Foundation of Soil Science in 1954 and the University's Kearney Agricultural Center in Parlier.

The early record shows that the in-house research staff of the Kearney Foundation was at the cutting edge of soils research. Their work had major spin-offs not only in agricultural production but also in human and animal health. For example, UC scientists funded by the Foundation studied the generation of radon gas in soils, discovered the importance of cobalt and molybdenum in nitrogen fixation, used ^{15}N isotopes for research, and determined selenium concentrations by X-ray fluorescence.

By the late 1960s, income from the endowment fund was insufficient to support the salaries and research programs of resident scientists, so the Foundation was reorganized to tackle new research missions every five years and to allocate research funds through a competitive grants process to existing faculty, Extension specialists, and farm advisors in the statewide Agricultural Experiment Station. The Foundation's research missions, established in five year cycles since 1970, have focused previously on nitrogen in the environment (1970-75), trace elements (1975-80), salinity (1980-85), and water penetration problems in irrigated soils (1986-91).

Administration

The Associate Vice President for Agriculture, Division of Agriculture and Natural Resources, appoints a Director of the Kearney Foundation from one of the three Agricultural Experiment Station campuses (Berkeley, Davis, or Riverside) to oversee carrying out the designated mission. The Director of the current mission is Dr. Andrew C. Chang, Professor of Agricultural Engineering and Agricultural Engineer in the Citrus Research Center - Agricultural Experiment Station at Riverside. A Technical Committee and an Advisory Committee are appointed by the Director to help establish research priorities, administer the competitive grants process, and ensure that sufficient research progress and information dissemination occur. Current members of the Technical and Advisory Committees are listed in the Appendix.

Information Dissemination

Since the 1980s, the Foundation has published an Annual Report of research progress. The Foundation also conducts workshops, holds seminars and technical conferences, and disseminates additional information, as needed, to fulfill each mission's research objectives and to communicate research accomplishments.

The report which follows is the first in a series of five Annual Reports on the current mission, Reactions of Toxic Pollutants in Soil Systems. Many of the 13 research projects are funded for two to three years; thus, this report represents initial progress. During the second year of the funding cycle, additional research projects, both fundamental and applied, will be added to the portfolio.

Effect of Sorption to Organic Matter on the Biodegradation of Organic Pollutants in Soil

KATE M. SCOW
Department of Land, Air and Water Resources, Davis Campus

Summary

The availability of pollutants to microbial populations capable of metabolizing these chemicals has a strong impact on rates of biodegradation in soil. Phenanthrene and naphthalene, both polyaromatic hydrocarbons and EPA priority pollutants, were selected to investigate the factors controlling rates of degradation of sorbed chemicals in soil and to explore methods with which to enhance their degradation.

The rate of biodegradation of phenanthrene in six surface soils varied with the organic matter content. In general, the rate of degradation was initially more rapid in low organic soils, and, later on, faster in the higher organic soils. Experiments conducted on the biodegradation of phenanthrene in soil containing different amounts of either activated carbon or hydrophobic chromatography beads showed a reduction in the rate and extent of mineralization as the amount of sorbent added was increased. There was no enhancement of the rate of phenanthrene degradation due to the addition of salicylic acid, phenol or glucose to soil. The rate of degradation of phenanthrene declined as the moisture content was increased from 16 to 100%; however, incubating the soil in slurries substantially increased the rate of biodegradation. The degradability of phenanthrene declined as the time of contact between the soil and chemical increased. Higher initial population densities of microorganisms able to degrade phenanthrene resulted in a greater percentage of the chemical being degraded in soil slurries.

Key Words: biodegradation, sorption, desorption, PAH's, pollutants, soil microbiology, coupled processes.

Project Objectives Addressed in 1991-92

(1) Determine how the sorption partition coefficient, the amount and quality of sorbent, presence of additional carbon sources, soil moisture content, age of phenanthrene in soil, and initial microbial population density influence the relationship between sorption and biodegradation rate in soil.

(2) Simplify an existing model describing diffusion, sorption and biodegradation in the presence of spherical aggregates to use for screening conditions when biodegradation may be limited by mass transfer.

(3) Develop and improve methodologies for working with sorbed chemicals.

Research Plan and Procedures

Measurement of biodegradation

The focus of the project this first year has been on the polyaromatic compounds, phenanthrene and naphthalene. Sorption and biodegradation studies were conducted in surface soils from California, including Yolo silt loam (1.7% organic matter), Auburn sandy loam (5.7%), Crozier silt loam (5.7%), Josephine silt loam (7%), McCarthy sandy loam (19%), and Windy loam (14%).

In biodegradation studies, from 10 to 50 g (dry wt) soil was usually incubated at 0.33 bar with phenanthrene at concentrations of 50 ng or 50 µg per ml soil solution. Biodegradation was measured in modified biometer flasks using ^{14}C-radiolabeled chemical to determine the amount of $^{14}CO_2$ evolved over time. The effect of adding carbon sources (e.g. glucose, salicylic acid, phenol) on the biodegradation of sorbed chemicals was tested by adding unlabeled or labeled material to flasks containing labeled or unlabeled phenanthrene, respectively. To determine quantitative relationships between biodegradation rate and quantity of sorbent, studies were conducted in Yolo soil amended with different amounts of artificial sorbents, including activated carbon and SM-7 (a spherical macroreticular acrylic polymer) chromatography beads. To distinguish between abiotic and biotic processes and for use in sorption/desorption experiments, soil samples were sterilized with cobalt-60 irradiation at Crocker Nuclear Lab on the UC Davis campus.

Measurement of desorption

Sorption isotherms of ^{14}C-phenanthrene were measured in sterilized soils and sorbents. Different ratios of sterile soil or sorbent to calcium chloride solution were tested. A mixture of radiolabeled and unlabeled phenanthrene at concentrations ranging from 0.1 ng to 1.0 µg per ml was added to tubes containing the sorbent-solution mixture and shaken for 4 h to 1 week. To sample, tubes were centrifuged and the supernatant measured for remaining ^{14}C.

Results

Determine How the Sorption Partition Coefficient, the Amount and Quality of Sorbent, Presence of Additional Carbon Sources, Soil Moisture Content, Age of Phenanthrene in Soil, and Initial Microbial Population Density Influence the Relationship Between Sorption and Biodegradation Rate in Soil

(a) Determination of sorption isotherms and desorption rates

Adsorption and desorption isotherms were determined for phenanthrene in Yolo, Crozier and Auburn soils. The adsorption isotherms were linear and desorption showed significant hysteresis in all three soils (Figs.1-3). The calculated sorption partition coefficients, normalized for organic carbon (K_{oc}), were 3150, 4730, and 4454 for Yolo, Crozier and Auburn, respectively. Desorption rates were measured in slurries of Auburn and Crozier soils by measuring changes in phenanthrene concentration following replacement of soil solution with fresh solution after equilibration for sorption. Desorption was rapid and completed within 6 h under these experimental conditions; however, only a small fraction (1-3%) of the original concentration could be desorbed. We are currently developing a method to measure sorption/desorption isotherms and rates in soils at field moisture levels for comparison to slurry results.

(b) Biodegradation of phenanthrene in soils of different organic carbon content.

The mineralization of radiolabeled phenanthrene at concentrations of 50 ng or 50 µg per ml soil solution was measured in six surface soils (0.33 bar moisture) that varied in organic carbon content from 1.02 to 11.07%. At the lower concentration, the rate and percentage mineralized varied with soil type (Fig. 4). There was no systematic relationship between organic carbon content and the pattern of degradation over the course of the study. There tended, however, to be a greater percentage of phenanthrene degraed in the early period of incubation (<200 h) in the lower organic soils, and, in the high organic soils, an increased percentage degraded in the later period of incubation. At the higher concentration, there was no degradation in some soils and, in soils in which degradation occurred, longer lag periods and slower rates (on a percent basis) than at the lower concentration. Yolo, the soil with the lowest organic matter content, showed a higher rate and percentage of phenanthrene degraded within 1400 h of incubation than any other soil.

(c) Biodegradation of naphthalene in Yolo soil amended with artificial sorbent

Naphthalene at a concentration of 500 ng per g soil exhibited a rapid rate of mineralization within the first 20 h of incubation. Over the period of 20 to 80 h, the rate slowly declined and stabilized at a slow and constant rate. The shape of the curves were similar in unamended soil as well as in soil to which 1.0 or 2.0 g SM-7 beads per 50 g soil had been added. However, the greater

the amount of beads added, the slower the initial rate of degradation and the lower the percent mineralized within 200 h. The percentage of radioisotope-labeled naphthalene mineralized was approximately 27, 22.5, and 20% for soil that had been amended with 0, 1.0 or 2.0 g beads, respectively.

(d) Sorption and biodegradation of phenanthrene in Yolo soil amended with artificial sorbent

Sorption isotherms were measured for phenanthrene on sterilized Yolo silt loam, activated carbon, and SM-7 chromatography beads. The chemical was incubated with the sorbents for different durations to determine the time at which an equilibrium concentration distribution was reached. Isotherms were linear over the concentrations tested for soil and sorbents. The K_{oc}'s for phenanthrene on synthetic sorbents were one and a half to two orders of magnitude higher than for soil, with values of approximately 2-6 x 10^6 for both activated carbon and beads. Sorption appeared to be irreversible for both artificial sorbents.

A preliminary experiment measuring the biodegradation of 10 μg phenanthrene per g Yolo silt loam, with and without the addition of 1 g activated carbon per 50 g soil, showed a strong effect of activated carbon on the rate of biodegradation. In the absence of activated carbon, the rate of mineralization of phenanthrene accelerated within the first 200 h of incubation, and then decelerated over the next 1300 h. At 1600 h, 27% of the phenanthrene was mineralized. In the presence of activated carbon, there was a lag period of approximately 180 h, and then the phenanthrene was mineralized at a slow, linear rate. By 1600 h only 10% had been mineralized in the presence of activated carbon.

A second experiment was designed to test the effect of phenanthrene concentration and activated carbon concentration on the kinetics of mineralization of phenanthrene. Fifty g of Yolo silt loam was amended with 0, 0.2, and 1.0 g of activated carbon and then mixed with either 50 ng (no-growth) or 2000 ng (presumably growth conditions) of phenanthrene per g of soil. At a concentration of 50 ng per g, phenanthrene degradation in unamended soil began immediately and the rate declined over time. By 1400 h, approximately 43% (21.5 ng per g) of the chemical had been mineralized. At the higher concentration, phenanthrene degradation in unamended soil showed an initial period of acceleration in the rate and then the rate declined. By 1400 h, 30% (600 ng per g) of the chemical had been mineralized. Activated carbon substantially lowered the rate of mineralization of phenanthrene. By 1400 h, less than 10% of either concentration of phenanthrene was mineralized in the presence of activated carbon.

Mineralization of 50 ng of phenanthrene per g soil (no-growth conditions) was measured in 10 g Yolo silt loam amended with 0, 100 or 500 mg SM-7 chromatography beads. In one set of treatments, pre-equilibrated chemical-sorbent complexes were added to soil; in another set, phenanthrene was added to soil containing SM-7 beads. There was a direct relationship between amount

of sorbent and the rate of mineralization in the treatments where the chemical was added to soil containing beads. There was no mineralization of the phenanthrene that had been pre-sorbed to 500 mg of beads; however, there was a slow, linear rate of degradation of the same mass of chemical pre-sorbed to 100 mg of beads.

(e) Effect of addition of other carbon sources on phenanthrene degradation

Three different carbon sources were tested for their ability to inhibit or acclerate the degradation of 50 ng of phenanthrene per ml in Yolo soil. The compounds tested were salicylic acid (SA), a metabolite and inducer of naphthalene and presumably phenanthrene metabolism; phenol, a chemical with structural similarities to salicylic acid but not a metabolite of phenanthrene metabolism; and glucose, a sugar not expected to have any specific interaction with phenanthrene. In an initial experiment, 50 µg SA per ml caused an acceleration in the rate of phenanthrene degradation resulting in degradation by 1300 h of 27% of the added phenanthrene compared to 19% of phenanthrene degraded in soil not amended with SA. Three subsequent studies with the compound, however, showed no effect on phenanthrene degradation and it was not possible to reproduce the initial observation. Studies of phenanthrene and SA in which the SA, rather than the phenanthrene, was radiolabeled showed that degradation of SA was completed in less than 30 h, whereas phenanthrene continued to be slowly degraded over a period of months. Neither glucose nor phenol were found to have a substantial effect on phenanthrene degradation.

(f) Effect of soil moisture content on degradation of phenanthrene

Numerous sorption studies are conducted in soils that are slurried rather than incubated at field moisture levels. To evaluate the effect of soil moisture on phenanthrene degradation, the degradation of 50 ng phenanthrene per ml was measured in Yolo silt loam at soil to solution ratios of 1:0.16 (equivalent to 70% of 0.33 bar); 1:10, and 1:50. The initial rate of degradation of phenenthrene was substantially higher in the slurried treatments than at field moisture level, and the percent degraded by 350 h was approximately 22, 20 and 9.5% for the soil to solution ratios of 1:50, 1:10, and 1:0.16, respectively (Fig. 5).

In another experiment, the effect of incubating Yolo soil at moisture contents of 8, 16, 50, and 100% on the degradation of 50 ng phenanthrene per ml was measured. Degradation was fastest at 16% moisture, and then increasingly slower at moisture contents of 50, 80 and then 100%. It is likely that the decline in rate was due in part to oxygen diffusion limitations at the higher moisture contents.

(g) Age of phenanthrene in soil

Over the course of time, sorbed chemicals often become less available than they were immediately following their incorporation into soil (Hamaker et al., 1972). This can have serious implications for predictions of the kinetics of

biodegradation of sorbed chemicals. Samples of sterile soil that had been incubated with phenanthrene for several weeks or to which phenathrene was just added were put into slurries and inoculated with an induced pure culture of bacterium able to degrade phenanthrene. There was virtually no degradation of the phenanthrene that had been preincubated in soil. However, recent additions of phenanthrene were readily degraded by approximately 30% by the pure culture (Fig. 6). A much lower percentage of recently added phenanthrene (<5%) was degraded by a pure culture of bacterium that was not pre-acclimated to phenanthrene in inoculum preparation.

(h) Effect of initial population density on degradation of phenanthene

Time-course measurements of biodegradation of sorbed chemicals in soil often show an initial rapid rate followed by a slower rate of degradation (Scow et al., 1986). One hypothesis for this phenomenon is that the fast rate results from degradation of readily degradable, non-sorbed material, while the slow rate observed in the later part of the curve results from degradation of material that is desorbed from the organic surface. Therefore, a higher initial population density of bacteria able to degrade the compound should result in higher initial rates and degradation percentage. Experiments were conducted using different initial population densities of a pure culture of bacterium able to degrade phenanthrene. The organisms were inoculated at three different population densities into a mineral salts medium or a sterile soil slurry containing 50 ng of phenanthrene per ml. The percentage of phenanthrene degraded was significantly greater in the mineral salts medium than in the soil slurry. The fraction of phenanthrene degraded in the mineral salts medium by 60 h was 21, 10, and 1% at initial population densities of 10^9, 10^7, and 10^5 cells per ml, respectively. The fraction degraded in the soil slurry by 60 h was 4.5, 2, and 1.5% at initial population densities of 10^9, 10^7, and 10^5 cells per ml, respectively (Fig. 7).

(i) Enhancement of polyaromatic hydrocarbon (PAH) degradation in soil

Two preliminary studies were conducted to determine the possibility of enhancement of the rate of degradation of sorbed chemicals in soil. Inoculation of soil with a surfactant and a naphthalene-degrading bacterium was tested. Addition of 0.5 ml of a 10% solution of the detergent, Tween 80, at the beginning of an experiment resulted in a slight stimulation of naphthalene mineralization (by 2%) within the first 16 h of incubation. Addition of Tween after 100 h of incubation with napthalene had no effect on subsequent degradation.

Several species of bacteria able to degrade naphthalene and/or phenanthrene were isolated from Yolo and other soils. One species, *Corynebacterium pseudodiphtheriticum* (Nap 2), a filamentous actinomycete isolated from Yolo soil, was re-introduced into sterile and nonsterile Yolo soil containing 1 μg naphthalene per g soil. Addition of Nap 2 caused a significant enhancement in both the initial and second phase rate of degradation. By 1580 h, approximately 52% of the naphthalene had been mineralized to CO_2, whereas 38% had degraded in uninoculated soil (Fig. 8). In the sterile soil, by

1580 h the Nap 2 degraded 32% of the added napthalene after a 50 h lag period.

Simplify An Existing Model Describing Diffusion, Sorption and Biodegradation in the Presence of Spherical Aggregates to Use for Screening Conditions When Biodegradation May be Limited by Mass Transfer

A process-based, kinetics model, the Diffusion-Sorption-Biodegradation (DSB) model, describes the biodegradation of chemicals limited in availability to microorganisms by diffusion and sorption (Scow and Hutson, 1992). Improvements to the DSB model were made during this past year. The model was adapted to include a mass transfer term across the surface of the aggregate and nonlinear conditions for adsorption. Also, a dimensionless group (analogous to a Thiele modulus) consisting of the diffusivity, the biodegradation rate constant, aggregate radius, and adsorption capacity was derived as a criterion for evaluating when intraparticle diffusion resistance can be ignored. The criterion was applied to data from the literature describing sorption and biodegradation of two chemicals in soil slurries and experimental results were confirmed. This simplification will facilitate use of the model as a screening tool without having to perform data-intensive and lengthy model simulations. These results are summarized in a submitted manuscript (Chung et al., 1992).

Develop and Improve Methodologies for Working with Sorbed Chemicals

(a) Effect of solvent used in phenanthrene stock solution on degradation

Phenanthrene has a very low solubility in aqueous solution (<1 ppm), thus requiring the use of a solvent in making up stock solutions. A comparison was made of the degradation of 50 ng phenenthrene per ml in Yolo soil that was added in various solvents: ether, methylene chloride, tetrahydrofuran, acetone and water. The solvents were given time to volatilize from the soil after their addition. Degradation of phenanthrene added in ethylene chloride and tetrahydrofuran was similar to water for at least portions of the degradation period (280 h). Acetone showed a slight depression and ether a significant depression (<8% mineralized by 280 h) in the degradation of phenanthrene compared to the water treatment (13.5% mineralized by 280 h). Subsequent experiments were performed using methylene chloride as the solvent.

(b) Development of method for extraction of phenanthrene from soil

Recoveries of 88 to 96% were measured for phenanthrene (incubated for 24 h in sterile soil) added at concentrations of 50 ng or 50 μg per ml soil solution. The extractant was methylene chloride and the samples were sonicated for 1 h. Efficiencies are now being determined for phenanthrene incubated in sterile soil for longer periods of time to be more representative of experimental conditions.

Discussion

Desorption isotherms in several soils suggest that sorption of phenanthrene is essentially irreversible. However, the percentage of phenanthrene that is degraded (especially if one assumes that CO_2 evolution represents approximately 50% of the total degradation, the remainder being incorporated into cells) far exceeds the percentage that is available in the soil solution after initial equilibration of the chemical between the solid and solution phase. This suggests that the desorption isotherms (conducted in sterile soil) are not representative of true conditions in soil or that microorganisms have means by which to promote desorption of phenanthrene. These questions will be pursued in future studies.

High organic soils initially appeared to have slower rates of degradation than did soils with lower organic contents; however, at a later time, degradation in high organic soils was often faster. The possibility that higher organic soils can maintain higher microbial populations or provide a secondary carbon source that enhances the rate of degradation of phenanthene will be considered in future studies.

It appears more difficult to enhance the degradation of phenanthrene and napthalene as the time of contact between soil and chemical increases. This observation is based on the results of studies of the effect of initial microbial population density on degradation; addition of a detergent at the beginning, rather than later in the incubation of a chemical in soil; the biodegradability of aged as compared to fresh phenanthrene in soil; and the rapid initial rate of degradation of sorbed chemicals generally seen in soils. Thus, research efforts should be directed at the bioremediation of chemicals that have been in contact with soil for some period of time rather than focusing only on recently added chemicals.

Results thus far indicate that the approach of using natural soil amended with different amounts of defined, artificial sorbent is feasible for the study of biodegradation of sorbed chemicals. Yolo silt loam is a reasonable test soil because its microbial populations can metabolize both naphthalene and phenanthrene, and the soil does not sorb the chemicals to such a degree that the effect of added sorbent is overshadowed. Although the sorption experiments suggested that sorption is irreversible, especially from activated carbon and beads, it appears that the reaction may be reversible in the presence of microorganisms.

Amendment of soil with additional carbon sources may, depending on the chemical, affect the degradation of a sorbed chemical, such as phenanthrene. Therefore, precautions (at least running the appropriate controls) should be taken in using organic solvents to prepare stock solutions of sparingly soluble chemicals. In this study, the rate of phenanthrene degradation was depressed in the presence of ether and, to a lesser degree, acetone.

References

Chung, G.-Y., B.J. McCoy, and K.M. Scow. 1992. Effect of sorption and intraparticle diffusion on biodegradation rates (in review).

Hamaker, J. W. In C. A. I. Goring and J. W. Hamaker (ed.) 1972. Organic chemicals in the soil environment. Marcel Dekker, New York, p. 253-340.

Scow, K. M., S. Simkins, and M. Alexander. 1986. Kinetics of mineralization of organic compounds at low concentrations in soil. Appl. Environ.

Scow, K.M. 1992. Effect of sorption-desorption and diffusion processes on the kinetics of biodegradation of organic chemicals in soil. (in press in SSSA Special Publication: Sorption and Degradation of Agricultural Chemicals in Soil).

Scow, K. M., and J. Hutson. 1992. Effect of diffusion and sorption on the kinetics of biodegradation: theoretical considerations. Soil Sci. Soc. Amer. J. 56:128-134.

Publications and Reports

Publications:

Chung, G.-Y., B. J. McCoy, and K. M. Scow. 1991. Effect of Intraparticle Diffusion and Sorption on Rate of Biodegradation.,n (In press).

Scow, K.M. 1992. Effect of sorption-desorption and diffusion processes on the kinetics of biodegradation of organic chemicals in soil. (SSSA Special Publication: Sorption and Degradation of Agrichemicals in Soil), (In press)..

Scow, K. M., and M. Alexander. 1992. Effect of diffusion and sorption on the kinetics of biodegradation: experimental results with synthetic aggregates. Soil Sci. Soc. Amer. J. 56:119-127.

Scow, K. M., and J. Hutson. 1992. Effect of diffusion and sorption on the kinetics of biodegradation: theoretical considerations. Soil Sci. Soc. Amer. J. 56:128-134.

Presentations:

March, 1992. Effect of desorption on the kinetics of biodegradation of organic chemicals in soil. Dept. of Chemical Engineering, Univ. of California, Davis, Ca.

Scow, K.M. and M. Fuller. 1991. Kinetics of biodegradation of sorbed chemicals in soil. A presentation at the Society of Environmental Toxicology and Chemistry Northern California Regional Chapter, Sacramento, May 29.

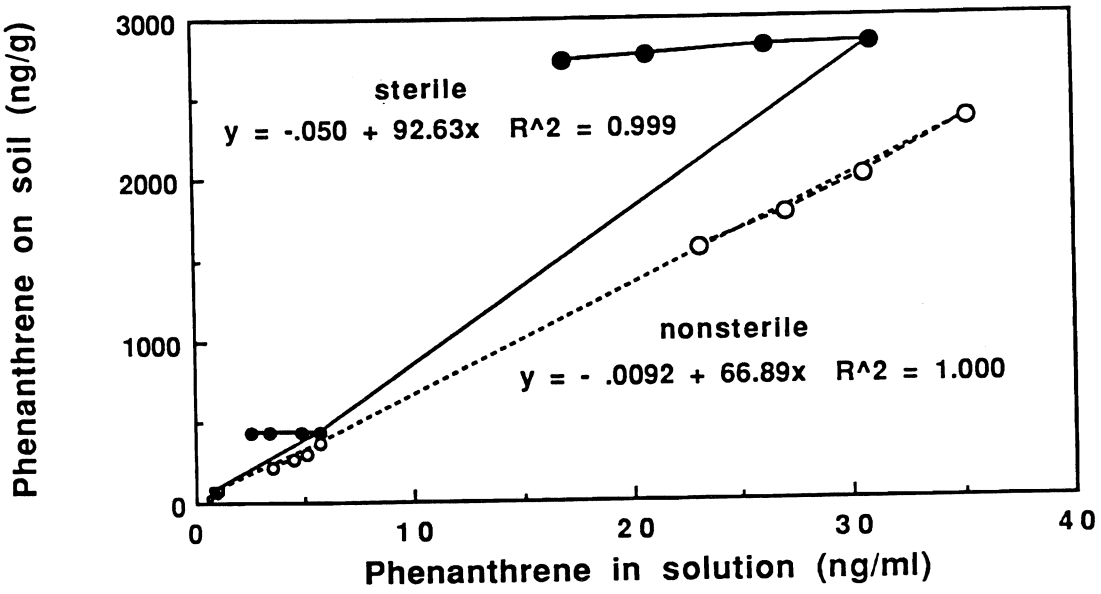

Figure 1. Adsorption isotherm in Yolo soil.

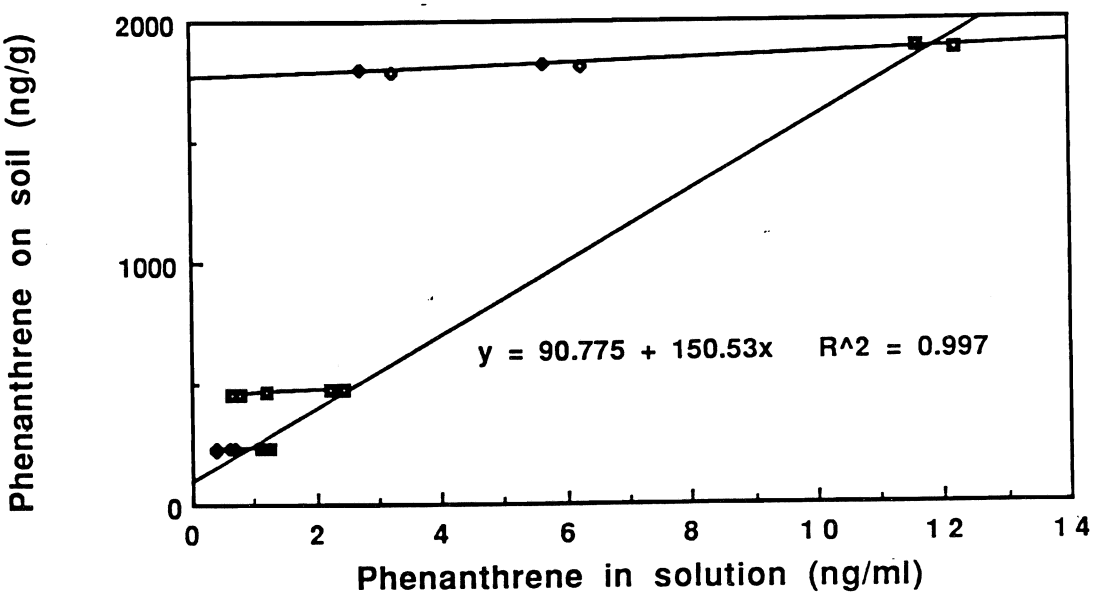

Figure 2. Adsorption isotherm in Auburn soil.

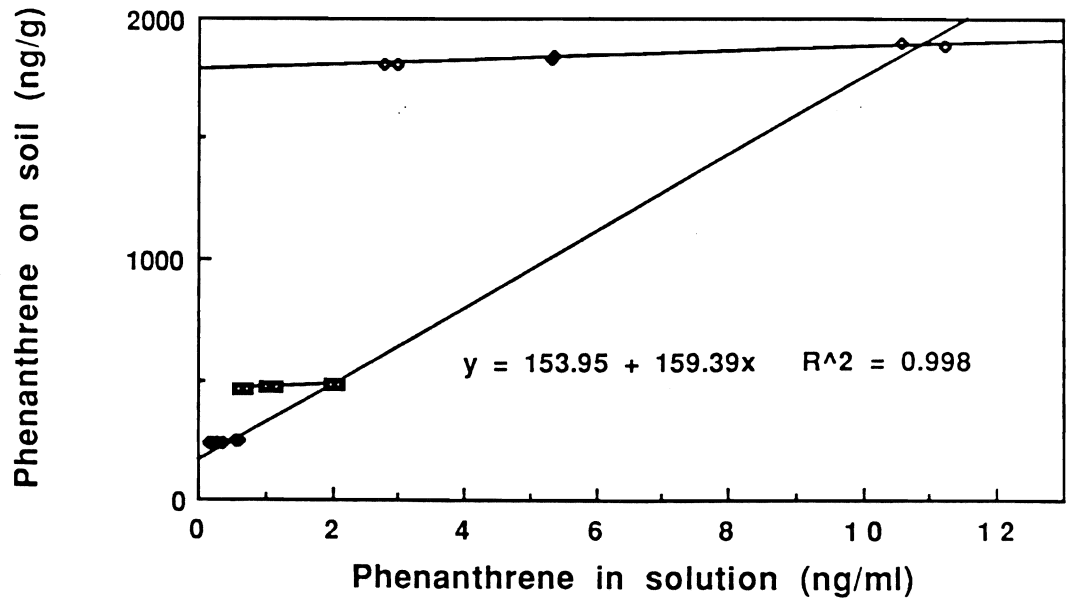

Figure 3. Adsorption isotherm in Crozier soil.

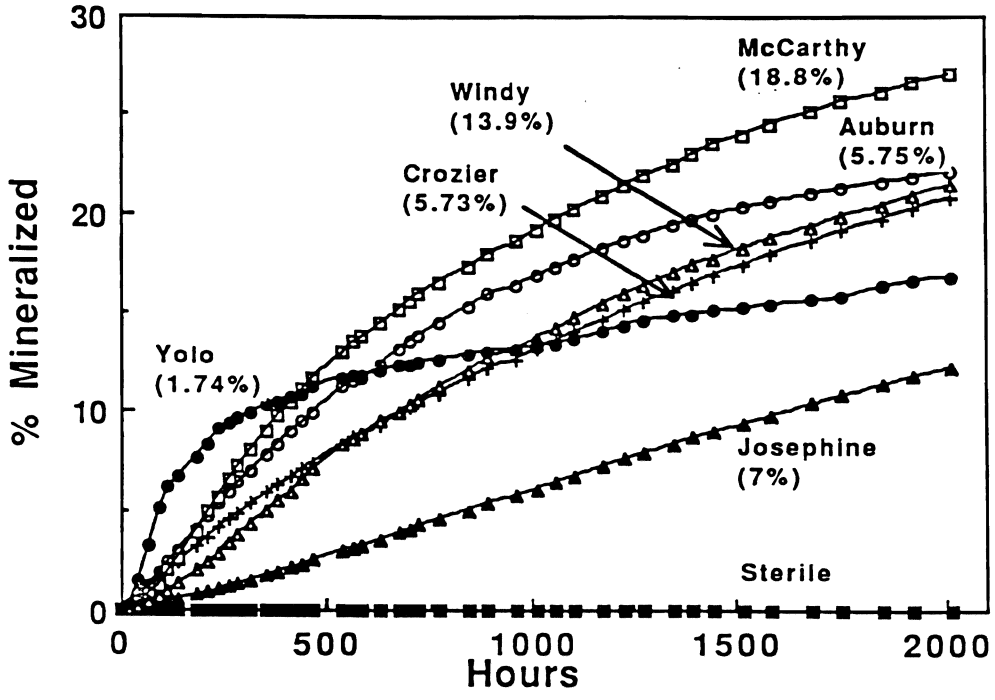

Figure 4. Biodegradation of phenanthrene (50 ng/ml) in soils with different organic matter contents.

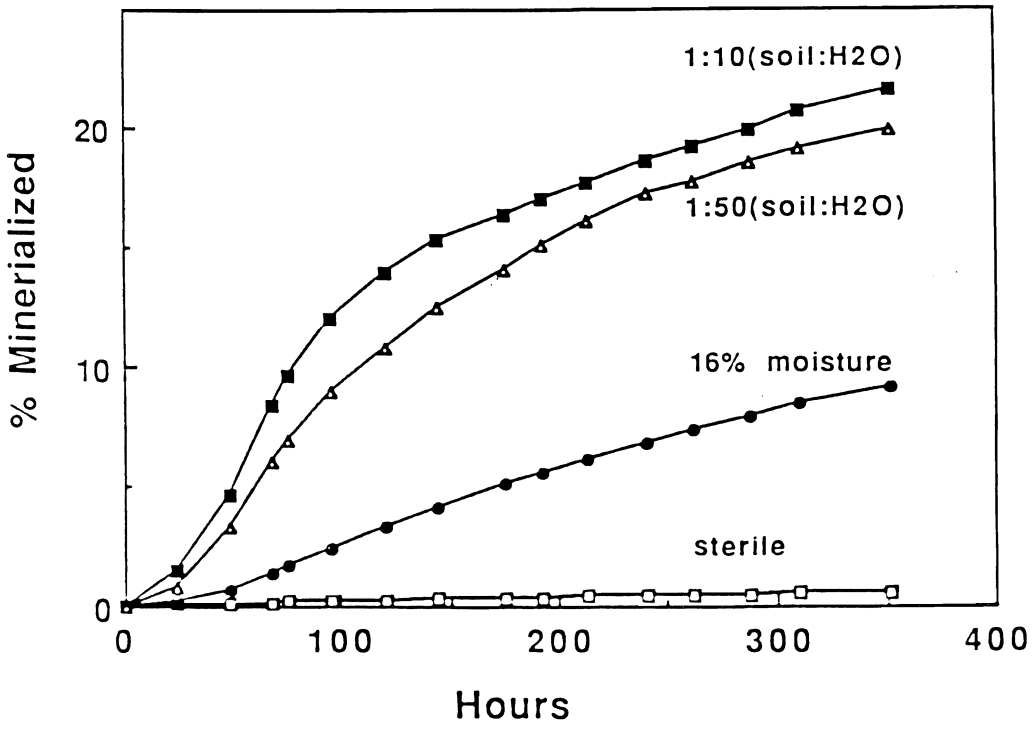

Figure 5. Biodegradation of phenanthrene in Yolo soil slurry.

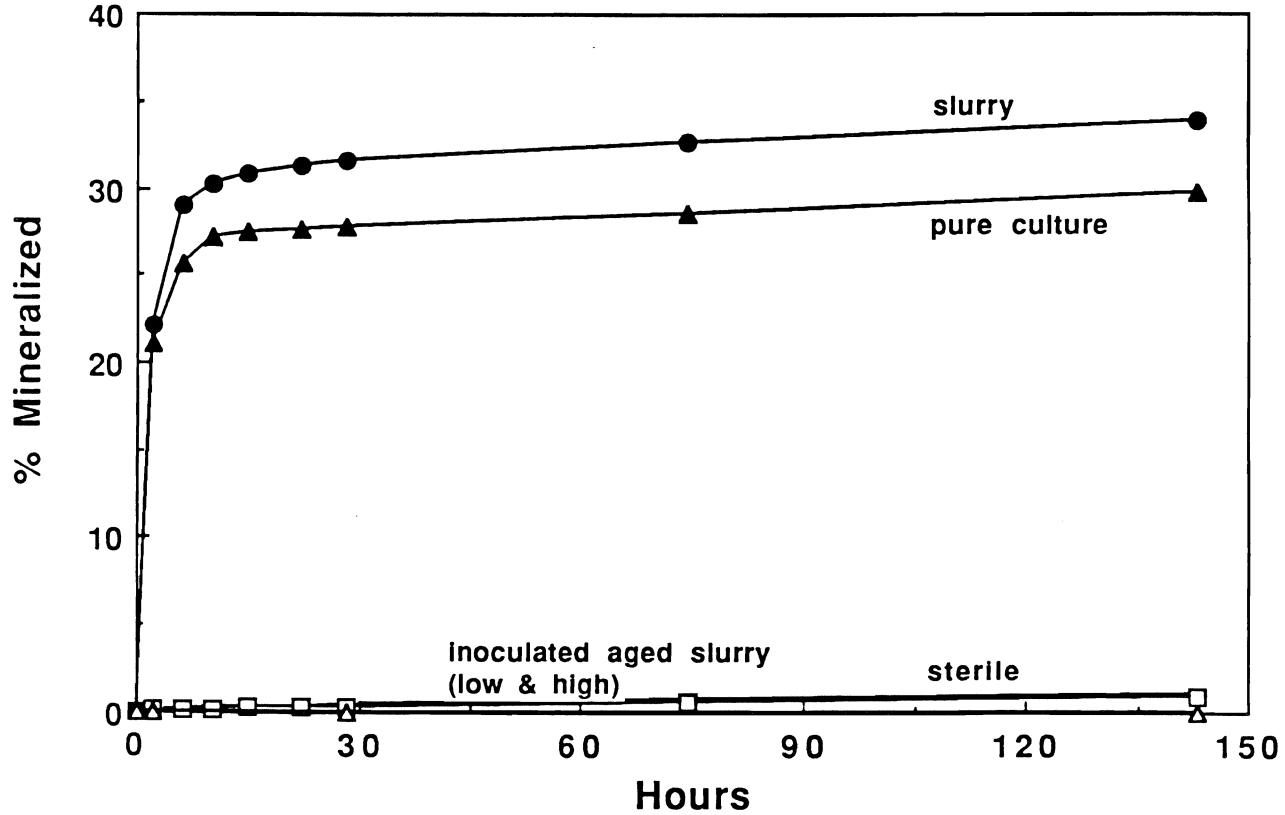

Figure 6. Effect of bound residue on phenanthrene biodegradation.

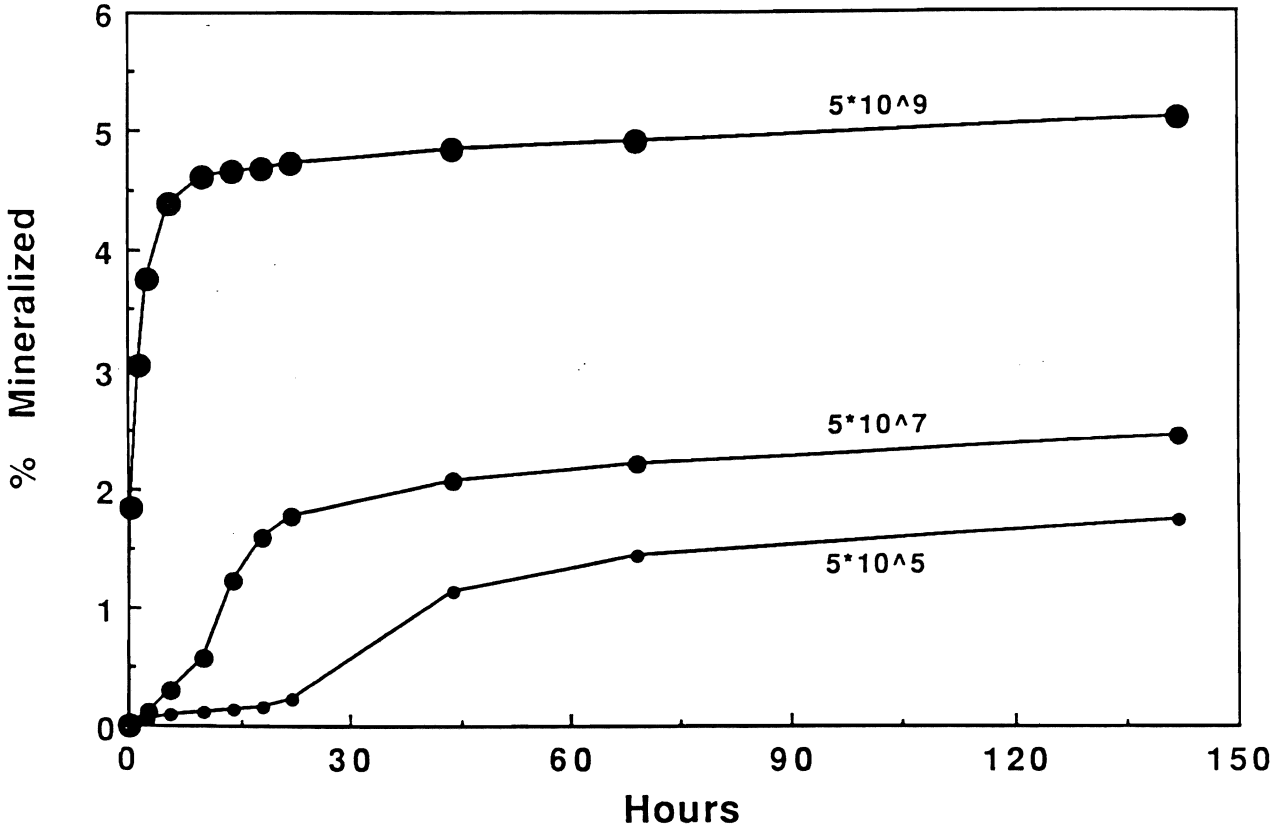

Figure 7. Effect of cell density on phenanthrene biodegradation in soil slurry.

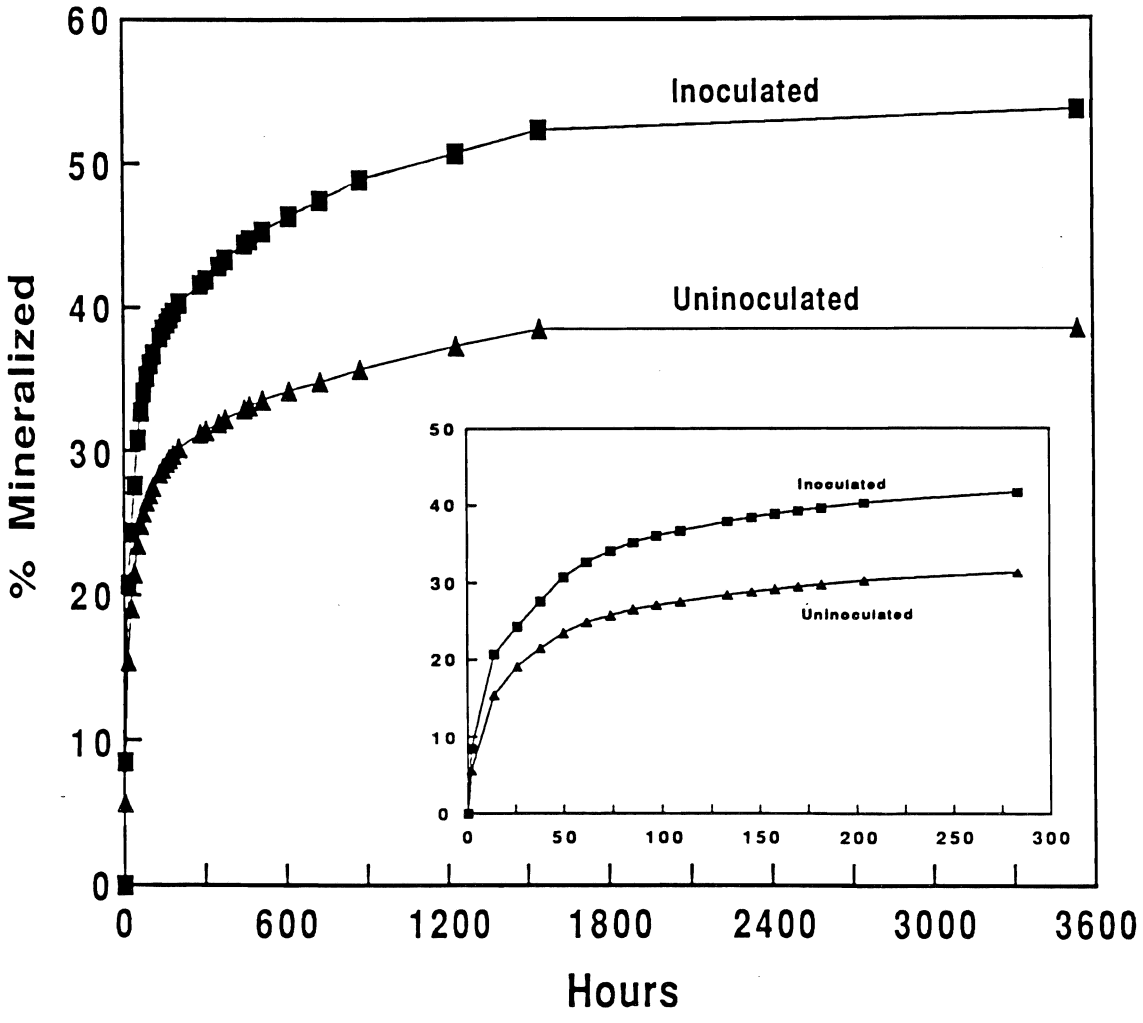

Figure 8. Effect of inoculation on the mineralization of naphthalene in Yolo soil.

Rhizosphere Effects on Degradation of Pesticides in Soil

DAVID E. CROWLEY
Department of Soil & Environmental Sciences, Riverside Campus

Summary

Biodegradation of persistent, chlorinated-hydrocarbon pesticides can be achieved in soil providing there are sufficient nutrients and microbial populations capable of metabolizing the target compound. Previously, much research has focused on metabolic pathways and genetics of pesticide biotransformations, whereas nutritional and ecological factors affecting degradation rates remain less well understood. Many bacteria and fungi that degrade pesticides colonize plant roots and have greater population numbers and metabolic activity in the rhizosphere than in bulk soils. Based on this rationale, it is hypothesized that plants may increase biodegradation rates ofsome pesticides or shorten the lag phase associated with biotransformation kinetics. The objectives of this research are to (1) determine whether plant roots, in fact, affect microbial mineralization rates of commonly used pesticides; (2) characterize the effects of root-induced pH shifts and root exudate composition on biotransformation rates and pathways of a model compound, chlorobenzoic acid; and (3) examine the effects of microbial competition during colonization of root surfaces on the biodegradation activity of a known pesticide-degrader bacterial strain.

Mechanistic studies in microbial ecology are being conducted to determine nutritional effects, such as competition for iron and composition of root exudates, on biotransformation rates. A reporter gene (luciferase) will be used to examine the effects of microbial competition during colonization of root surfaces on the biodegradation activity of a known pesticide-degrader bacterial strain. In the experiments with plants, pesticide mineralization rates will be examined using glass "rhizotron" tubes in which roots grow through pesticide-amended soil. Soil extracts from the rhizotron tubes, bulk soil, and from soil incubated without plants will be analyzed by TLC, and GC, or by HPLC methodologies. Knowledge obtained from these studies should provide basic information on rhizosphere processes that affect pesticide persistence in soil, and may aid in development of technology aimed at bioremediation of contaminated soils.

Key Words: biodegradation, microbial ecology, pesticide, root, rhizosphere

Project Objectives Addressed in 1991-92

1. To determine whether plant roots influence the rates of biodegradation or disappearance of chlorobenzoate and other representative chlorinated hydrocarbons from soil.

2. Characterize the effects of root exudates on biotransformation of chlorinated hydrocarbons.

Research Plan and Procedures

In the first year of this project, our research group has focused on the primary objective of our proposal, which is to determine whether mineralization of pesticides occurs more rapidly in the presence of plant roots than in bulk soils. This has involved a considerable start up effort and preliminary experimentation including (1) development of techniques for quantitative extraction and detection of representative chlorinated hydrocarbons from soil, (2) isolation of microbial consortia that utilize chlorinated hydrocarbons employing enrichment culture techniques, and (3) methodology for testing the effects of plant roots on pesticide disappearance/biodegradation from contaminated soils. Our research group is pleased to report not only our success in this initial start up, but also what we believe are promising results that should allow us to generate the first publications of our data early in the coming year. In our initial efforts, we have worked primarily with the model compound 4-chlorobenzoate. The general procedures that we have employed for quantitative analysis of this compound are based on soil extractions with water or acetonitrile and separation of chlorobenzoate from the soil extracts using reverse phase HPLC with UV detection. These techniques are then being employed in studies with the termaticide Chlordane, which is water insoluble, but which can still be extracted with an organic solvent. The HPLC procedures we are using should be compatible for a planned survey of several other compounds for which we have obtained EPA reference standards. While our main goal is to determine mechanistic effects of plant root interactions with degrader microorganisms, an applied goal of our research also will be to survey plant effects on microorganisms provided with a variety of chlorinated compounds that are highly recalcitrant to degradation.

To achieve our objective in understanding potential plant effects on pesticide biodegradation, a critical component of our research effort has involved the isolation of various microbial consortia or single microbial species that are capable of growing on 4-chlorobenzoate and various chlorinated hydrocarbons when provided as a sole carbon source. After isolation, these strains are then being tested as inocula on plant roots to examine the relative rate of disappearance of chlorobenzoate and other chlorinated hydrocarbons in the presence and absence of roots. A variety of plant species, including a turf grass, and two crop plants, bean and corn, are being used as model species. Based on our progress to date, we are planning to conduct a series of experiments in the nutritional ecology of selected strains or consortia to

determine nutritional factors that can be manipulated to improve their competitiveness on plant roots and enhance their biodegradation activity. We have also conducted a number of practical experiments to test the phytotoxic effects of chlorobenzoate and a second representative pesticide, Chlordane, on the growth of plants. This will allow us to determine the working range for using plants in the bioremediation of contaminated soils. One unanticipated finding has been that plants readily absorb water soluble chlorobenzoates. This presents a novel method for bioremediation of soils, and also suggest there may be some hazard with food chain transfer, but, from a practical standpoint, it has complicated our efforts to quantitatively assay root effects on microbial degradation processes. In our future efforts to determine the fate of chlorobenzoates with respect to plant uptake, microbial uptake, chemical binding, and degradation, we are planning to conduct mass balance studies using radioisotope ^{14}C-chlorobenzoate.

The experimental systems we are presently using to study root effects on degradation of chlorinated hydrocarbons include pot cultures, plants grown in sand media in continuous flow columns, and plants grown in root boxes. Once we have perfected our procedures, we anticipate that small scale field trials may be conducted on the Agricultural Experiment Station at Riverside. Each of the different systems has various specific advantages. Pot cultures are used to examine phytotoxic effects on the plant material over a range of pesticide concentrations. A more complicated system developed by Paul Haby, one of our graduate research assistants, uses recirculating flow columns in which chlorobenzoate and/or other materials are continually pumped over the surface of a 30 cm long column used for plant culture. Leachate passing through the media and out through the bottom is returned to the top of the column with a peristaltic pump and sampled at time intervals for determination of chlorobenzoate concentrations (see results below). In essence, this system not only allows continuous sampling, but also serves as a chemostat for producing bacterial enrichment that grow on plant roots and utilize chlorobenzoate as a carbon source.

In addition to the two plant culture methods, we have developed a system employing "rhizotubes" (Figure 1) that allows us to examine microsite effects of plant roots on chlorinated hydrocarbon degradation. This novel system developed in our lab is based on root boxes that have a removable side for access to the roots. Pesticides or chlorobenzoate are loaded into agar or sand media in microcentrifuge tubes that are then placed underneath a growing root tip. After the root has grown through the media, the root is severed and the root exudate, soil solution and remaining pesticide are extracted by spinning the column with a microcentrifuge. This has proven to be a very versatile system that we will continue to use for examining specific inoculation effects and microsite conditions that affect the disappearance of chlorinated hydrocarbons.

Results

Extraction and Quantification of Target Compounds Using standard procedures, chlorobenzoates and polyaromatic hydrocarbons are extracted from soils using organic solvents and specific extraction techniques that depend upon the degree to which they are adsorbed to the soil matrix. Among chlorinated hydrocarbons, chlorobenzoates are relatively easy to extract because of their solubility in water, which ranges from 70 to 250 ppm for its various isomers. In studies with chlorobenzoate, we have obtained 80% or greater extraction efficiency with a single water extraction. We also tested various organic solvents, and hot water extractions that were not any better than water. Other compounds we are working with, such as Chlordane, are much more insoluble and require multiple extractions with acetonitrile from a sand medium or soxhlet extraction with strong solvents for soil containing clay or organic matter. Once extracted, all of the materials we have worked with are readily quantified by HPLC chromatography using a C18, reverse-phase column with a water-acetonitrile gradient. Chlorobenzoate also requires the addition of 3% acetic acid to the solvent system in order to protonate the benzoic acid group and give good retention on the column. A typical chromatogram for 4-chlorobenzoate is shown in Figure 2. Based on the ultraviolet absorption spectrum of chlorobenzoate, we have determined an absorbance peak of 238 nm, with a high extinction coefficient that allows detection of quantities as small as 10 ng. With a standard injection quantity of 10 ul, this allows detection of chlorobenzoate in an extract solution at a concentration of 1ppm. Chlordane, a second compound we have conducted several experiments with, is less readily detected having an absorbance peak of 213nm and detection threshold of 100 ng. Published procedures for chlordane normally employ gas chromatography with electron capture detection. However, the HPLC procedures we have developed require simpler sample preparation and work well over the concentration range we have selected. Concentration curves have been generated for both chlorobenzoate and chlordane and are now incorporated into our software for peak quantification.

Enrichment Culture of Chlorinated Hydrocarbon Degrader Populations A primary goal of our research during the first year has been to obtain and characterize specific microorganisms or various consortia of microbial species that can utilize specific chlorinated hydrocarbons as a carbon source for growth. One of the difficulties in microbial ecology research is that very few (less than 0.1%) soil organisms are culturable on solid agar media. Thus, to select for populations that utilize chlorinated hydrocarbons *in situ*, we have employed standard enrichment culture techniques in which a soil inoculum is placed in minimal media and provided with either chlorobenzoate or chlordane as a sole carbon source. These populations are then maintained in long term cultures on the substrate to amplify their population numbers that function in the utilization of the carbon source. Our initial experiments with chlorobenzoate have employed a soil from the citrus orchards on the Riverside campus that was amended with chlorobenzoate and used to grow ryegrass. After the end of a three week period, the pot cultures were harvested and extracted to measure

chlorobenzoate. Our analyses showed that chlorobenzoate was no longer detectable in the pot culture. Subsequently, to further study and enrich the degrader consortium, rhizosphere soil from the plant cultures was placed in a bioreactor under aerobic conditions and supplied with 250 ppm of chlorobenzoate (Figure 3).

After isolation from rhizosphere soil and maintenance in continuous culture in chlorobenzoate media, we have now obtained a microbial consortia that can reduce 500 ppm of 4-chlorobenzoate to nondetectable levels in less than one week in a liquid mineral salts medium. Recently, we have tested a number of media supplements, including root extracts, for their effects on the growth of this consortium. Results of these experiments show that enrichment of the media with yeast extract and an alternate carbon source, mannitol, slowed the disappearance of chlorobenzoate, whereas addition of root extracts, root exudate, or soil did not. Using these additions to the medium, it also appears that various subsets or species from within the consortia have undergone further selective enrichment such that we may have selected for single strains. One culture appears to have selected an organism preliminarily identified as *Pseudomonas aeruginosa*. These cultures are now being plated out on selective media containing chlorobenzoate in an attempt to obtain this or other single strains that can use chlorobenzoate as a carbon source. Identification of such a strain would be highly beneficial for our future studies in which we would like to incorporate a reporter gene marker into selected strains to follow their growth and activity after inoculation on to plant roots in contaminated soils.

Parallel studies employing enrichment cultures are also being conducted with chlordane and lindane. With chlordane, aerobic enrichment cultures were inoculated with one of three soils obtained from agricultural fields that have a history of DDT contamination. Since chlordane is not soluble in aqueous media, the pesticide was sprayed onto ceramic beads that were then placed into Erlenmeyer flasks containing media and the soil inoculum. Chlordane concentrations were then determined by extracting three randomly selected beads with acetonitrile. Preliminary data indicate that chlordane disappears from the media very slowly with approximately 30% disappearance after 25 days in culture when provided at 200 ppm. At a lower starting concentration of 50 ppm, levels of chlordane were nondetectable after 25 days. At this point, it is too early to determine whether we have in fact isolated a Chlordane degrader consortium, which would be a breakthrough since chlordane's very high substitution with chlorine (see appendix) makes it extremely recalcitrant to degradation. Production of humic material or bacterial polysaccharides could also increase disappearance by nonspecific binding. Lastly, low solubility is a concern with this compound since the pesticide is inaccessible for microbial uptake when it is strongly sorbed onto a solid matrix. Future experiments will continue these enrichment cultures and explore the use of nutrient supplements and surfactants to increase solubility in the culture media. In the meantime, we have already begun plant experiments with this recalcitrant compound to examine potential root stimulatory effects on degradation as well as phytotoxicity.

Phytotoxicity effects on plant growth One concern in biodegradation research is distinguishing mineralization of the target compound from other processes such as uptake, binding, and volatilization. For this reason we are using the term 'disappearance' until we have established the true fate of the compounds we are examining. Several of the chlorobenzoate based materials, such as chloramben, dicamba, and 2,3,6-TBA, are used as herbicides and thus are taken up by plants. For example, chloramben (3-amino-2,5-dichlorobenzoic acid) is a preemergent herbicide that is taken up by both susceptible and tolerant plants, but detoxified by tolerant plant species (Frear et al., 1978). Another chlorobenzoate, Dicamba (3,6-dichloro-2methoxybenzoic acid) is also readily absorbed by plants and has plant growth regulator properties that impede plant growth. Interestingly, several strains of bacteria have now been isolated that metabolize dicamba, some of which have been employed recently as rhizosphere inoculants to protect dicamba-susceptible plant species (Krueger et al., 1991). Given this background information, it is essential in our studies examining plant effects on microbial degradation that we obtain mass balance information on the relative quantities of chlorobenzoate that are being taken up versus degraded.

In our first experiments examining root effects on chlorobenzoate, we observed that root growth of ryegrass was strongly inhibited at chlorobenzoate concentrations of greater than 100 ppm. Concentrations greater than 250 ppm also kill bean and corn. Chlordane appears to have unexplained phytotoxic effects that result in the development of leaf tissue chlorosis in bermuda grass when applied at concentrations above 200 ppm. In effect, these concentrations have determined our upper working limit for studies on plant root effects on degradation. One method we are using for examining uptake of chlorinated hydrocarbons by plants has been to collect xylem exudate. With this procedure, the plant is severed at the base of the stem and a tube is place over the top to collect 100 to 200 ml of exudate that accumulate in the tube over a 2 hr period. Other procedures have involved sampling of individual plant parts that are homogenized and centrifuged, after which the resulting supernatant is injected directly into the HPLC. These methods have shown that although chlorobenzoate is not commercially used as an herbicide, it is readily taken up by plants and translocated to the stems and leaves. On the other hand, we have not found any evidence for uptake of Chlordane, which suggests that plant uptake will be less of a concern with the more nonpolar, less water soluble compounds. As we test other compounds, we will continue to employ these controls to assay for phytotoxicity and plant uptake of the test materials.

Root Effects on Pesticide Degradation/Disappearance Since the inception of this project, we have accumulated considerable data supporting our hypothesis that plant roots enhance the biodegradation activity of chlorobenzoate degrader organisms. Experiments examining this hypothesis have employed a variety of experimental approaches, including simple pot cultures of plants in chlorobenzoate-amended sand media, recirculating columns, enrichment cultures with root exudates or root extracts, and rhizotube experiments in root boxes. When inoculated with a microbial consortia, the primary effect seems to

be to shorten the lag phase that occurs prior to disappearance of the compound. This is most readily apparent in a recirculating column that allows repeated time point sampling of the soil solution. To eliminate disappearance by root uptake, root extracts were prepared by homogenizing the plant root material and filtering it through a Whatman 1 filter. Figure 4 shows the results of one particular experiment in which the recirculating column amended with chlorobenzoate and root extract gave disappearance of chlorobenzoate in 7 days. In the column without the root extract, the chlorobenzoate persisted for over 20 days at which time the experiment was terminated.

In addition to the recirculating column experiments, we have also conducted several experiments with the rhizotube system in which a small amount of chlorobenzoate was loaded into a microfuge spin filter tube in agar or sand media. In experiments with bean or corn, we routinely found 90% disappearance of the chlorobenzoate after inoculation of the roots, versus 44% disappearance in inoculated tubes cultured for the same period of time without roots. In the future, we anticipate that this system will be particularly useful for mass balance studies with radiolabeled compounds. Use of the rhizotron tubes allows precision and reproducibility in pesticide loading, bulk density, and soil moisture, and also minimizes handling of radiolabeled materials that can be used at high specific activities in a minimum soil volume. Soil properties such as pH, nitrogen content, nitrogen source, and organic matter can also easily be altered to create unique microsite environments using similarly grown plant material. To alter microbial degrader and nondegrader populations in the rhizosphere for competition studies, specific microbial inocula may be loaded at high densities into the tube media.

Discussion

Chlorinated hydrocarbons have been used extensively as pesticides in agriculture for several decades. Faced with the concern that these compounds and their breakdown products now occur commonly in most agricultural soils, considerable efforts have been made to determine the processes involved in their biodegradation and their possible toxicity to living organisms. This research has shown, in accord with the earliest reports (Audus, 1949), that biodegradation represents a major pathway for elimination of xenobiotic compounds and that many common soil microorganisms have the capability to degrade even the most persistent compounds under the right nutrient and environmental conditions (see review of Rochkind-Dubinsky, 1987). With continuing breakthroughs in the genetic engineering of microbes for improved degradation abilities, it is anticipated that new technology for bioremediation of contaminated soil and water systems will become available in the foreseeable future (see review of Chaudry and Chapalamadugu, 1991). Presently, however, there is a great deal of knowledge on the metabolism and genetics of biodegradation but very little information on environmental factors that affect mineralization and transformation of compounds by microorganisms in their natural habitat. This lack of information represents a large gap in knowledge that is needed to optimize both the utilization of pesticides and the bioremediation of pesticide-contaminated soils.

Early research on the degradation of various pesticides in the plant rhizosphere has been very limited, but the consensus in the literature has been that roots significantly enhance microbial degradation rates of the few materials that have been examined (eg. parathion, Hsu and Bartha, 1979; and organophosphates, Reddy and Sethunathan, 1983). From our survey of the literature there has been very little work since these early reports, until recently. Several current publications in this area (Walton and Anderson, 1990; Aprill and Sims, 1990) provide evidence for a rapidly growing interest in using plants for bioremediation purposes, and in determining the effects of plant roots on microbial degradation of xenobiotics. Once we proceed beyond documentation of the rhizosphere effect, real application of plants and microorganisms in bioremediation will require a better understanding of the nutritional ecology of the rhizosphere and how competition affects various microbial populations and processes. The long term goals of our research group over the next several years will be to identify key nutritional factors that govern microbial activity in the rhizosphere. After the first year, our research has progressed to examining specific factors involved in degradation of the model compound, chlorobenzoate, and we have begun in-depth study on the general applicability of ecological principles in degradation processes. Presently, two graduate students, Paul Haby and Steve Reis, are working full time on this project. Under the auspices of this grant, they are assisted by Ms. Susan Hackett, a Lab Assistant I and Mr. Dirk Adams, a part time undergraduate student worker. In the fall of 1992, two new students, Ms. Cathy Irwin and Mr. Sam Alvey, began working in my lab on rhizosphere effects on pesticide degradation. With the synergism that comes from a team approach, this should be an exciting year that will bring continued rapid progress.

Among one of the more promising tools to have emerged in recent years for monitoring bacterial activity in soils is the use of a bioluminescent reporter gene that can be stably incorporated into the genome of specifically selected organisms (Shaw et al., 1992). Incorporation of bioluminescence into a bacterial strain results in the production of light which can be detected as photons in a scintillation counter or by (nonradioactive) autoradiography using photographic x-ray film. In a recent, particularly relevant application of this methodology, the bioluminescence reporter was engineered so that expression of the luciferase gene was coupled to a promoter for napthalene degradation in a strain of *Pseudomonas fluorescens* (Heitzer et al., 1992). Using this strain, the authors have now developed a bioassay that allows quantitative assessment of napthalene bioavailability in water and soil samples. However, one limitation of this particular gene construction is that an aldehyde substrate required for bioluminescence is not produced in sufficient quantities and consequently must be artificially added for the luciferase enzyme to produce light. In our research group, Dr. Maria Brennerova, a postdoctoral research associate supported by the University of California Biotechnology Research and Education Program, has been working on an improved version of the reporter which utilizes a constitutively expressed ribosomal promoter to control the bioluminescence (*lux*) operon. After extensive testing, we have determined that this promoter is very strongly expressed during the exponential growth

phase of the marked strain. In our subsequent experiments, we have since used the bioluminescence reporter to localize zones of exponential growth of the bacterium (*P. fluorescens*) on plant roots (Figure 6). We believe that this gene construction should be very useful in our Kearney Foundation work next year since the reporter (incorporated into a transposon, *Tn7*) can readily be incorporated into other bacterial strains. One of our immediate goals will be to use this reporter to mark specific individual strains of a chlorobenzoate degrader that will then be inoculated onto plant roots.

Anticipated Research Plan for Year 2 In the second year, one of our goals will be to conduct final experiments that are still needed prior to publication. To this end, Mr. Paul Haby will continue his radioisotope work on chlorobenzoate. After these studies are finished, he has expressed an interest in examining whether plant-produced surfactants in root exudates are able to mobilize nonpolar chlorinated hydrocarbons in the rhizosphere. Mr. Steve Ries will continue his research on chlordane and lindane, and tentatively has decided to focus on aerobic/anaerobic effects on pesticide degradation in the rhizosphere. He may also examine nutritional effects and would like to set up field plot experiments examining rhizosphere effects and the use of plants for bioremediation. Ms. Cathy Irwin has just started and has begun research on iron nutritional effects on degradation and the importance of iron competition in regulating the population of a pesticide degrader in the plant rhizosphere. She is presently working with strains isolated from Paul Haby's enrichment cultures and would like to employ one of the well-characterized chlorobenzoate degraders from Dr. Dennis Focht's laboratory. Lastly, Mr. Sam Alvey will have the opportunity to put together a topic that reflects his interest and that is within the scope of the original proposal. Possibly, this may involve experiments with the bioluminescence marker for tagging and monitoring degrader populations in soil.

References

Aprill, W. and R. C. Sims. 1990. Evaluation of the use of prairie grasses for stimulating polycyclic aromatic hydrocarbon treatment in soil. Chemosphere. 20: 253-265.

Audus, L. J. 1949. The biological detoxication of 2:4-Dichlorophenoxyacetic acid in soil. Plant and Soil 2:31-36.

Chaudhry, G. R. and S. Chapalamadugu 1991. Biodegradation of halogenated organic compounds. Microbiol Reviews 55:59-79.

Frear, D. S., H. R. Swanson, E. R. Mansager, and R. G. Wein. 1978. Chloramben metabolism in plants: isolation and identification of glucose ester. J. Agric. Food Chem. 26: 1347-1351.

Heitzer, A., O. F. Webb, J. E. Thonnard, and G. S. Sayler. 1992. Specific and quantitative assessment of naphthalene and salicylate bioavailability by using a bioluminescent catabolic reporter bacterium. App. and Env. Microbiol. 58: 1839-1846.

Hsu T.S. and R. Bartha. 1979. Accelerated mineralization of two organophosphate insecticides in the rhizosphere. App. and Env. Microbiol. 37: 36-41.

Krueger J.P., R.G. Butz, and D.J. Cork. 1991. Use of dicamba-degrading microorganisms to protect dicamba susceptible plant species. J. Agric. Food Chem. 39: 1000 - 1003.

Reddy B. B. and N Sethunathan. 1983. Mineralization of parathion in the rice rhizosphere. App and Env. Microbiol. 1983. 45: 826-829.

Rochkind-Dubinsky M. L., Sayler G. S., Blackburn J W. 1987. Microbiological decomposition of chlorinated aromatic compounds. Marcel Decker, NY.

Shaw, J.J., F. Dane, D. Geiger, and J.W. Kloepper. 1992. Use of bioluminescence for detection of genetically engineered microorganisms released into the environment. App. and Env. Microbiol. 58:267-273.

Walton, B. T. and T. A. Anderson. 1990. Microbial degradation of trichloroethylene in the rhizosphere: potential application to biological remediation of waste sites. App. and Env. Microbiol. 56: 1012-1016.

Publications and Reports

As of this first annual report, we have not yet generated any formal publications. However, I believe we have made considerable progress in achieving our first year objectives and that solid publications in refereed journals will be forthcoming. The first year has involved much preliminary startup work including method optimization for soil extractions and detection techniques, the isolation of microbial consortia from enrichment cultures, testing of phytotoxicity and plant culture methods, and initial trials to test the general validity of our hypotheses. During the second year, we will continue to pursue the most productive avenues identified during the first year and will carry out a series of detailed, replicated experiments necessary for high quality research publications. I also anticipate that we will present the results of this research at an appropriate national scientific meeting to be decided upon in the near future.

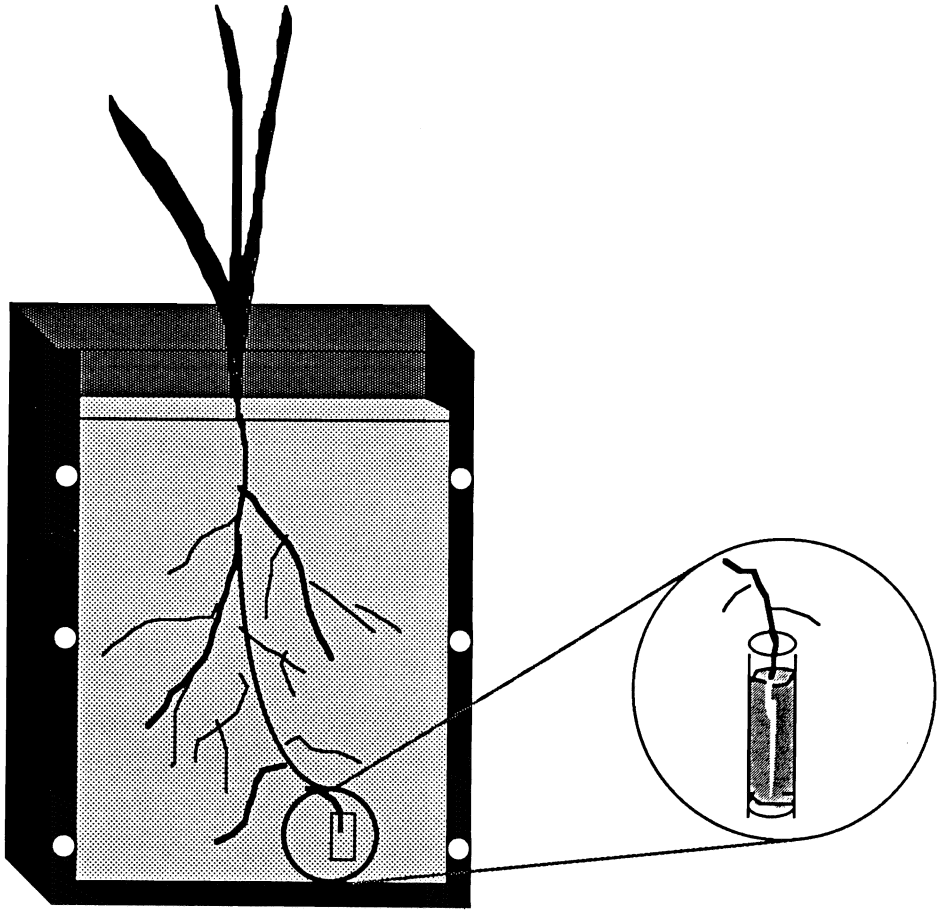

Figure 1. Root boxes employing removable side and rhizotubes for examination of microsite effects on the degradation or disappearance of chlorinated hydrocarbons.

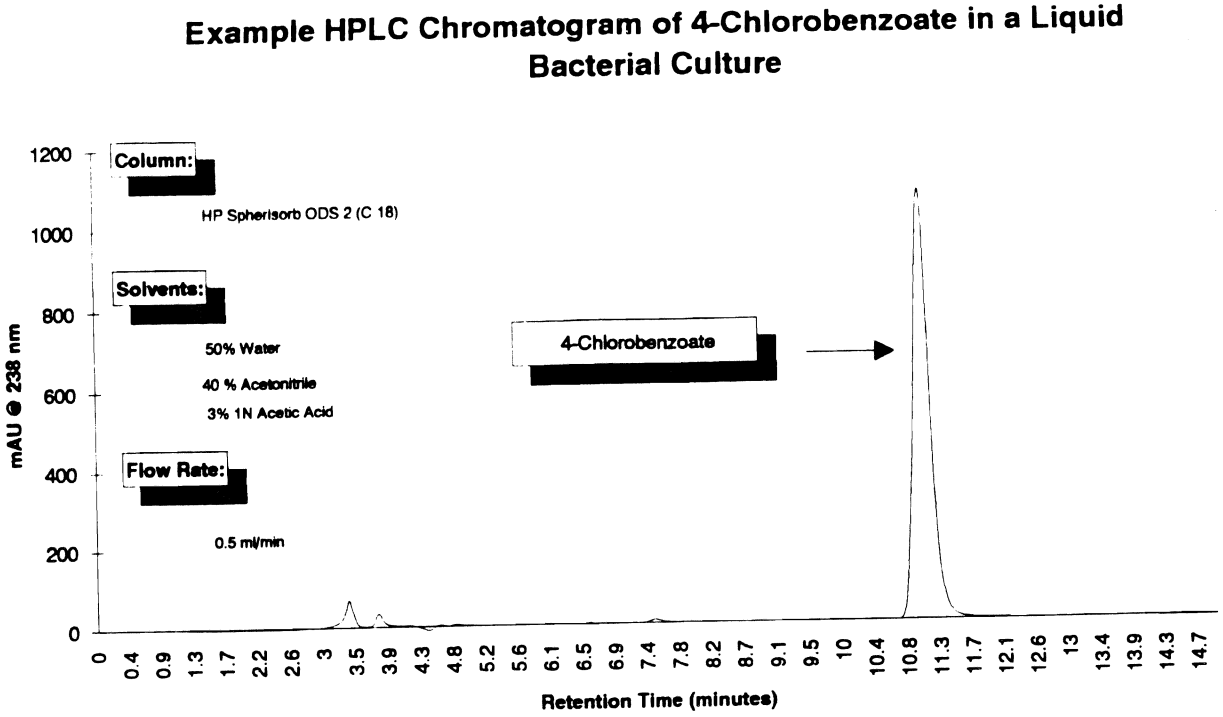

Figure 2. HPLC chromatogram of 4-chlorobenzoate sampled from a liquid bacterial culture.

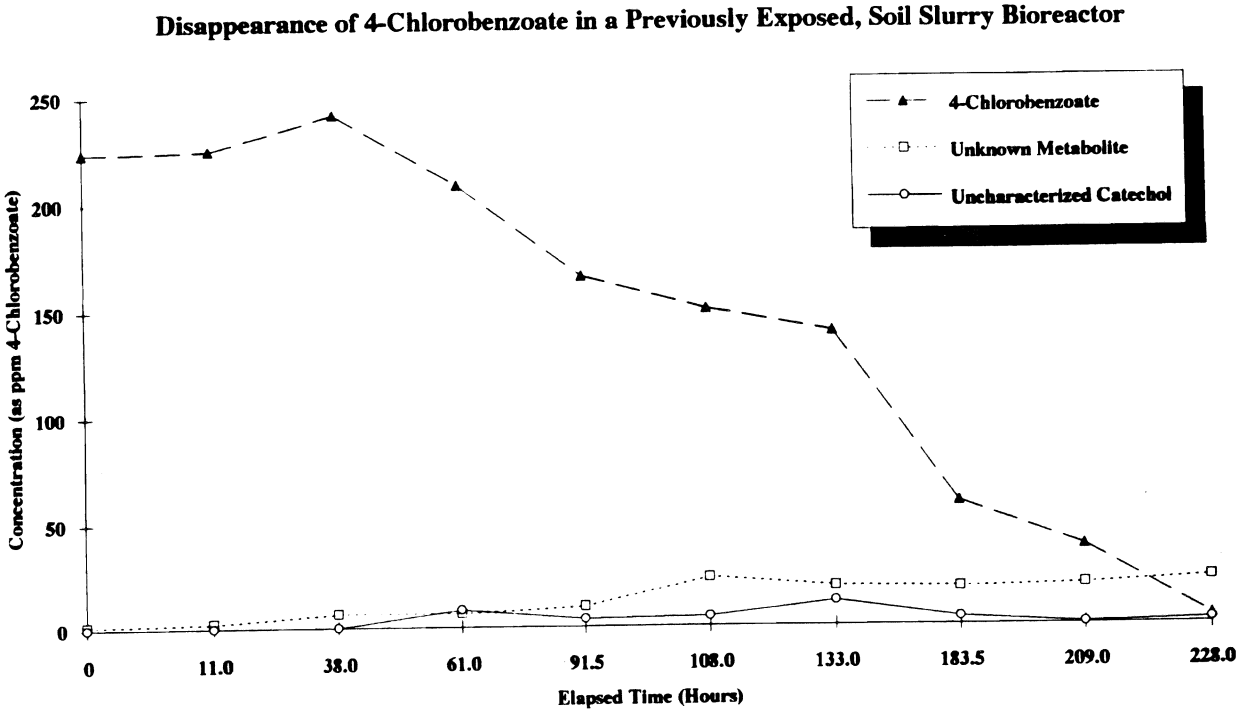

Figure 3. Enrichment culture of a 4-chlorobenzoate degrader population from rhizosphere soil of ryegrass.

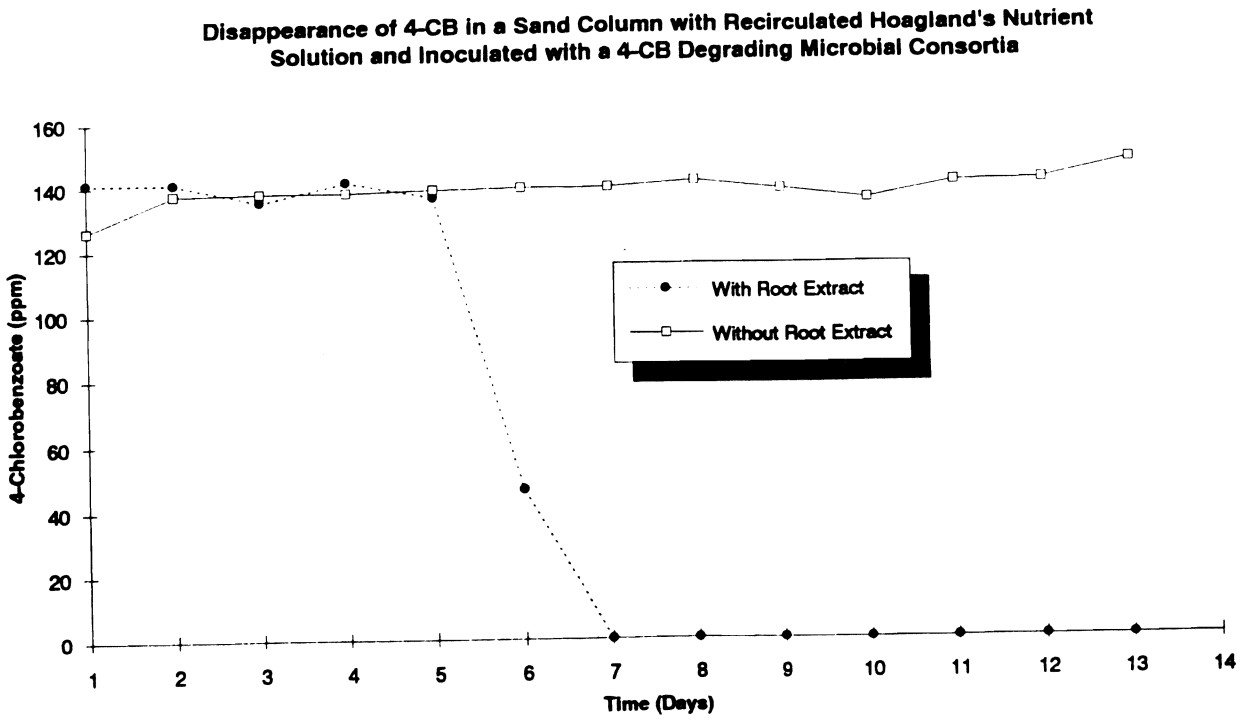

Figure 4. Disappearance of 4-CB in a sand column with recirculated Hoagland's nutrient solution and inoculated with a 4-CB degrading microbial consortia.

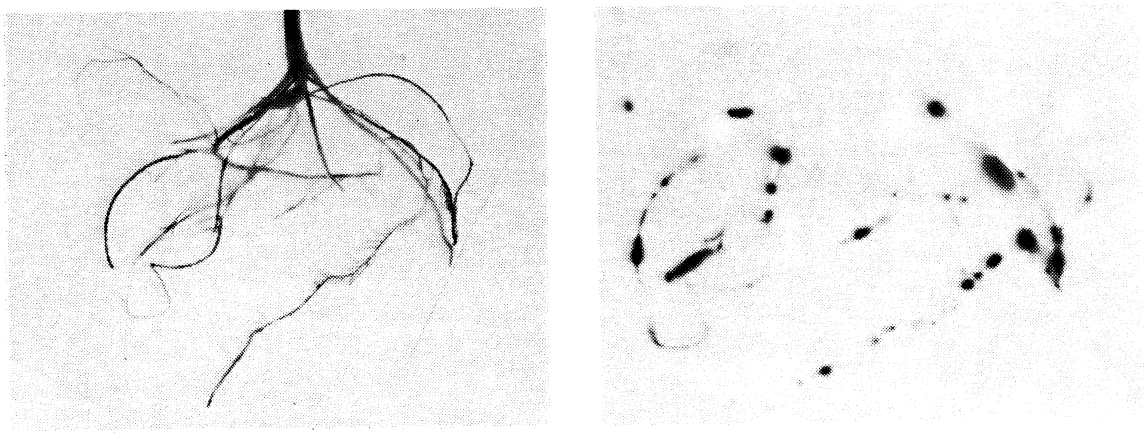

Figure 5. Autoradiography of corn roots inoculated with *Pseudomonas fluorescens* containing a bioluminescence reporter gene. Left side: corn roots. Right side: autoradiograph showing zones of exponential growth of the bacterium on the root surface.

Mechanisms of Chromium Redox Reactions and Transformations in Rhizosphere and Bulk Soil

ROBERT J. ZASOSKI AND RICHARD G. BURAU
Department of Land, Air and Water Resources, Davis Campus

Summary

This two-year study is developing information on the reactivity and cycling of chromium (Cr) in conditions reflective of bulk soil and the near-root environment that will be useful in modeling the fate, transport, and remediation of high Cr areas in California and elsewhere. Mechanisms controlling Cr conversion between the immobile Cr(III) and the more mobile and toxic Cr(VI) are being investigated. The oxidation of Cr(III) by manganese (Mn) oxides, the only known oxidant of Cr(III) in soils with pH levels <9.0, is being studied in the first phase of this research project to determine the mechanism of the oxidation process. The current literature does not appear to resolve the mechanism for Cr oxidation by Mn-oxides. In the second phase, the influence of root-related organic compounds that can reduce and chelate Cr and Mn will be investigated. In the third phase, rhizosphere soil will be used to test the conclusions derived from phases one and two. This research project will lead to a better understanding of the mechanisms of Cr(III) oxidation and Cr(VI) reduction in the rhizosphere and bulk soils and will generate parameters useful for the modeling of Cr transport in soils. In light of the numerous areas in California where Cr is elevated and the importance of these areas to watersheds draining into the Central Valley, this information will be timely and critical. Mechanistic details of Cr transformations will also be useful in remediation of contaminated sites and in examining Cr availability to plants.

Three different manganese (Mn) oxides - birnessite, pyrolusite and hausmannite - were synthesized and tested for their capacity to oxidize Cr(III) to the more mobile and toxic Cr(VI). Each oxide could oxidize Cr(III). However, the response to Cr concentration and pH were different for each oxide. Characterization of the oxides found large differences in crystallinity, zero point of charge, surface area and Mn(III) content. The Mn(III) content was qualitatively related to oxidation capacity. A surface nucleation of $Cr(OH)_3$ could explain the reduced oxidation at higher pH for birnessite (δ -MnO_2). Pyrolusite (β-MnO_2) exhibited an increased oxidation capacity as pH increased. The hydrogen dependence of the proposed reaction is consistent with greater oxidation at higher pH. The data are also consistent with the suggestion that the product (CrO_4) is inhibiting the reaction. The lower oxide (hausmannite) contains Mn(III) and had a large oxidation capacity for Cr(III). The details of the mechanism are still under investigation and surface analyses are scheduled for next year. It has been shown that commonly occurring soil Mn-oxides can oxidize Cr(III) to the more mobile and toxic Cr(VI) which would be available for plant uptake or transport in the soil.

Key Words: Hausmannite, pyrolusite, birnessite, manganese oxides, pH, oxidation, Cr(III), chromate.

Project Objectives Addressed in 1991-92

The objective of this project is to define the mechanisms controlling Cr conversion between the immobile Cr(III) and the more mobile and toxic Cr(VI) in the near-root environment and bulk soils. Since Mn-oxides are the only compounds known to oxidize Cr(III) in soils, the first phase of the project examined Cr(III) interactions with Mn-oxides. In this initial year of the project, various Mn-oxides were synthesized and characterized and their ability to oxidize Cr(III) was addressed.

Research Plan and Procedures

To determine the mechanism of Cr(III) oxidation by Mn-oxides, the oxidation process was investigated using three different Mn-oxides - birnessite ($MnO_{1.96}$), pyrolusite (MnO_2), and hausmannite (Mn_3O_4).

Preparation of Mn-oxides

Birnessite was prepared by adding HCl to an excess of $KMnO_4$ as described by Buser et al. (1954). The resulting oxide was washed with deionized water and 0.5 *N* $HClO_4$ alternatively until the residual K content was less than 1 % and then dried at 40°C, and ground to passed through an 80-mesh sieve.

Pyrolusite (β-MnO_2) can be purchased as reagent grade manganese dioxide. The 0.106-0.150 mm size fraction was washed repeatedly in deionized water, leached in a 10% HCl solution for 30 min and again repeatedly rinsed in deionized water, and dried at 60°C.

A suspension of hausmannite was prepared by adding 0.5 *N* NaOH to a stirred 0.05 *M* $MnSO_4$ solution which was maintained at 25°C while being flushed with CO_2-free air (Lind, 1988). A Radiometer pH-stat controlled the micro-drop addition of NaOH at a rate that kept the pH at 8.5. The resulting solid phase was washed with deionized water. Because of the rapid oxidation of hausmannite, a fresh suspension was used in the equilibrium studies, and freeze-dried sample was used for characterization.

Characterization of the prepared Mn-oxides

To identify the prepared Mn-oxides, zero point of charge (ZPC), O/Mn ratio, and surface area were measured using a salt titration method (Sakurai et al., 1988), the iodometric method (Murray et al., 1984), and the ethylene glycol monoethyl ether method (Carter et al., 1986), respectively. Transmission electron micrographs and X-ray diffractograms were obtained for each oxide.

Cr(III) oxidation study

The ability of Mn-oxides to oxidize Cr(III) was examined using a batch method to obtain steady-state data. Mn-oxides were placed in 50-ml polyethylene tubes to yield an initial solid surface area to solution volume ratio of 25 m^2 L^{-1}. The supporting electrolyte was 0.001*N* $NaNO_3$. Solution pH was adjusted to range between 3.0 and 5.0. Chromium nitrate was used as a Cr(III) source. Prior to the studies at pH 5.0, the solution was purged of CO_2 with N_2 gas. After a 24 h shaking period at 24 ± 1°C, the suspensions were filtered through a 0.45-μm pore membrane filter and the filtrates were analyzed. Chromium(VI) was determined by s-diphenylcarbazide procedure (Bartlett and James, 1979), and solution Mn was determined by atomic absorption.

Mn(III) effect on Cr(III) oxidation

Manganese(III) was leached from or loaded onto the Mn-oxides to study the effect of Mn(III) ion on the Cr(III) oxidation. In the leaching runs, Mn-oxides were shaken for 10 h at 25°C in 0.27*M* sodium pyrophosphate solution at pH 6.0. After centrifugation, absorbance of the extracts were measured at 480 nm. Absorbance at 480 nm was unique to complexes of Mn(III). Manganese (II) in the presence of sodium pyrophosphate does not absorb at 480 nm. To load Mn(III) ions onto the Mn-oxides, the Mn-oxides were suspended in 0.001*M* Mn(III) acetyl acetonate solution for 1 day and washed with 0.001*M* $NaNO_3$ solution. Chromium (III) oxidation was examined by suspensions of these Mn(III)-treated Mn-oxides.

Results

Characterization of the Mn-oxides

The zero point of charge, surface area and O/Mn ratio determined for the synthesized oxides correspond very well with published criteria of each preparation. The data are summarized in Table 1. The X-ray diffraction data (Table 2) are in good agreement with *d* spacing for those oxides found by other workers. Since the birnessite is nearly amorphous, it has fewer reflections and weak diffraction intensities. Some representative transmission electron micrographs of the oxides are presented in Figures 1-3. The birnessite sample consists of characteristic clumps or balls of needles (Figure 1). Pyrolusite (Figure 2) shows much more crystalline form than birnessite or hausmannite (Figures 1 and 3 respectively). The hausmannite samples (Figure 3) have a few needles which are characteristic of γ-MnOOH in addition to the cubic or bipyramid shape of the hausmannite matrix. In contact with oxygen, hausmannite is slowly converted to manganite (γ-MnOOH) (Lind, 1988).

The oxides prepared for use in the experimental phase of this project represent a range of oxidation states and contain varying levels of Mn(II), Mn(III), and Mn(IV). They also vary in crystallinity and charge characteristics. The high surface area and nearly amorphous nature of birnessite suggest that it

would be highly reactive. The low zero point of charge for this preparation indicates that at pH values above 2.9 the surface would be negative and capable of adsorbing Cr(III). In contrast, the zero point of charge associated with hausmannite and pyrolusite indicates a positive surface and a reduced ability to retain Cr(III) under the experimental conditions examined in this phase of the study. However, at the pH levels used, hausmannite and pyrolusite should be able to adsorb and retain CrO_4^{2-}.

Cr(III) oxidation equilibrium

The oxidation of Cr(III) by the three different forms of Mn-oxide were characterized over a range of initial Cr(III) concentrations and pH values in matrix of 0.001 and 0.1 *M* $NaNO_3$.

The equilibrium isotherms are presented in Figures 4, 5, and 6. To compare the oxidation capacity of each Mn-oxide, nearly the same surface area to solution volume ratio was used in all of the equilibrium studies. Each Mn-oxide shows different oxidation capacity. Hausmannite and birnessite oxidized much greater amounts of Cr(III) than pyrolusite. Interestingly, even though hausmannite has a lower surface area and higher ZPC than birnessite, it was capable of oxidizing more Cr(III) than the highly amorphous birnessite. Hausmannite contains a significant level of Mn(III) and is represented as $Mn^{2+}Mn_2^{3+}O_4$ or Mn_3O_4.

Solution pH had a significant effect on the Cr(III) oxidation by Mn-oxides. At low pH, birnessite and hausmannite suspensions approached their maximum potential oxidizing capacity (CrO_4^{2-} production); however, as solution pH increased, oxidation capacity gradually decreased. Chromium (III) oxidation by pyrolusite has been examined by Eary and Rai (1987) in the pH range between 3.0 and 4.7. They reported that the oxidation rate increased at lower pH. However, in this study, oxidation capacity increased as pH increased from 3 to 5.

The effect of ionic strength on the Cr(III) oxidation by pyrolusite at pH 3 and 5 is shown in Figure 7. Increased electrolyte concentration substantially increased Cr(III) oxidation in this suspension.

Mn(III) effect on the Cr(III) oxidation

In contrast to the presumably more reactive birnessite, hausmannite, which contains Mn(III), has a large capacity to oxidize Cr(III), as noted above. To examine further the effects of Mn(III) on the Cr(III) oxidation, the Mn-oxides were extracted with 0.27*M* sodium pyrophosphate at pH 6.0. This reagent is known to form stable Mn(III) complexes and it has been used to remove Mn(III) from Mn-oxides (Rophael and Boulis, 1982). Manganese extracted by pyrophosphate from the Mn-oxides is shown in Figure 8. The amount of extractable Mn was qualitatively related to the oxidation capacity of the Mn-

oxides. Hausmannite was completely dissolved by the pyrophosphate treatment and therefore could not be used as a post-pyrophosphate treatment.

The Cr(III) oxidation capacity of pyrophosphate-leached oxide was higher than the untreated oxide (Figure 9). Both birnessite (pH=4.0) and pyrolusite (pH=5.0) exhibited the same response to pyrophosphate leaching.

Manganese (III) treatment of birnessite at pH 3 and 4 had little effect on Cr(III) oxidation except at higher Cr additions where a slight depression in oxidation by Mn(III)- treatment was found (Figure 10). In the case of pyrolusite, there was a strong interaction with pH. At low pH Mn(III) treatment inhibited oxidation, while at pH 5 a stimulation of Cr oxidation was observed (Figure 11).

These studies show that the surface of Mn-oxides can be modified by treatment with pyrophosphate or Mn(III) ions. Several questions remain to be answered. These include defining the state of Mn on the oxide surface following treatment with Mn(III) or leaching with pyrophosphate. Does pyrophosphate really leach Mn(III) or does it remove other Mn forms as well? Is the Mn(III) loading treatment effective at leaving Mn(III) on the surface or does the Mn(III) undergo conversion to Mn(II) and Mn(IV)? These questions and evaluation of particle charge characteristics will be examined in the second year of this research project.

Discussion

Each Mn-oxide exhibited different oxidation capacities. Solution pH and ionic strength had significant effects on the Cr(III) oxidation capacity of the Mn-oxides. These different effects, which are dependent on the oxide characteristics and solution variables, are not easily explained.

There are a few possibilities. The pH effect on the Cr(III) oxidation in the case of birnessite may be explained by the adsorption and surface nucleation of $Cr(OH)_3$. At higher pH and Cr(III) concentration, the formation of the hydroxide would inhibit further oxidation. This explanation has been advanced previously (Fendorf and Zasoski, 1992) and these new data are consistent with this hypothesis. Fendorf et al. (in press) have provided some additional evidence for surface nucleation. Since pyrolusite has a ZPC of 7.2, it would have a positive net surface charge in the pH range of this study and the possibility of surface nucleation is reduced. If this is true, then oxidation capacity should increase with pH as was observed. Adsorption of anionic Cr(VI) species may inhibit the reaction as suggested by Eary and Rai (1987). The data for pyrolusite are consistent with this suggestion, as chromate is strongly adsorbed by pyrolusite in acidic solutions, and this adsorption increases as pH decreases (Figure 12). Therefore, the differences in Cr(III) oxidation between pyrolusite and birnessite in relation to pH can be rationalized. Hausmannite has a ZPC of 7.3 which is very close to that of pyrolusite. But, unlike pyrolusite, Cr(III) oxidation decreases as pH increases. Inhibition by adsorption of Cr(III) and nucleation of $Cr(OH)_3$ is less likely and adsorption of the product (CrO_4) is also

less likely to reduce oxidation since adsorption and oxidation capacity trends proceed in opposite directions.

The effects of Mn(III) on the process are also unclear. Qualitatively, the Mn(III) content of the oxide is related to Cr(III) oxidation capacity, but removing Mn(III) from the oxide does not consistently reduce the oxidation capacity. Rophael and Boulis (1982) suggested that the rate of Cr(III) oxidation in solution may depend on the availability of free Mn(III) ions in the oxidant solid. However, Manceau and Charlet (1992) suggested that the oxidation rate strongly depends on the structure of the oxide and that the oxidizing agent is Mn(IV) rather than Mn(III) ions. The suggested mechanism is that Cr(III) ions diffuse toward vacancies of the oxide structure where the electron transfer with the nearest Mn(IV) ions takes place and then chromate ions are released into the solution. However, this explanation is also wanting because the process is a three electron transfer. Reduction of Mn(IV) to Mn(II) only yields two electrons. It seems that Mn(III) must also be involved in the process.

Support for both possibilities can be gleaned from the present study. Manganese (III) leaching may leave vacancies on the oxide surface for Cr(III) oxidation by electron transfer with Mn(IV). Manganese (III) loading may block the vacancies on the oxide surface and inhibit the oxidation process. If the oxidation rate is dependent on the number of vacancies, as suggested by Manceau and Charlet (1992), then the oxidation should increase as the vacancies in the structure increase, and the rate of reaction should increase with time. However, this contradicts the observed oxidation capacities.

In order to understand more fully the mechanisms involved, it is necessary to know the oxidation state of surface-bound Mn on the various oxides. Surface analysis of the various preparations as well as analysis of their electrophoretic mobilities are planned for the upcoming year. At this juncture, the research has shown that a variety of Mn-oxides can oxidize Cr(III) to Cr(VI). This conversion increases the toxicity and mobility of Cr in soils. Both leaching and transport of Cr will be facilitated by this conversion. In addition, the mobility and availability to plants will be enhanced. Reduction and interaction of this oxidized Cr with bulk soil and rhizosphere soil will determine the fate of oxidized Cr. Research on this question is scheduled for upcoming phases of this project.

References

Bartlett, R.J. and B. James. 1979. Behavior of chromium in soils: III. Oxidation. J. Environ. Qual. 8:31-35.

Buser, W., P. Graf and W. Feitknecht. 1954. Beitrag zur kenntis der mangen(II)-manganit und des d -MnO_2. Helv. Chim. Acta. 37:2322-2333.

Carter, D.L., M.M Mortland, and W.D. Kemper. 1986. Specific Surface. *In* A. Klute (ed.) Methods of Soil Analysis, Part I. Agronomy 9:413-423. Am. Soc. Agron. Inc., Madison, WI.

Eary, L.E. and D. Rai. 1987. Kinetics of chromium(III) oxidation to chromium(VI) by reactions with manganese dioxide. Environ. Sci. Technol. 21:1187-1193.

Fendorf, S. and R.J. Zasoski. 1992. Chromium(III) oxidation by δ-MnO_2: 1. Characterization. Environ. Sci. and Technol. 26:79-85.

Fendorf, S.E., M. Fendorf, D.L. Sparks, and R. Gronsky. 1992. Inhibitory mechanisms of Cr(III) oxidation by δ-MnO_2. J. colloid Interface Sci. (in press)

Lind, C.J. 1988. Hausmannite (Mn_3O_4) conversion to manganite (γ-MnOOH) in dilute oxalate solution. Environ. Sci. Technol. 22:62-70.

Manceau, A. and L. Charlet. 1992. X-ray absorption spectroscopic study of the sorption of Cr(III) at the oxide-water interface: I. Molecular mechanism of Cr(III) oxidation on Mn oxides. J. Colloid Interface Sci. 148:425-442.

Murray, J.W., L.S. Balistrieri, and B. Paul. 1984. The oxidation state of manganese in marine sediments and ferromanganese nodules. Geochim. Cosmochim. Acta. 48:1237-1247.

Rophael, M.W. and S.N. Boulis. 1982. Kinetics of the oxidation of chromium(III) ions by trimanganese tetroxide and by manganese(III) oxide. Surface Technology. 16:243-248.

Sakurai, K., Y. Ohdate and K. Kyuma. 1988. Comparison of salt titration and potentiometric titration methods for the determination of zero point of charge (ZPC). Soil Sci. Plant Nutr. 34:171-182.

Table 1. Zero point of charge (ZPC), surface area and oxygen to manganese ratio of the prepared Mn-oxides.

	Birnessite	Pyrolusite	Hausmannite
ZPC	2.9	7.2	7.3
Surface area, m^2/g	263.3	5.6	30.3
O/Mn ratio	1.94	2.02	1.39

Table 2. X-ray diffraction data for the prepared Mn-oxides.

	The most intense *d* spacings, nm				
Birrnessite	0.752(100)	0.327(50)	0.247(61)		
Pyrolusite	0.312(100)	0.241(43)	0.163(39)	0.211(14)	0.156(14)
Hausmannite	0.249(100)	0.277(73)	0.154(47)	0.309(39)	0.496(37)

*Values in ( ) are relative intensities

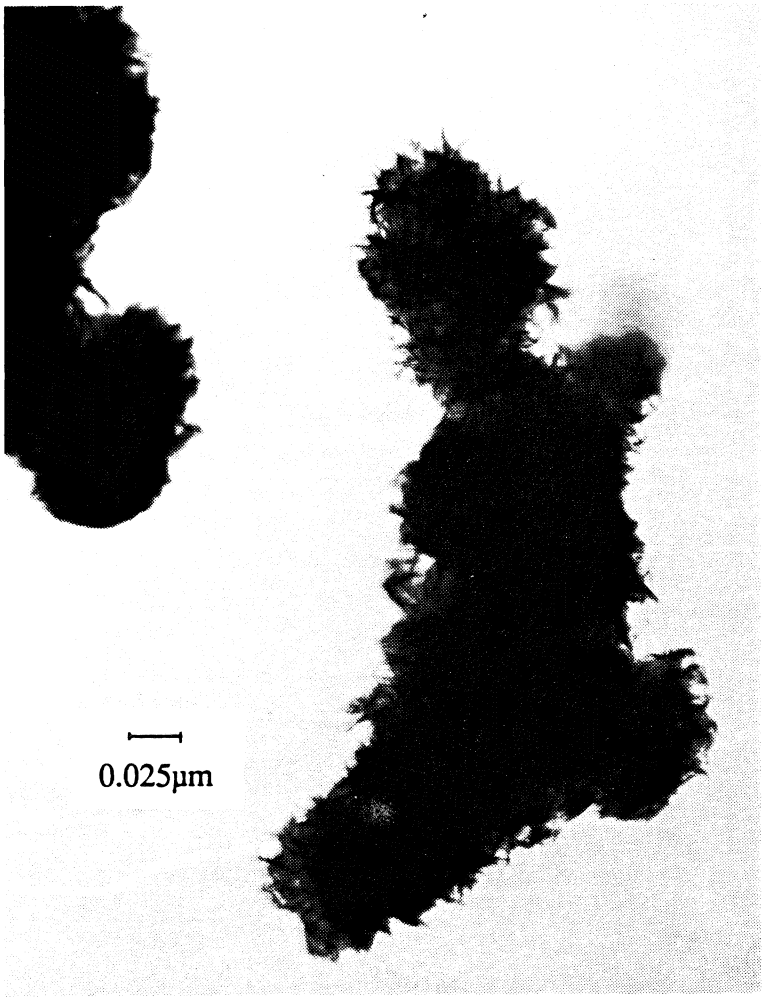

Figure 1. Transmission electron micrograph of birnessite, 280,000X

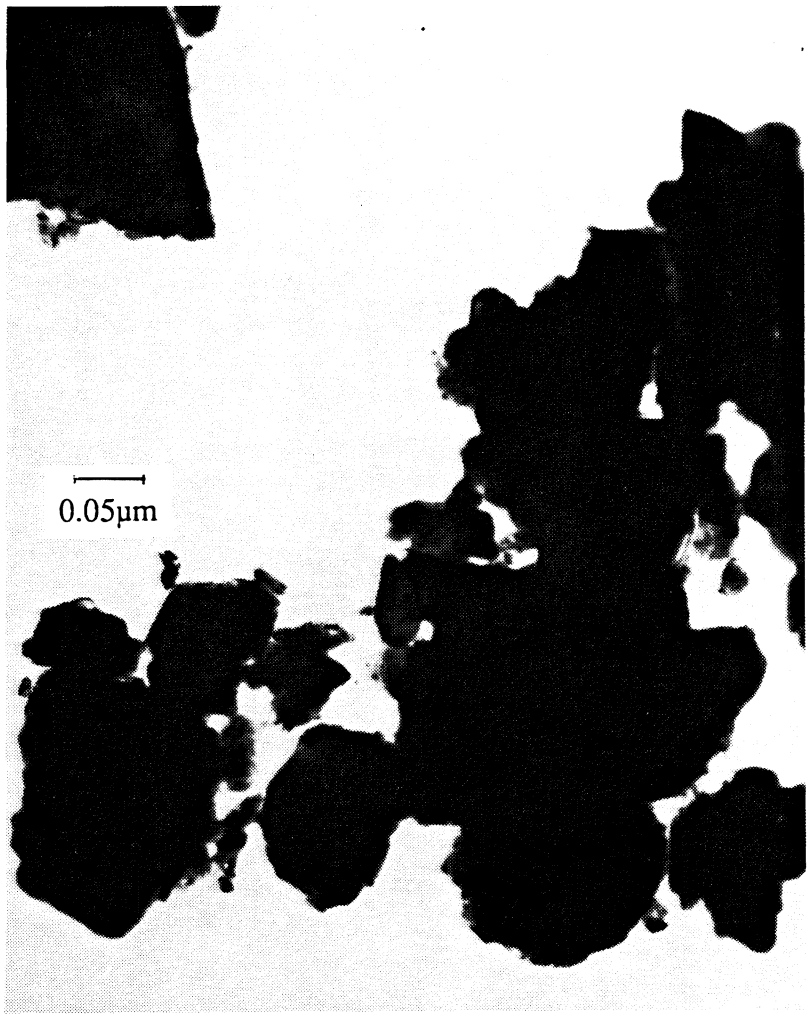

Figure 2. Transmission electron micrograph of pyrolusite, 181,400X.

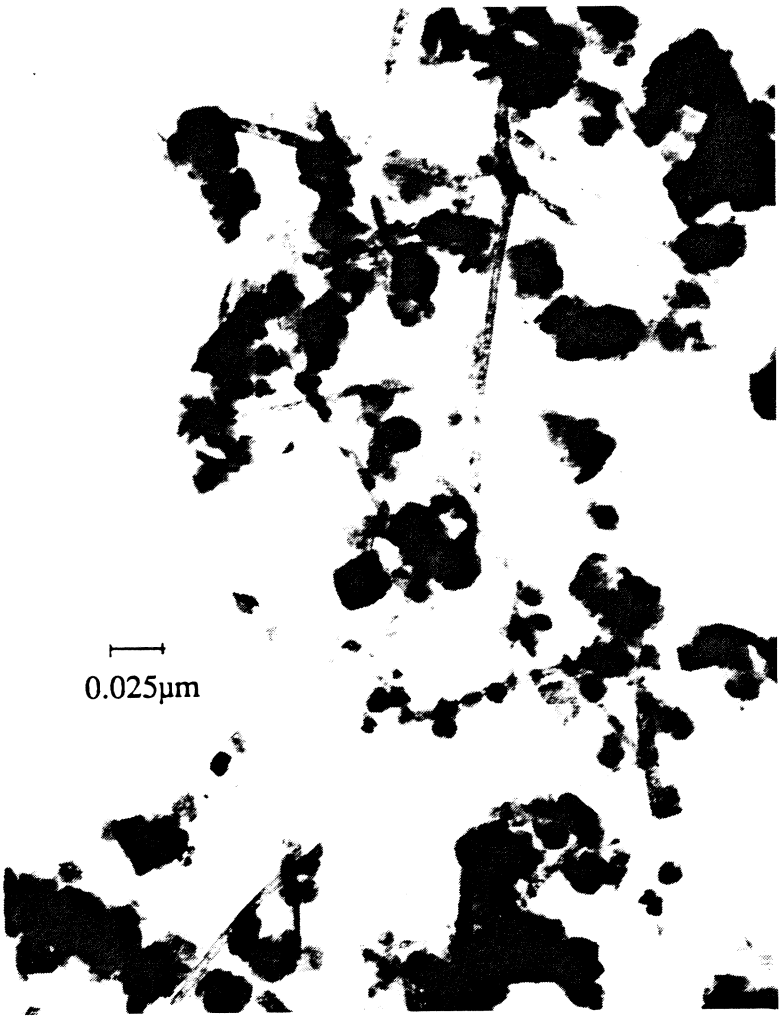

Figure 3. Transmission electron micrograph of hausmannite, 280,000X.

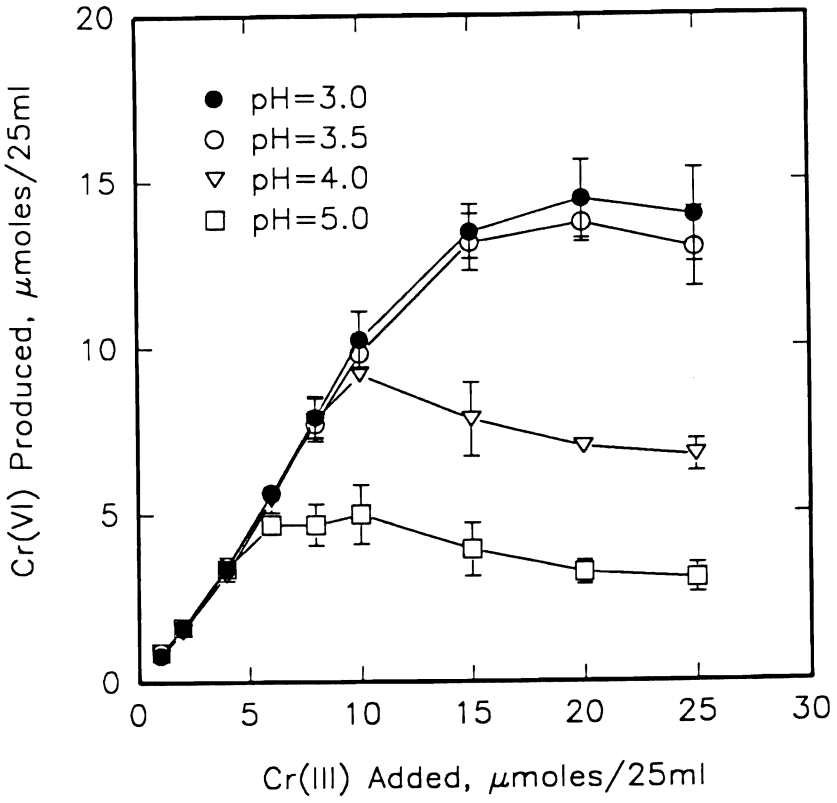

Figure 4. Cr(III) oxidation by birnessite as a function of added Cr(III) concentration and pH. Surface to solution volume ratio was equal to 25 m^2L^{-1}.

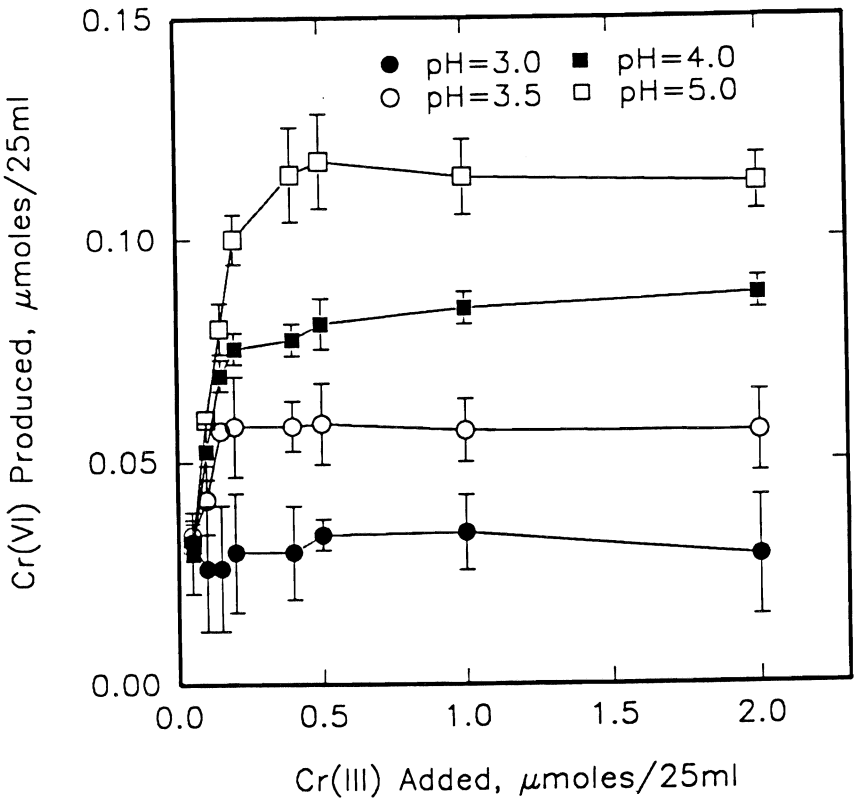

Figure 5. Cr(III) oxidation by pyrolusite as a function of added Cr(III) concentration and pH. Surface to solution volume ratio was equal to 25 m^2L^{-1}.

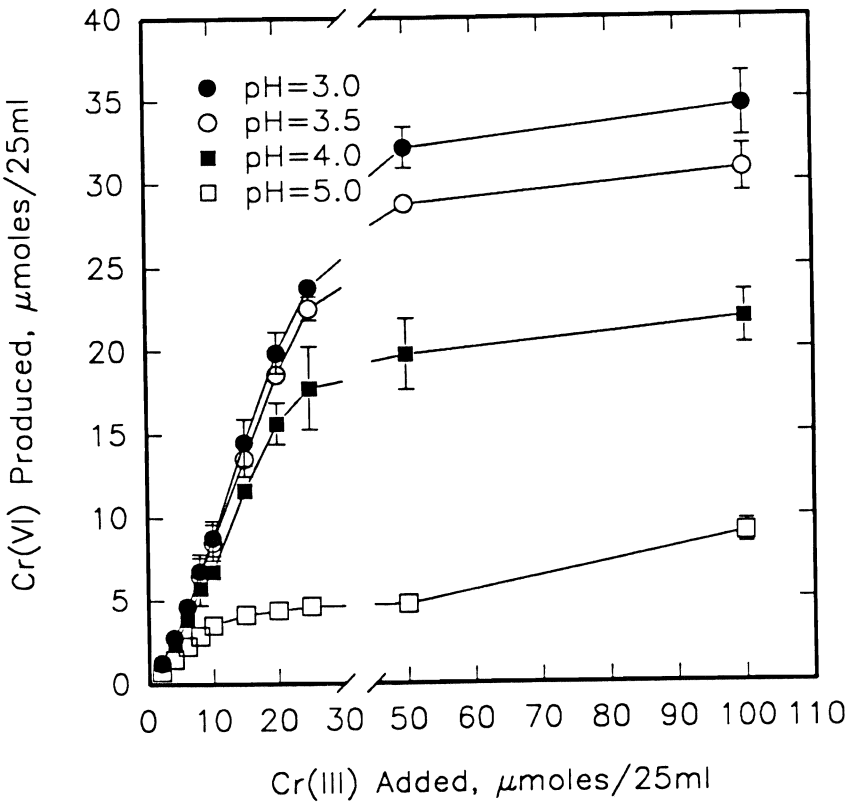

Figure 6. Cr(III) oxidation by hausmannite as a function of added Cr(III) concentration and pH. Surface to solution volume ratio was equal to 25 m^2L^{-1}.

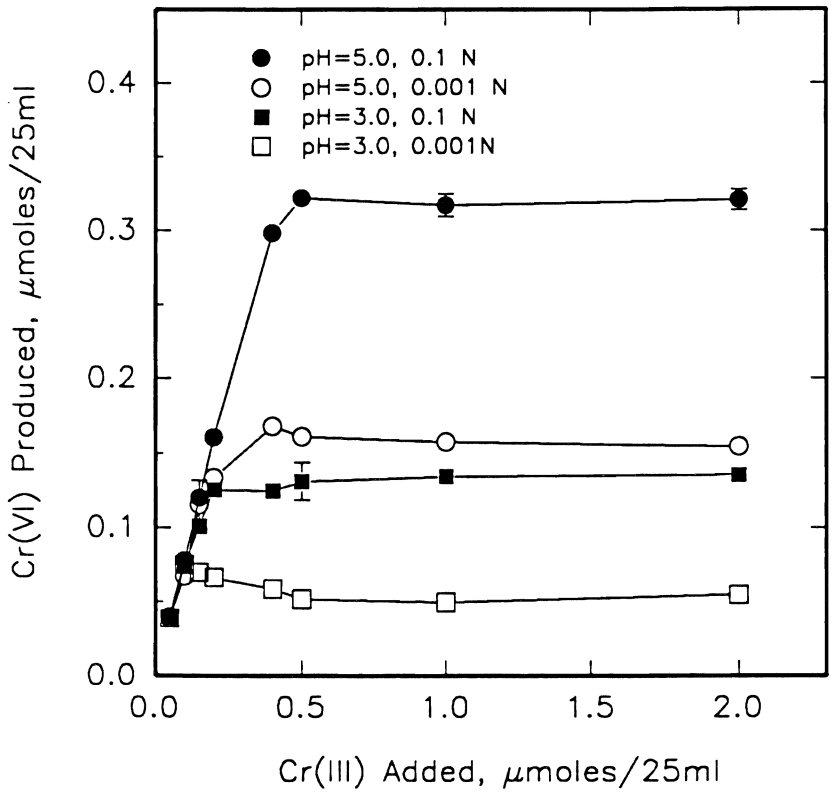

Figure 7. Ionic strength effect on Cr(III) oxidation by pyrolusite.

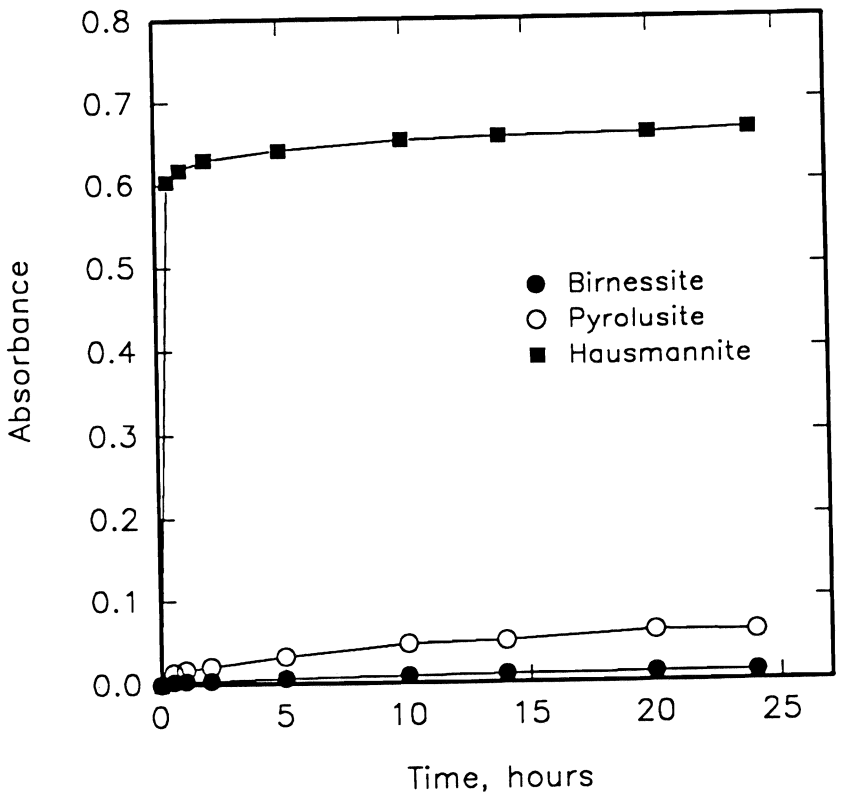

Figure 8. The rate of Mn(III) release from the Mn-oxides when reacted with 0.27 M $Na_4P_2O_7$ (pH=6.0). The solid to solution volume ratio was 250 gL^{-1} for hausmannite.

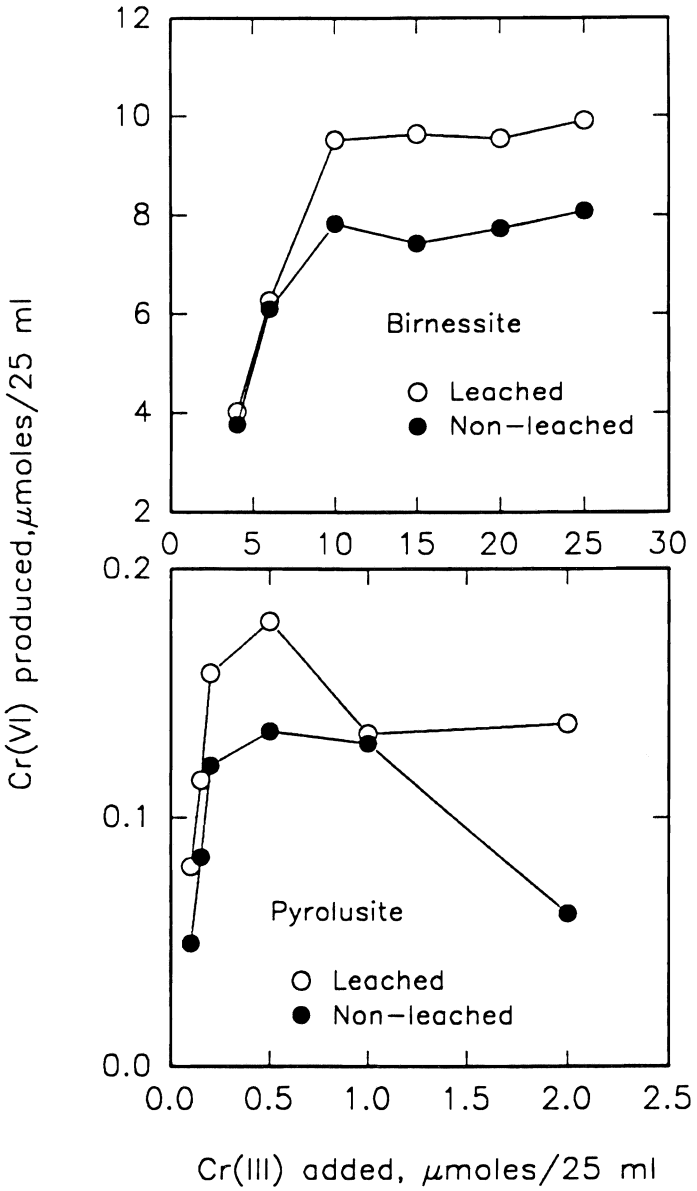

Figure 9. Effect of pyrophosphate leaching on the Cr(III) oxidation by birnessite (pH=4.0) and pyrolusite (pH=5.0)

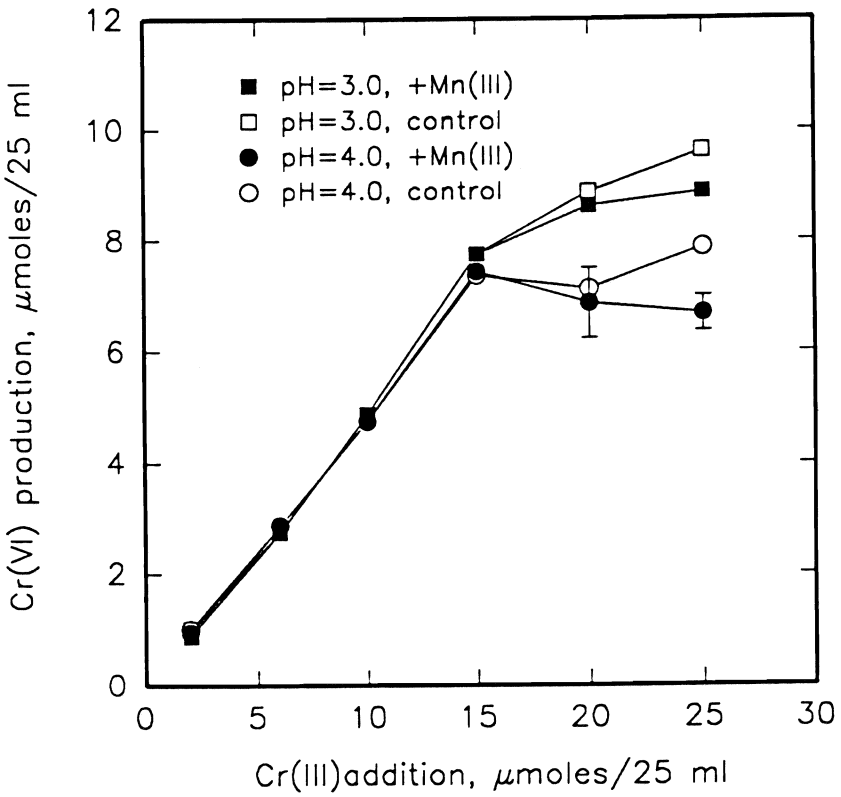

Figure 10. Effect of Mn(III) treatment on oxidation by birnessite. Surface to solution volume ratio was equal to 25 m^2L^{-1}.

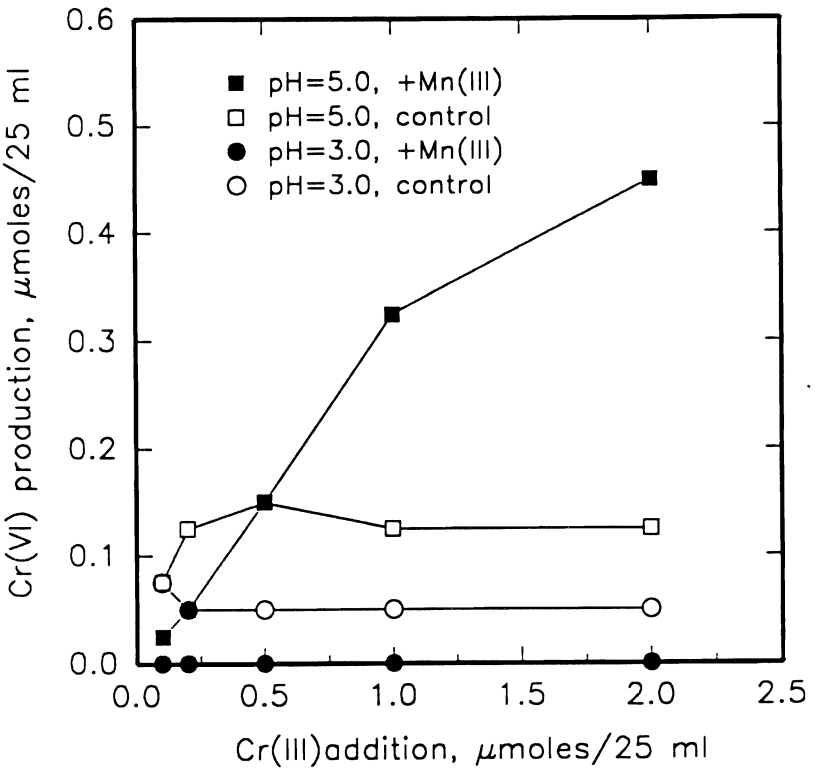

Figure 11. Effect of Mn(III) treatment on oxidation by pyrolusite. Surface to solution volume ratio was equal to 25 m^2L^{-1}.

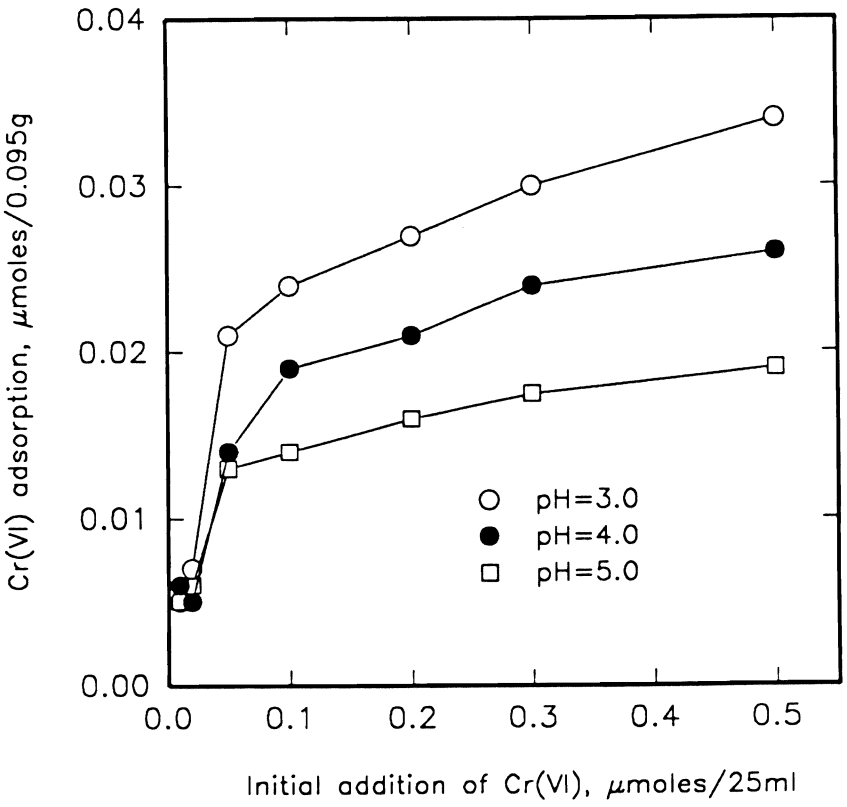

Figure 12. Cr(VI) adsorption on pyrolusite at different pH levels at 25 m^2L^{-1} surface to solution volume ratio.

Project Objectives Addressed in 1991-92

Determine the effect of organic pollutant sorption kinetics on the chemical factors that influence flocculation.

Research Plan and Procedures

A stock suspension was prepared from a Hanford sandy loam soil that was sampled from the upper 0.2 m of the profile in May 1989 at the Kearney Agricultural Center. The soil sample has been stored in the laboratory in plastic-lined soil cartons since then. The stock suspension was prepared according to the procedure outlined by Sposito et al. (1990), in which the (silt + clay) size fraction is dispersed and then saturated with Na. The pH value of the resulting suspension was 8.27; its solids concentration was 158 g (clay + silt) kg^{-1}. After preparation, the soil suspension was stored in a refrigerator.

Carbon tetrachloride (CCl_4) and the herbicide picloram (4-amino-3,5,6-trichloropyridine 2-carboxylic acid) were selected as the organic chemicals for study in sorption experiments. The importance of these prototypical pollutant compounds in soil and water quality issues is well documented (Graham-Bryce, 1981; Sawhney and Brown, 1989). Quantitation of the two compounds in the sorption experiments involves liquid scintillation counting, so both were obtained in ^{14}C labelled form.

Radiolabelled CCl_4 with a reported specific activity of 4.1 mCi $mmol^{-1}$ was obtained in February 1992 from NEN Research Products. Its radiochemical purity was assessed at 99% in January 1992. The $^{14}CCl_4$ sample was received in a glass breakseal tube. The tube was placed in an acetone-CO_2 bath, and approximately 2 mL of methanol was placed above the glass seal. The seal was broken with a glass rod, and the resultant methanol-$^{14}CCl_4$ mixture was extracted with a 2.5 mL gastight syringe and an elongated needle. The stock methanol-$^{14}CCl_4$ mixture then was stored upside down and refrigerated in a glass vial with a teflon-silicon septum. A ^{14}C-labelled n-hexadecane standard (Amersham International, 99% chemical purity, 97.5% radiochemical purity) was used to measure the specific activity of the methanol-$^{14}CCl_4$ solution. This standard was added directly to 15 mL of a "scintillation cocktail" with a 10 L syringe.

A sample of radiolabelled picloram was received in April 1992 from Dow Chemical. Its radiochemical purity was reported as 99+%, and its specific activity was 35.9 mCi $mmol^{-1}$. It was diluted in 1 L Millipore™ water to provide a solution with a specific activity of 1.35×10^{-2} Ci mL^{-1}.

A method for timed $^{14}CCl_4$ sorption experiments with the Hanford soil suspension was developed, after extensive preliminary experimentation, from the methodology reported by Ball (1989). A spiking solution was prepared in a glass vial with a teflon™ septum that could be closed by a stainless steel pin.

The 5 mL spiking solution comprised the appropriate volumes of methanol-$^{14}CCl_4$ solution, unlabelled CCl_4 and Millipore™ water to give 200 mg CCl_4 L^{-1}. The reaction vessels for the sorption experiments were 10 mL glass ampules (Wheaton Scientific). Each ampule was weighed and 10.0 g soil suspension was added. A gastight syringe (Hamilton Co.) was used to add an aliquot of 5 L spiking solution below the surface of the suspension in each ampule. Precision and reproducibility were improved by fitting the syringe with a Chaney adaptor (Hamilton Co.). Immediately after addition of the spiking solution to an ampule, it was sealed with a flame-sealer (oxygen-propane) for ampules (Ampuseal, Bioscience, Inc.).

The samples were wrapped with padding and inserted into plastic centrifuge tubes. The centrifuge tubes containing the ampules then were rotated lengthwise at 1 RPM without interruption. After the sorption reaction period ended, the ampules were placed in rubber sleeves and centrifuged at 3000 RPM for 30 min. The ampule then was broken open at its collar. An aliquot of 2 g mass was removed with a gastight, 2.5-mL syringe (Hamilton Co.) and inserted below the surface of a preweighed scintillation vial containing 15 mL "scintillation cocktail." Each vial was then reweighed and allowed to stand in the dark for 30 min (or longer), until the random counts induced by light were below 2%, at which time counting commenced on a Beckman LS 9000 scintillation counter for 10 min. The time at which the ampule was removed from the centrifuge and a 2.0 mL sample introduced into the "cocktail" was considered to be the actual sampling time.

Results

A preliminary sorption experiment with $^{14}CCl_4$ was run for nine days. Samples were prepared and counted in duplicate; they included 5-mL aliquots of the spiking solution in both 10 g Millipore™ water and 10 g soil suspension. No soil suspension blanks were reacted. The results (Table 1) showed that measurable sorption of $^{14}CCl_4$ took place after a one-week period.

Discussion

Experiments planned for the upcoming year include additional measurements of CCl_4 and picloram sorption by the Hanford soil colloids. These measurements will establish sorption and desorption time scales leading to the principal experiments to be conducted to determine the flocculation behavior of organic pollutant-containing soil colloids.

References

Ball, W. P. 1989. Ph.D. Dissertation. Stanford University.

Graham-Pryce, I. J. 1981. The behavior of pesticides in soil. p. 621-670. *In* D.J. Greenland and M. H. B. Hayes (eds.). The chemistry of soil processes. John Wiley, New York.

Sawhney, B. L., and K. Brown. 1989. Reaction and movement of organic chemicals in soils. Soil Science Society of America, Madison, WI.

Sposito, G., A. Yang, and D. Heil. 1990. Colloidal properties of soil illite influencing surface crust formation. Fourth-year annual report of the 1986-91 mission. Kearney Foundation of Soil Science, University of California,Davis.pp.10-15.

TABLE 1. Results of a duplicated preliminary $^{14}CCl_4$ sorption experiment on Hanford soil colloids.

Reaction time (hr)	Adsorbate ("None" = water blank)	Counts (dpm)
2	None	794 ±39
2	Soil	788 ±22
97	None	838 ±20
97	Soil	794 ±7
118	Soil	807 ±40
187	None	796 ±01
187	Soil	776 ±04

Kinetics and Mechanisms of Degradation of Herbicides in California Forest Soils

JOHN G. MCCOLL
Department of Soil Science, Berkeley Campus

Summary

The sorption of herbicides and other xenobiotics in soils has been attributed to partitioning into organic matter or sorption onto clay mineral surfaces (e.g. Rao and Davidson, 1982). The increased use of herbicides in forests and the paucity of research on the adsorptive and degradative properties of clay minerals common to California forest soils point to a problem area addressed in this study. In temperate forest soils, such as those in California, organic matter is concentrated in the litter layer on the soil surface. Managed forest soils can have very low concentrations of organic matter because certain management practices, such as burning of slash after clear-cutting, result in removal of the litter layer, which drastically changes the sorptive properties of these soils.

Many hydrologic models use the octanol-water partitioning coefficient and K_d values (for clay minerals) to predict herbicide movement. Forest soils have very low concentrations of 2:1 clay minerals. Due to the low concentrations of clay minerals and the low concentrations of organic matter in forest soils, hydrologic models used to predict the fate and movement of herbicides to groundwater could fail to predict how rapidly an organic contaminant might move through forest soils.

This study attempts to determine how important the sesquioxide fraction of forest soils is in the adsorpiton of commonly used herbicides with differing chemical properties. Next to organic matter, sesquioxides are considered the most sorptive and reactive fraction in forest soils. We examined this hypothesis using forest soils and synthetic clay minerals with two of four chosen herbicides, atrazine and picloram. Adsorption isotherms at pH 4 to 7 were used to determine how well ferrihydrite and birnessite adsorbed the two herbicides. Greatest atrazine adsorption occurred at pH 6 on ferrihydrite, and pH 4 on birnessite, and birnessite was found to be the most absorbent mineral (0.04 versus 0.18 mmol kg^{-1}). Ferrihydrite adsorbed picloram at higher levels than atrazine with both maxima occurring at pH 4 to 5. Ferrihydrite adsorbed dramatically higher amounts of picloram than birnessite (1.32 and 0.08 mmol kg^{-1}). This higher adsorption can be attributed to the carboxylic acid group on picloram which is capable of forming complexes with the surface of ferrihydrite, and not with the more lewis acid surface, birnessite.

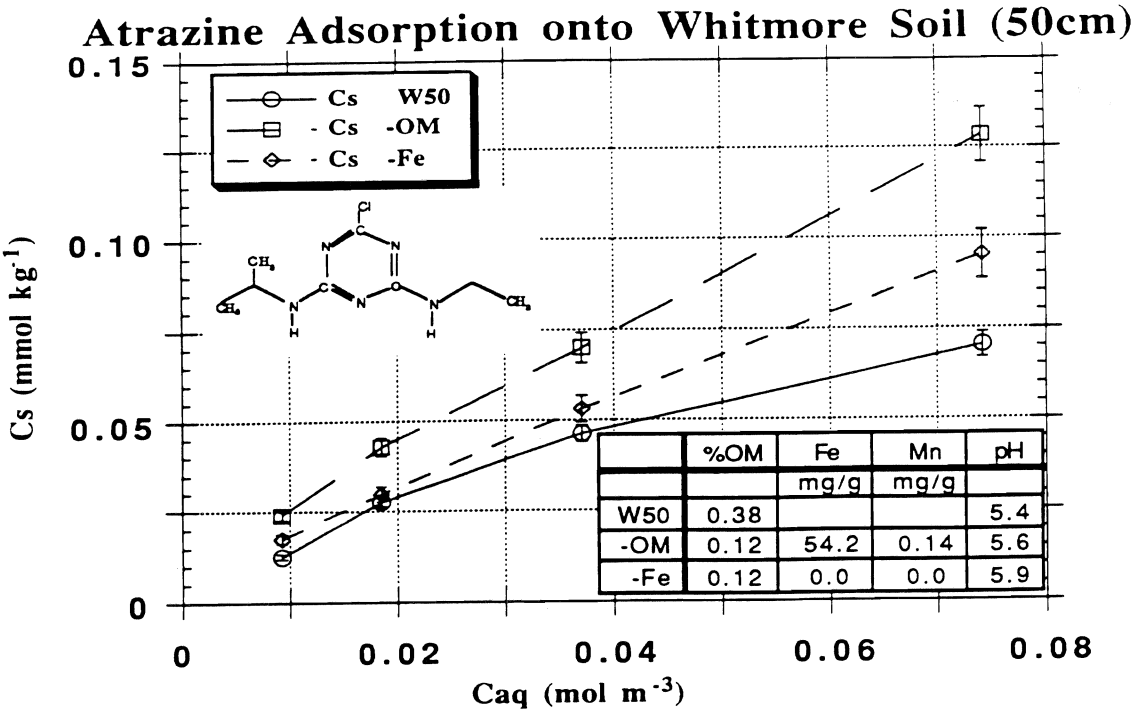

Figure 5: Sorption of atrazine onto a Whitmore soil B horizon (depth 50cm); whole soil (W50), organic matter removed (-OM), -OM and sesquioxides removed (-Fe).

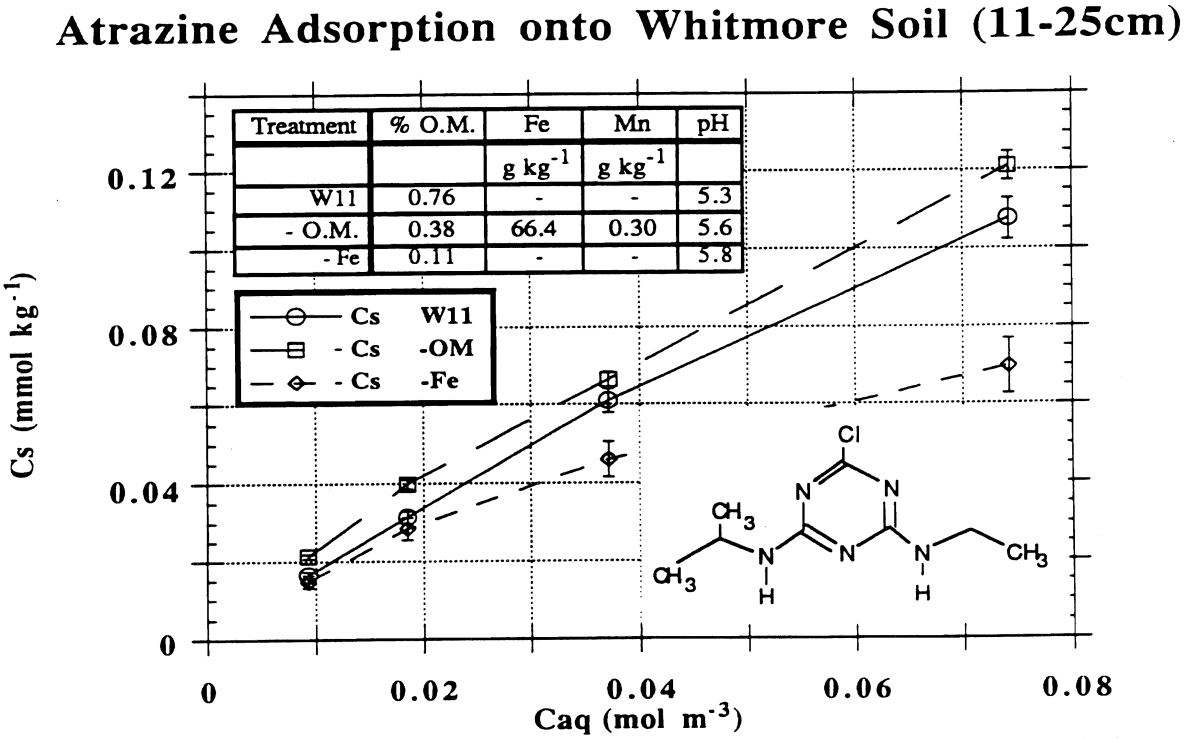

Figure 6: Sorption of atrazine onto a Whitmore soil B horizon (depth 11-25cm); whole soil (W11), organic matter removed (-OM), -OM and sesquioxides removed (-Fe).

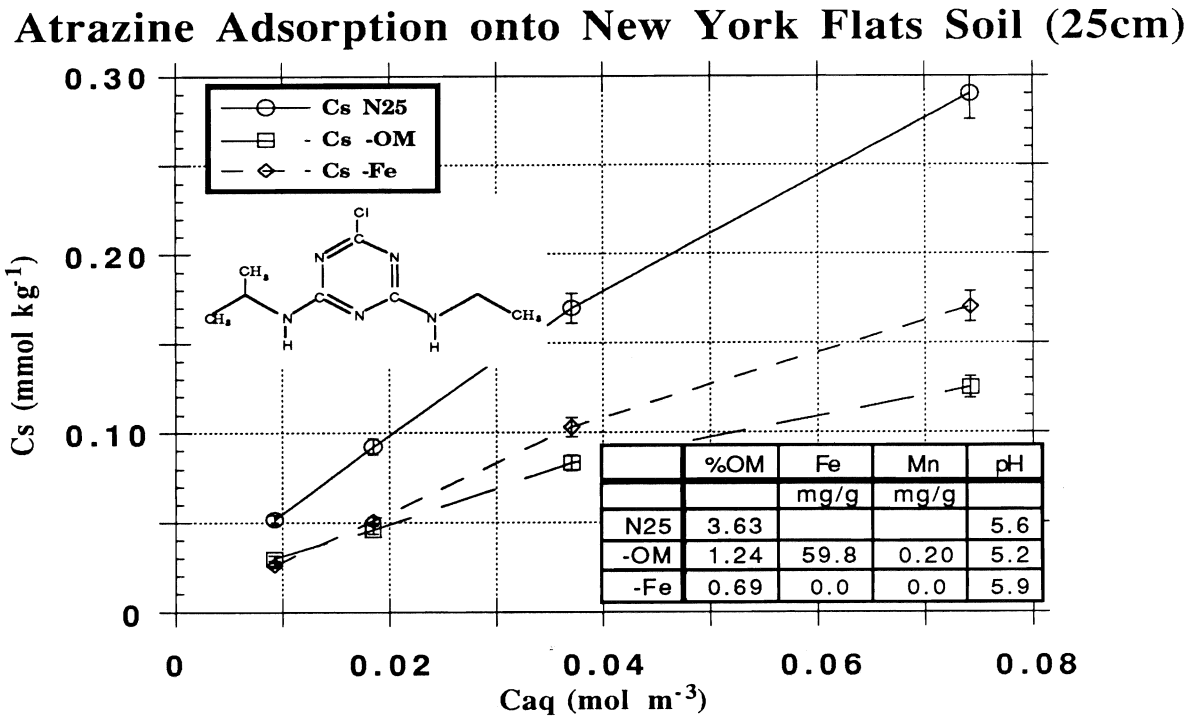

Figure 7: Sorption of atrazine onto a New York Flats soil B horizon (depth 25cm); whole soil (N25), organic matter removed (-OM), -OM and sesquioxides removed (-Fe).

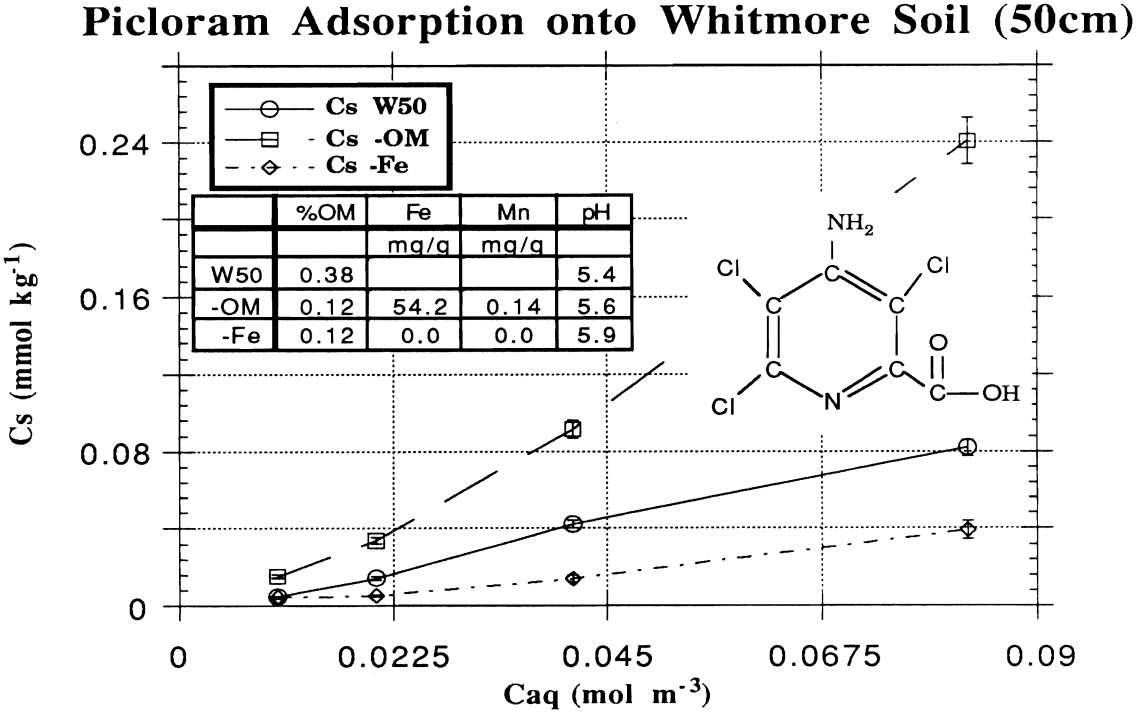

Figure 8: Sorption of picloram onto a Whitmore soil B horizon (depth 50cm); whole soil (W50), organic matter removed (-OM), -OM and sesquioxides removed (-Fe).

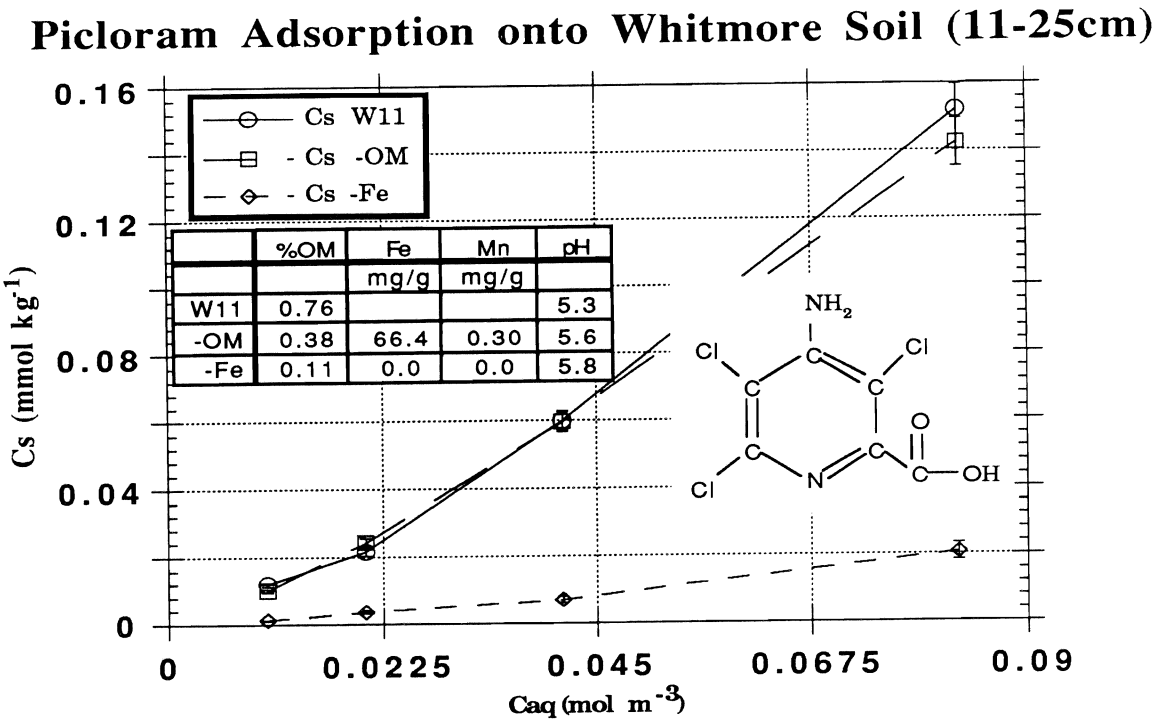

Figure 9: Sorption of picloram onto a Whitmore soil B horizon (depth 11-25cm); whole soil (W11), organic matter removed (-OM), -OM and sesquioxides (-Fe).

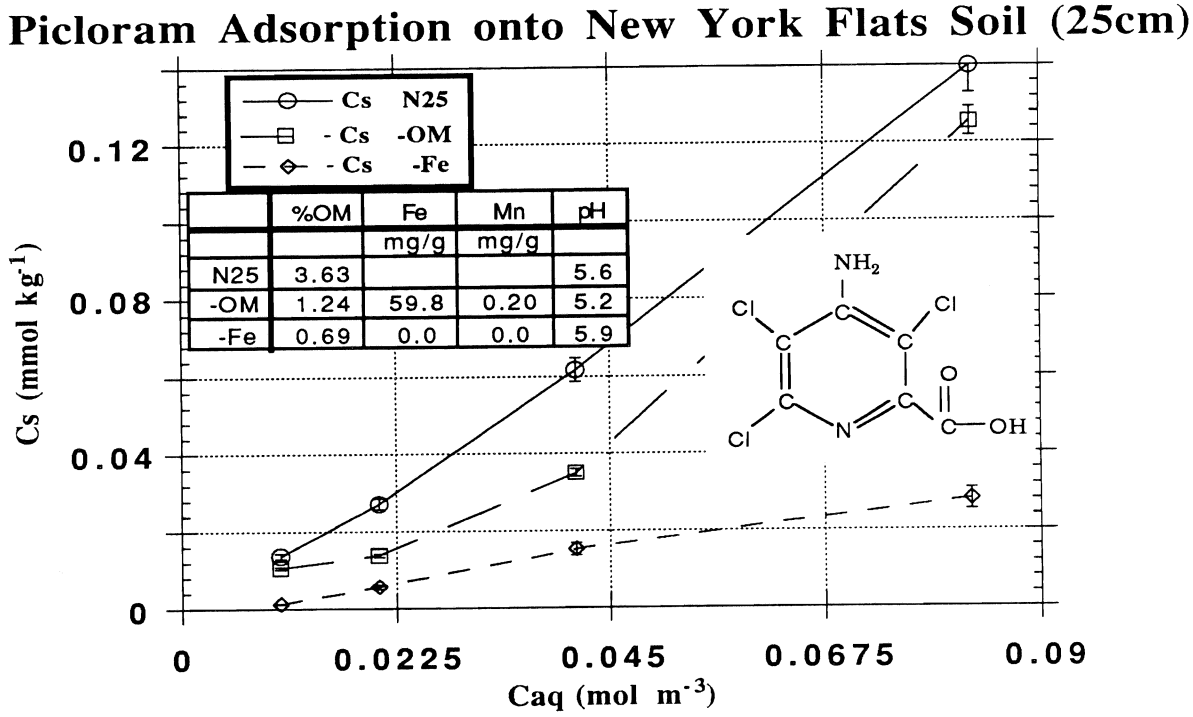

Figure 10: Sorption of picloram onto a New York Flats soil B horizon (depth 25cm); whole soil (N25),organic matter removed (-OM), -OM and sesquioxides removed (-Fe).

Pesticide Transport Via a Soil Particle Carrier Mechanism and Interactions with Polymers

JOHN LETEY AND WALTER J. FARMER
Department of Soil and Environmental Sciences, Riverside Campus

Summary

Developing management practices to mitigate water pollution requires a complete understanding of transport mechanisms whereby pesticides may be transported to non-target destinations. A majority of the research on pesticide transport through soil has focused on understanding transport in solution with appropriate consideration of adsorption, diffusion, and dispersion. Comparatively little research has been directed toward identifying the importance of pesticide transport on a carrier. This two-year investigation focuses on identifying the conditions under which transport on mineral particle carriers through the vadose zone or in furrow runoff become significant. High molecular weight polymers, frequently added to soils to promote soil aggregation through their effects on soil dispersion, flocculation, and aggregate stability, may also affect pesticide transport in solution or on a carrier. High molecular weight polymers may significantly alter pesticide sorption-desorption interactions with soil, increasing or decreasing the pollution potential of a pesticide for entering surface waters or groundwater.

The objectives of this two-year research project are as follows: (1) evaluate the migration of pesticide through soil via a clay carrier mechanism for various soil characteristics and water quality; (2) investigate the interactions between polymers and pesticides on adsorption behavior and particulate transport and the implications of these interactions on pesticide mobility in soil; and (3) evaluate the surface transport of pesticides via particulate movement in furrow irrigation with and without polymer treatment.

In the first year of the study, objective two, listed above, was addressed. Several polymers were used to investigate their effects on the sorption of two carbon-14 labeled herbicides, nonionic napropamide and anionic picloram, by an Arlington sandy loam and a Tulare clay. Sorption and desorption isotherms in the presence (200 mg L^{-1}) and absence of polymers were determined by the batch equilibrium method. The sorption-desorption of napropamide was essentially unaffected by the presence of any of the polymers. Picloram soil sorption was completely inhibited by each of the cationic guars (a natural polysaccharide polymer); an anionic guar had little effect on the sorption or desorption of picloram. Several polyacrylamide-based polymers (PAM), both anionic and cationic, reduced picloram sorption by soil. Pretreatment drying of either soil with 800 mg kg^{-1} of anionic PAM did not affect the sorption of napropamide. Also, pretreatment drying of the Arlington soil with 400 mg kg^{-1} of

anionic PAM on cationic guar did not affect the sorption of picloram. In the case of picloram sorption, solution phase interactions between picloram and certain of the polymers appear to enhance the solution phase concentration of picloram, thus decreasing sorption by soil.

Key Words: sorption-desorption, isotherms, napropamide, picloram, polyacrylamide, guar

Project Objectives Addressed in 1991-92

Investigate the interactions between polymers and pesticides on adsorption behavior and the implications of these interactions on pesticide mobility in soil.

Research Plan and Procedures

Two ^{14}C labeled herbicides, nonionic napropamide [2-(alpha-naphthoxy)-N,N-diethyl propionamide] and anionic picloram (4-amino-3,5,6-trichloropicolinic acid), were investigated in this study. The soil materials used were Arlington sandy loam (coarse-loamy, mixed Thermic Haplic Durixeralf) and Tulare clay (fine, montmorillonitic, Thermic Vertic Haplaquolls). The samples were collected from the upper 30 cm of the soil profile, air-dried, ground, and passed through a 2-mm sieve. Some of the physical and chemical characteristics of these soil samples are given in Table 1. The Tulare clay sample was taken from a plot irrigated with high saline water, resulting in a relatively high exchangeable sodium percentage (ESP) and electrical conductivity (EC) in the saturation extract. Six polymers used in the study were provided by Rhone-Poulenc (Louisville, KY). Three were PAM polymers of high molecular weight (10-15 million g mol^{-1}) with substitution of NH_2 by OH at 2 (2J), 21 (21J), and 40% (40J) to create various magnitudes of negative charge. The other three polymers, known as guar, were derivatized natural polysaccharides of lower molecular weight (0.2-2 million g mol^{-1}) than PAM. The guar compounds were higher charged cationic (T-4141), lower charged cationic (CP-14), and anionic (T-4246). Four other polymers were provided by Allied Colloids (Suffolk, VA). One of these polymers was identified as Percol 333, a very high molecular weight nonionic PAM. The other three were copolymers of quatenary acrylate salt and acrylamide of high molecular weight. Percol 747 had medium cationic charge density; Percol 763 had high cationic charge density; and Percol 757 had very high cationic charge density.

Sorption and desorption isotherms of napropamide were measured on the two soil materials. The residual water content in the air-dried soil was determined and samples equivalent to 10 g of oven-dried material were placed in a 20-ml solution of carbon-14 labeled napropamide in 50-ml Teflon-coated stainless steel tubes. Napropamide concentrations of 1, 5, 10, 20 and 40 mg L^{-1} in distilled water were used. The tubes were capped and mounted on a reciprocating shaker in a constant-temperature 25°C incubator for 24 h. The samples were then centrifuged at 12,000 rpm for 20 min at a constant temperature of 25°C. One ml of the clear supernatant solution was transferred into a 20-ml scintillation vial containing 10 ml of scintillation cocktail (Budget Solve product by Research Product Corp., Prospect, IL). The ^{14}C activity was determined using a soft Beta counting spectrometer (Beckman LS5000 TD liquid scintillation system, Beckman Instruments, Inc., Fullerton, CA). The amount sorbed was calculated from the differences between the readings of the standard (blank not exposed to soil) and the reading of the solution after exposure to the soil. A desorption isotherm was measured by removing one-half of the supernatant solution and replacing it with distilled water. The soil

and solution were mixed and shaken for 24 h, after which the ^{14}C concentration was measured in the equilibrium solution.

The above-stated procedures were repeated for both soils, except that napropamide was mixed with distilled water containing 200 mg L^{-1} of anionic PAM polymer (21J). In a third study, napropamide was dissolved in a solution of 0.005 M $CaCl_2$ solution and the sorption-desorption curves were measured only on the Arlington soil.

In other studies, only one point on the sorption-desorption curve was measured. In one set of measurements, sorption and desorption of napropamide from a solution containing 40 mg L^{-1} of napropamide and 200 mg L^{-1} of either 2J, 40J, T-4246, T-4141, or CP-14 was done on Arlington soil. In another case, the two soils were treated with anionic PAM 21J at a rate of 800 mg kg^{-1} and allowed to dry. After drying, the sorption and desorption of napropamide from a 40 mg L^{-1} solution in distilled water were measured.

A series of measurements were made using anionic picloram on Arlington soil. One point on the sorption isotherm was measured using a picloram concentration of 400 mg L^{-1} incorporated with 200 mg L^{-1} of each of the 10 polymers. In another set of measurements, the Arlington soil was treated with 400 mg kg^{-1} of anionic PAM 21J and cationic guar T-4141 and dried. The sorption of picloram dissolved in distilled water at a concentration of 400 mg L^{-1} was measured on these two soils pretreated with polymers.

Measurements were made to determine whether picloram affected the adsorption of 21J and T-4141 on Arlington soil. Solutions containing 200 mg L^{-1} of tritium-labeled 21J or T-4141 with non-labeled picloram at concentrations of 0, 100, 200, and 400 mg L^{-1} were used for the adsorption measurements. Tritium-labeled polymers were obtained as described by Malik and Letey (1991).

All pesticide sorption measurements were done in duplicate and the polymer adsorption measurements were done in triplicate.

Results

The sorption-desorption isotherms for napropamide in distilled water for the two soils (Table 2) were characterized as linear, extrapolating to near the origin, with no hysteresis between sorption and desorption. The linear sorption coefficient, K_d(L kg^{-1}), values were greater for Tulare clay soil than for the Arlington sandy loam. This increased sorption of the Tulare soil is attributed to its higher organic carbon content.

The K_d values obtained from a complete isotherm of napropamide on Arlington and Tulare soil samples with various treatments are presented in Table 2. Note that neither the sorption nor desorption of napropamide on either soil is greatly affected by the electrolyte in solution, anionic PAM 21J in solution, or previous treatment of the soil with PAM 21J.

The K_d values for sorption-desorption, which were determined using only one concentration, were computed on the assumption of a linear extrapolation from the data point to the origin. The K_d values of napropamide and picloram from solutions of several polymers are presented in Table 3. The K_d value of napropamide was about the same in distilled water or when mixed with any of the polymers. There was no significant interaction between any of the polymers and napropamide on the sorption of napropamide by the Arlington soil. The K_d value for desorption was slightly higher than for sorption in the polymer solutions in each case, but the difference was not great. For napropamide there was very little, if any, interaction between the pesticide and the polymers in the soil solution system.

The sorption and desorption of the anionic picloram was affected by the presence of a polymer in solution. Indeed, the cationic guars completely prohibited the sorption of picloram by the Arlington soil. These results were confirmed by redoing the measurements eight times. The anionic guar T-4246 had almost no effect on the sorption or desorption of picloram. On the other hand, the lower charged anionic PAMs, which have larger molecular weight than the guar, reduced the sorption of picloram. Increasing the negative charge density on the PAM decreased the effect.

Thus the picloram molecule interacted with the polymer molecules in a manner to affect the picloram sorption. The anionic picloram may have become electrostatically associated with cationic guar and kept completely in solution. The anionic guar would have repelled the anionic picloram and not affected its sorption. Increasing the anionic charge density of the PAM may have led to increased repulsion of the picloram, making it more available for sorption. On the other hand, there appears to have been an association between the picloram and the lower charge anionic PAM in a manner to reduce its sorption.

The one-point K_d values for picloram in Arlington soil and the high molecular weight Percol polymers are presented in Table 4. The K_d values for picloram on Arlington soil which had been pretreated with anionic PAM-21J and cationic guar T-4141 and dried are also presented in Table 4. The data for the Percol polymers are presented in the order of increasing cationic charge density. There was a consistent trend of increasing K_d with increasing cationic charge density. In all cases, however, the sorption was reduced by having the picloram associated with the polymers. The sorption from a picloram-Percol solution is inconsistent with the results with the cationic guar. In association with the cationic guars, there was no sorption of picloram. On the other hand, increasing the positive charge density of Percol increased the sorption. Pretreating the soil with polymers and drying the soil before doing the sorption experiments had very little effect on adsorption of picloram. For the cationic

guar T-4141, sorption of picloram was completely inhibited when the polymer was in solution, but when the polymer was applied to the soil and dried, there was very little, if any, effect on picloram sorption.

Since polymers are adsorbed to soils (Malik and Letey, 1991; Nadler and Letey, 1989), it would seem that if the picloram were associated with the polymer, that adsorption of the polymer should lead to some apparent adsorption of the picloram. This was not observed for the T-4141. It was hypothesized therefore that the picloram-polymer solution might alter the adsorption of the polymer. The results of adsorption of cationic guar T- 4141 and anionic PAM 21J in the presence of various picloram concentrations are presented in Table 5. There was a consistent trend of decreasing adsorption of T-4141 with increasing picloram concentration, but the magnitude was relatively small. Picloram sorption by soil in the presence of the Guar T-4141 remained at zero at all picloram concentrations. There was no consistent trend between picloram concentration and adsorption of PAM 21J. The adsorption of PAM 21J was not greatly affected by the picloram association. The mechanism by which the cationic guars completely inhibited adsorption of picloram remains unexplained. An electrostatic attraction between the polymers and picloram could have prevented the picloram association with the soil particles. But there was sorption of the polymer (Table 5); therefore, if there was any picloram associated with the polymer it should have been partially adsorbed with the polymer.

In summary, the nonionic napropamide sorption was not affected by any of the polymers; however, a slight decrease in desorption of the napropamide in the presence of the polymer (Table 3) did occur. On the other hand, the anionic picloram sorption was significantly affected by association with the polymers in solution. The polymers either had no effect on sorption or decreased sorption of picloram, in some cases completely preventing sorption. The mechanism by which the picloram and polymer interact to affect picloram sorption is not explained because of apparent inconsistencies in the results.

References

Malik, M. and J. Letey. 1991. Adsorption of polyacrylamide and polysaccharide polymers on soil materials. Soil Sci. Soc. Amer. J. 55:380-383.

Publications and Reports:

Malik, M., J. Letey and W. J. Farmer. Sorption of two pesticides as affected by polymers. (In preparation).

Table 1. Physical and chemical characteristics of the soil samples.

	Clay	Silt	Sand	CEC	ESP	EC	pH	OC
	----------%----------			mmol kg^{-1}		dS m^{-1}		g kg^{-1}
Arlington sandy loam	10	31	59	150	1.0	0.83	7.1	7.8
Tulare clay	55	38	7	315	8.0	2.8	8.1	20.9

Table 2. K_d (L kg^{-1}) of napropamide on Arlington and Tulare clay soil samples.

Treatment	Arlington soil		Tulare clay soil	
	Sorption	Desorption	Sorption	Desorption
Distilled water	2.44	2.40	12.1	11.5
0.005 M $CaCl_2$	2.44	2.36	--	--
In solution with anionic PAM 21J	2.56	2.58	11.4	11.3
Soil treated with anionic PAM 21J and dried	2.48	2.52	12.2	12.3

Note: r^2 for all cases is equal to 0.99.

Table 3. K_d (L kg^{-1}) of napropamide and picloram in equilibrium with different polymers Arlington soil.

Treatment	Napropamide		Picloram	
	Sorption	Desorption	Sorption	Desorption
Distilled water	2.41[a]	2.40[a]	0.11	0.27
Anionic PAM 2J	2.45	2.94	0.05	0.11
Anionic PAM 21J	2.56[a]	2.58[a]	0.08	0.14
Anionic PAM 40J	2.00	2.44	0.10	0.07
Anionic guar T-4246	2.46	3.04	0.12	0.27
Cationic guar CP-14	2.20	2.78	0.00	--
Cationic guar T-4141	2.28	2.70	0.00	--

[a]Complete isotherm. For all others average of 4 replicates of 40 mg L^{-1} for napropamide and 400 mg L^{-1} for picloram. Concentration of polymer is 200 mg L^{-1}.

Table 4. K_d (L kg^{-1}) of picloram in equilibrium with different polymers on Arlington soil and Arlington soil that had been pretreated with 21J and T-4141.

Treatment	K_d
Distilled water	0.11
Nonionic PAM Percol 333	0.015
Cationic acrylate-acrylamide Percol 747	0.019
Cationic acrylate-acrylamide Percol 763	0.038
Cationic acrylate-acrylamide Percol 757	0.065
21J treated soil	0.10
T-4141 treated soil	0.10

Table 5. K_d (L kg^{-1}) of cationic guar T-4141 and anionic PAM 21J as affected by different concentrations of picloram.

Picloram concentration	Cationic guar T-4141	PAM 21J
(mg L^{-1})		
0	1.10	0.91
100	1.00	0.96
200	0.96	1.01
400	0.90	0.91

Dissolution of Nonaqueous Phase Liquids in Soil

WILLIAM A. JURY, MICHAEL A. ANDERSON, AND ZBIGNIEW J. KABALA
Department of Soil & Environmental Sciences, Riverside Campus

Summary

When a nonaqueous phase liquid (NAPL) enters the soil through a leaking storage tank or waste spill, a residual portion of the mass becomes trapped in the soil or aquifer matrix. Subsequently, it acts as a source of contamination through slow dissolution of its mass into the surrounding water. This three-year research project is characterizing the dissolution process using a newly-developed modeling philosophy that allows the diffusion-limited mass transfer from the NAPL to be isolated from the transport process, thereby allowing the rate coefficient governing the transport to be measured separately. The protocol for this analysis involves adding an inert water tracer, such as Br, to characterize the water flow pathways and expressing the NAPL dissolution and movement through the soil in terms of the observed behavior of the tracer. To aid model development, a series of experiments is being conducted in which resident NAPLs (single compounds and binary mixtures) are being leached through packed columns of saturated or unsaturated soil. The shape of the initial distribution is being varied to create different interfacial surface areas between the phases, and experiments are being conducted at several flow rates, pore size distributions, and in heterogeneous as well as homogeneous soil. The goal of the study is to develop a generic description of the initial value problem, together with a characterization of the rate constant in terms of the observable properties of the medium and the NAPL. Such a model will be of great value in the design of remediation strategies and in estimation of the potential environmental impact of a spill.

First-year activities of this three-year research project included an evaluation of soil NAPL- and water-wettability through contact angle (θ) measurements. NAPL residual saturation is dependent upon a number of factors, including surface wettability. The contact angles for water in equilibrium with soil constituents exceeded 0, the value generally assumed, and ranged from 5 - 56°. Humic acid and goethite, which tend to form coatings on soil particles, both yielded contact angles for solid-water-vapor systems significantly greater than 0 (56± 1 and 24± 1°, respectively). NAPLs wetted mineral surfaces more readily than water in solid-NAPL-vapor systems (θ of 0 - 7° for benzene, toluene and PCE in equilibrium with mica, kaolinite and bentonite surfaces). Wetting properties changed substantially in solid-NAPL-water systems; however, where non-wetting behavior (θ measured through the NAPL > 90°) was observed for these NAPLs in equilibrium with biotite mica surfaces.

As vapor transport in the unsaturated zone and dissolution into soil water and ground water are additional potentially important modes of contamination, first-year activities also included an evaluation of vapor-liquid partitioning.

Equilibrium partitioning of benzene, toluene and o-xylene between vapor and water phases were significantly altered in the presence of surfactants and humic acid. The presence of surfactants was found to lower substantially equilibrium vapor concentrations relative to water at constant added chemical mass to closed vessels. A 3-phase model was developed which fits experimental vapor phase concentration data. The model assumed linear solute-surfactant partitioning with Henry's law written using derived, aquated concentrations in lieu of total liquid phase concentrations. Solute-surfactant partition coefficients were similar to octanol-water coefficients.

Key Words: surface tension, wetting properties of soil, vapor-liquid partition

Project Objectives Addressed in 1991-92

The overall objective of this project is to evaluate NAPL dissolution-mass transfer in saturated and unsaturated soils. Toward that end, research activities during this first year have focused on two topics important to NAPL residual saturation and dissolution-mass transfer: (1) an evaluation, through contact angle measurements, of the wetting properties of soil constituents in equilibrium with selected NAPLs and water, and (2) the influence of aqueous phase composition on vapor-liquid partitioning.

Research Plan and Procedures

Wetting Properties of Soil Components

Contact angles of water and selected common contaminant NAPLs in equilibrium with a number of solid phase soil components were determined using sessile drop and captive bubble techniques (Anderson, 1986; Adamson, 1990). The sessile drop method was used for solid-liquid-vapor systems, while the captive bubble technique was used for solid-liquid-liquid systems where one of the immiscible liquids was an aqueous solution containing dissolved chemical.

Briefly, the sessile drop method involves placing a drop of liquid (water or NAPL) on a flat, smooth surface. The angle formed by the liquid in equilibrium with the solid and its vapor was then measured using a telemicroscope fitted with a goniometer. The captive bubble method involved evaluating the angle formed by an NAPL in contact with a solid surface immersed in deionized water. A 100 μL syringe filled with an NAPL was fitted to a capillary tube, with the tube then immersed and carefully placed adjacent to the solid surface. A drop of NAPL was formed at the tip of the capillary tube and then brought in contact with the surface. Advancing and receding contact angles were determined by measuring the angle formed by the water as the NAPL drop size was enlarged or reduced.

Kaolinite, bentonite, goethite and solid-phase fulvic and humic acid surfaces were prepared from clay materials under 100 MPa pressure. Biotite mica was used without preparation. Wetting properties of Teflon were also evaluated.

Vapor-Liquid Partitioning

Equilibrium vapor-liquid partitioning of selected organic chemicals in the presence of humic acid and two synthetic surfactants was evaluated using closed vessel equilibrations (Lincoff and Gossett, 1984). Fifty mL of 0 to 7.5 x 10^{-2} M sodium dodecyl sulfate (SDS) or Witconol SN70 solutions, or 0 to 500 mg C/L humic acid solutions were added to 120 mL serum bottles. All solutions were prepared in 0.03 M NaCl. Seven μL of benzene, toluene, or o-xylene were injected below the water surface and the bottles rapidly sealed with aluminum crimp caps and Teflon-lined septa. It was calculated that addition of this mass of

chemical was below the solubility limit in water of all three chemicals. Equilibrations were preformed in triplicate at ambient temperature (23± 1° C). Vapor phase concentrations were determined by withdrawl of 100 L samples using a gas-tight syringe and injection into a Hewlett-Packard Model 5890 Series II gas chromatograph configured with a split/splitless injector port, a Hewlett-Packard capillary HP-5 column (cross-linked 5% Ph Me silicone; 25 m x 0.32 mm x 0.52 μm), and FID detector.

Apparent solubilities of benzene, toluene, and o-xylene in the presence of these surfactants were determined following the procedure of Chiou et al. (1986) where an excess of chemical was added to sealed vessels containing surfactant solutions. Liquid phase concentrations (i.e., apparent solubilities) were determined from sample absorbance at 254 nm using Spectronic 1001 UV/Vis spectrophotometer.

Results

Wetting Properties of Soil Components

Wetting behavior is a balance of adhesive and cohesive attractive forces in 3-phase systems (solid-liquid-vapor or solid-liquid-liquid) (Adamson, 1990). Where adhesive attractive forces between a fluid (fluid A) and solid exceed that fluid's cohesive forces and also exceed the adhesive attraction of the solid for the second fluid (fluid B), fluid A will tend to spread over the solid surface, thereby maximizing the liquid-solid interface and minimizing the free energy of the system. Fluid A can be considered to be a wetting fluid when θ is 0°. Interactions of the competing fluid B (liquid or vapor) with the solid are limited (i.e., fluids for which a low solid-liquid adhesive force exists and cohesive forces predominate, the liquid will tend to interact only weakly with the surface, being readily displaced from the solid surface by the wetting phase). As a result, wetting fluids generally intimately contact the solid phase and reside in the smaller pore spaces, whereas the nonwetting fluid is displaced to larger pores with less direct contact with the solid surface (Mercer and Cohen, 1990).

The wetting properties of these solid surfaces were evaluated first for solid-liquid-vapor systems. Contact angles (θ) for water in equilibrium with biotite, bentonite, goethite, kaolinite and solid-phase fulvic acid were similar, ranging from 5 - 26 ° (Table 1). It is notable that a cleaved and freshly exposed biotite surface yielded a lower mean θ than that of an aged surface. Aging apparently renders the surface more hydrophobic, likely through surface contamination with airborne organic compounds. Given the high surface tension of water (72.8 mN/m), which is a measure of the cohesive forces of water molecules, these low values for θ indicate that these solids may be considered high-energy surfaces. That is, adhesive attractive forces associated with the solid are able to overcome the attractive forces within the water drop, distend the water drop, and create a substantial water-solid interface. The theoretical case of a water drop suspended in free space, without a solid surface present, can be considered the no-adhesive force scenario. Under this scenario, the water drop assumes a

perfect spherical shape (θ approx. 180 °). The Teflon surface, with a θ of 111° (Table 1), represents a low-energy surface. The adhesive attractive forces existing between the Teflon surface and the water molecules are limited; as a result, cohesive forces predominate and the water drop retains qualitatively a spherical shape. We observed that the solid-phase humic acid exhibits wetting properties intermediate between the Teflon surface, where water can be considered a non-wetting fluid, and the clay minerals, where water can be considered a wetting fluid (Table 1). From the Young-Dupre' equation, the work of adhesion, W_A, may be calculated:

$$W_A = \gamma_{LV}(1+\cos\theta) \qquad (1)$$

where $_{LV}$ is the surface tension of the fluid (Table 1).

Contact angles of selected NAPLs in equilibrium with biotite, kaolinite and bentonite surfaces are provided in Table 2. o-xylene was found to wet completely all mineral surfaces, as did, for all practical purposes, tetrachloroethene (PCE), though tetrabromoethane yielded finite contact angles ranging from 24 - 42° (Table 2). Thus, for solid-liquid-vapor systems, these NAPLs, like water, also tend to wet mineral solid surfaces.

Under most relevant environmental scenarios, however, water is present and a competition between water and NAPLs for the solid surface exists. As a result, wetting behavior is a balance of adhesive and cohesive forces in this solid-NAPL-water system. For these systems, contact angle measurements were made for NAPLs in contact with mineral surfaces immersed in water. The solid surfaces formed from clay minerals all readily dispersed when immersed in water, so these determinations were limited to the biotite and Teflon surfaces. The general similarity of the contact angles for mica and the other mineral phases for water and NAPLs from solid-liquid-vapor systems implies that results from solid-NAPL-water systems may be extrapolated, at least qualitatively, to the other minerals.

The captive bubble method allowed determination of both advancing and receding contact angles. To allow for comparison with Table 2, the contact angles are reported through the NAPL, though the convention is generally to report the angles measured through water. Considering the case of PCE, we noted that while previously wetting the freshly exposed mica surface (θ =1°), when the competing fluid was its vapor, the presence of water profoundly changed its wetting properties (Table 3). The PCE interacted only weakly with the mica surface, with the competing water phase predominating the solid surface. For this case, PCE was relegated to a non-wetting status, and when present in soil saturated with water, it will generally be excluded from micropores and occupy only the larger pore spaces (Mercer and Cohen, 1990). The difference between advancing and receding contact angles is an indication of hysteresis: during advance, the PCE is encountering a water-wet surface; while receding, the PCE is backing through a PCE-wet mica surface. The PCE may change the character of the mineral surface sufficiently to alter the

measured θ. A similar trend was noted for benzene, which completely wet the mica surface when vapor was the competing fluid, whereas it interacted with the surface only in a limited capacity when water was present (Table 3). The wetting properties of tetrabromoethane were relatively unaffected by the presence of water. The presence of water had only a modest influence on the interactions of benzene with a Teflon surface as well.

Vapor-Liquid Partitioning

An organic chemical within an unsaturated soil will partition mass to the vapor phase. With water present in the soil such that a 4-phase system (solid-NAPL-water-vapor) exists, chemical partitioning between the vapor and water (liquid) phases also occurs. At equilibrium, vapor-aqueous phase partitioning is described by Henry's law, provided here in the nondimensional form:

$$C_g = HC_{aq} \tag{2}$$

where C_g is the concentration in the gas or vapor phase (M/L^3), C_{aq} is the concentration in the aqueous phase (M/L^3), and H is the nondimensional Henry's constant. The presence of dissolved organic matter (DOM) has been shown to affect solubility and sorptive properties of organic chemicals (Chiou et al., 1986; Chin et al., 1990), though the influence of DOM on vapor-liquid partitioning has been evaluated only minimally (Callaway et al., 1984). In particular, the influence of surfactants on vapor-liquid partitioning has not been investigated. With the proposed use of surfactant-washing in remediation of NAPL-contaminated soils (Abdul et al., 1990), it is also important to understand this relevant partitioning phenomena.

Three-phase model

A 3-phase model was developed to describe chemical partitioning among vapor, aquated, and surfactant-associated phases. It was first assumed that partitioning of chemical to the surfactant follows a simple linear isotherm (Kile et al., 1990) described by:

$$S = KC_{aq} \tag{3}$$

where S is the amount partitioned to unit mass of surfactant (M/M) and K is the linear solute-surfactant partition coefficient (L^3/M). The total liquid phase concentration, C_l, and the aquated concentration (i.e., the concentration of chemical not associated with surfactant) are related by:

$$C_l = C_{aq} + SX \tag{4}$$

where X is the concentration of surfactant (M/L^3), which, when substituted into Eq. 3 yields:

$$C_{aq} = C_l/(1+KX) \tag{5}$$

Thus the aquated or "free" chemical concentration can be determined from the total liquid phase concentration. Assuming then that only the aquated form participates in liquid-vapor exchange, Henry's law (Eq. 2) can be rewritten using Eq. 5 as:

$$C_g = HC_l/(1+KX) \quad (6)$$

Apparent Solubility

Linear increases in the apparent solubilities of benzene, toluene, and o-xylene with increasing SDS concentrations were observed (Fig. 1), with $r > 0.99$ for linear regressions of apparent solubilities with SDS concentration. Evaluation of the apparent solubility in the presence of SN70 was stymied by the formation of a second liquid phase within the sealed vessels when an excess of chemical was equilibrated with the SN70 solutions. As a result, no apparent solubility data are provided for this surfactant. Apparent solubility of organic chemicals in the presence of humic substances has been demonstrated in previous studies (Chiou et al., 1986) and was not reassessed here. The data from Fig. 1 were used to calculate K values of 190, 560, and 1280 for benzene, toluene, and o-xylene, respectively, which were in relatively good agreement with reported K_{ow} values of 132, 537, and 891 (Mercer and Cohen, 1990).

Vapor Phase Concentrations and Apparent Henry's Constants

Equilibrium vapor phase concentrations for the three chemicals in the absence of surfactant were between 21 and 24 mg/L. At constant added chemical mass to the vessels, vapor phase concentrations were significantly reduced at moderate to high SDS concentrations (Fig. 2). Vapor concentrations were reduced most significantly for o-xylene, followed by toluene, and benzene. Apparent Henry's constants (vapor concentration over total liquid concentration, here denoted H^*) necessarily followed these same trends and decreased with increasing SDS concentration (Table 4).

Partition coefficients derived from the apparent solubility experiments yielded predicted gas concentrations significantly less than those observed for all three compounds (not shown). Partition coefficients calculated from gas concentration data using a mass balance equation and Eq. 6 were lower than those derived from apparent solubility data (Table 5).

The Witconol SN70 was somewhat more efficient at reducing vapor phase concentrations than the SDS at equal surfactant concentrations (Fig. 3). As a result, apparent Henry's constants were correspondingly lower at similar surfactant concentrations (Table 4). At the highest SN70 concentration, the apparent Henry's constant of o-xylene was reduced to less than 10% of that in water. Like that for SDS, Eq. 6 could be fit to the gas phase data and a K determined; solute-surfactant partition coefficients were considerably higher than those for the shorter-chained anionic SDS (Table 5).

No discernible decrease in benzene and toluene vapor concentrations was noted for the humic acid solutions, though the gas phase concentration of o-xylene did decrease slightly with increasing humic acid concentration (Fig. 4). As a result, apparent Henry's constants for benzene and toluene in the presence of humic acid were unchanged (Table 1) and the extent of partitioning was below that for which K could be derived. A solute-surfactant partition coefficient of 850 was calculated for o-xylene, a value intermediate between SDS and SN70.

Discussion

Wetting Properties of Soil Components

The contact angles for water in equilibrium with soil constituents exceeded 0 in all cases, the value generally assumed. Goethite, and particularly humic acid, which generally form coatings on soil particles, both yielded values of θ for solid-water-vapor systems significantly greater than 0.

Mercer and Cohen (1990) point out that residual saturation results from capillary forces and depends upon a number of factors, including wettability. Capillary pressure is related to contact angle, for interfaces that form subsections of a sphere, through (Anderson, 1987; Mercer and Cohen, 1990):

$$P_c = \frac{2\gamma\cos\theta}{r} \tag{7}$$

where r is the radius of a water-filled pore and is the interfacial tension. For an NAPL to enter a water-saturated porous medium, the NAPL pressure head must exceed the capillary forces. The threshold entry pressure can be estimated as an equivalent head of water by the capillary rise equation:

$$h_c = \frac{2\gamma\cos\theta}{r\rho_w g} \tag{8}$$

where h_C is the capillary rise, $_W$ is the density of water, and g is the gravitational constant. From these considerations, then, contact angles are very important to NAPLs and water retention in soils.

Vapor-Liquid Partitioning

The presence of surfactant resulted in a significant reduction in the equilibrium vapor phase concentration, and thus apparent Henry's constants, of benzene, toluene, and o-xylene. Gas phase concentrations were described by a simple 3-phase model which partitions mass to the vapor, aquated and surfactant-associated phases. Gas-liquid phase partition was described by Henry's law with the aquated (i.e., non-surfactant associated component) concentration used in lieu of the total liquid phase concentration. Aquated and surfactant-associated components were described by a linear partition

equation, though the partition coefficient was found to be a function of solute concentration. Aldrich humic acid exhibited little influence on the equilibrium vapor phase concentrations and apparent Henry's constants for benzene and toluene, but did result in some reductions for o-xylene.

The role of this phenomenon in the air-water partitioning of more hydrophobic chemicals in natural waters can be inferred based upon data from available literature. For example, the reduction in apparent Henry's constant for 2,2',4,5,5'-PCB can be calculated for a soil solution with a DOM content of 100 mg/L, assuming a partition coefficient of 1.17×10^4, a Henry's constant of 1.16×10^{-2}, and a total liquid concentration at its solubility limit in water of 1.1×10^{-2} mg/L (Mercer and Cohen, 1990). From Eq. 4, an equilibrium gas concentration of 5.88×10^{-5} mg/L is predicted. This soil solution would yield an apparent Henry's constant of 5.35×10^{-3}, a reduction of 54 % in H^*. Thus, for hydrophobic organic chemicals in waters and soil solutions relatively high in DOM or surfactants, significant reductions in H^* can be anticipated. These conditions are met in many high organic carbon soils, and soils and aquifers in which surfactant-washing is performed.

References

Abdul, A.S., T.L. Gibson, and D.N Rai. 1990. Selection of surfactants for the removal of petroleum products from shallow sandy aquifers. Ground Water 28:920-926.

Adamson, A.W. 1990. Physical chemistry of surfaces. 5th ed. John Wiley & Sons, New York, NY.

Anderson, W.G. 1986. Wettability literature survey - Part 2: Wettability measurement. J. Petrol. Technol. Nov. 1986:1246- 1262.

Anderson, W.G. 1987. Wettability literature survey - Part 4: Effects of wettability on capillary pressure. J. Petrol. Technol. Oct. 1987:1283-1300.

Callaway, J.Y., K.V. Gabbita, and V.L. Vilker. 1984. Reduction of low molecular weight halocarbons in the vapor phase above concentrated humic acid solutions. Environ. Sci. Technol. 18:890-893.

Chin, Y.-P., W.J. Weber, Jr., and B.J. Eadie. 1990. Estimating the effects of dispersed organic polymers on the sorption of contaminants by natural solids. 2. Sorption in the presence of humic and other natural macromolecules. Environ. Sci. Technol. 24:837-842.

Chiou, C.T., R.L. Malcolm, T.I. Brinton, and D.E. Kile. 1986. Water solubility enhancement of some organic pollutants and pesticides by dissolved humic and fulvic acids. Environ. Sci. Technol. 20:502-508.

Kile, D.E., C.T. Chiou, and R.S. Helburn. 1990. Effect of some petroleum sulfonate surfactants on the apparent water solubility of organic compounds. Environ. Sci. Technol. 24:205-208.

Lincoff, A.H and J.M. Gossett. 1984. The determination of Henry's constant for volatile organics by equilibrium in closed systems. p.17-25. In W. Brutsaert and G.H. Jirka (ed.) Gas transfer at water surfaces. D. Reidel, Dordrecht, Holland.

Mercer, J.W. and R.M. Cohen. 1990. A review of immiscible fluids in the subsurface: Properties, models, characterization and remediation. J. Contaminant Hydrol. 6:107-163.

Publications and Reports

Hung, A.Y.C and M.A. Anderson. 1992. Contact angles of water and nonaqueous phase liquids on soil constituents. Agron. Abstr. (p. 239).

Anderson, M.A. 1992. Influence of surfactants on vapor-liquid partitioning. Environ. Sci. Technol. 26:2186-2191.

Table 1. Wetting properties of selected solid surfaces in solid-water-vapor systems.

Surface	θ	W_A[a]
Mica-fresh	5±10	144.9
Mica-aged	26±18	137.9
Fulvic acid	15±1	142.7
Humic acid	56±1	113.2
α-FeOOH	24±1	138.9
Kaolinite	15±1	142.7
Bentonite	19±2	141.6
Teflon	111±3	46.6
Paraffin	111±4	46.6

[a] γ_{LV}^{w} = 72.8 mN/m

Table 2. Contact angles of NAPLs on the surfaces of mica, kaolinite, bentonite, and teflon in solid-NAPL-vapor systems.

	θ			
Surface	Benzene	o-Xylene	PCE	TBE
Mica-fresh	0±0	0±0	1±2	35±4
Mica-aged	0±0	0±0	7±3	42±3
Kaolinite	0±0	0±0	2±2	28±6
Bentonite	0±0	0±0	0±0	24±4
Teflon	36±1	41±1	37±2	76±3

Table 3. Contact angles of NAPLs on the surfaces of mica and Teflon in solid-NAPL-water systems.

	θ		
Surface	Benzene	PCE	TBE
Mica	145±4/135±2[a]	165±2/153±2	148±6/110±4
Teflon	52±3/42±3	ND	ND

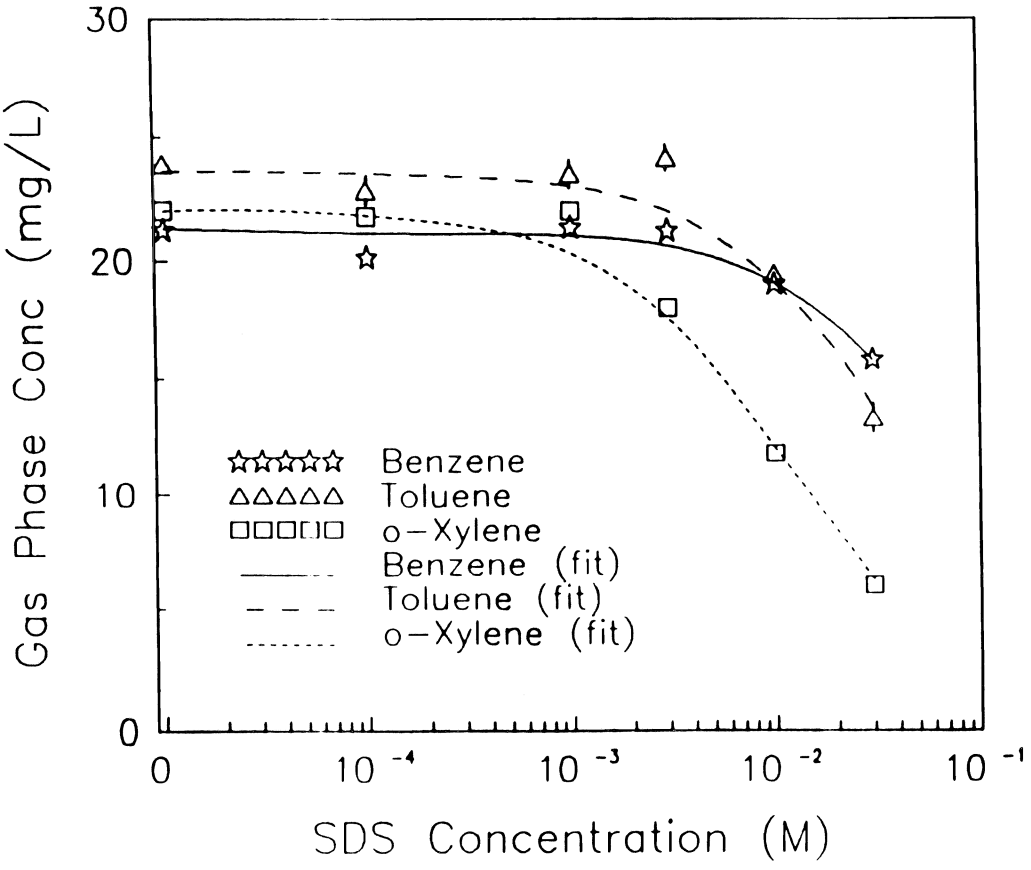

Figure 2. Observed and model-fitted edquilibrium gas phase concentrations of benzene, toluene, and o-xylene versus logarithm of SDS concentration. Error bars provided when standard deviations exceed symbol size.

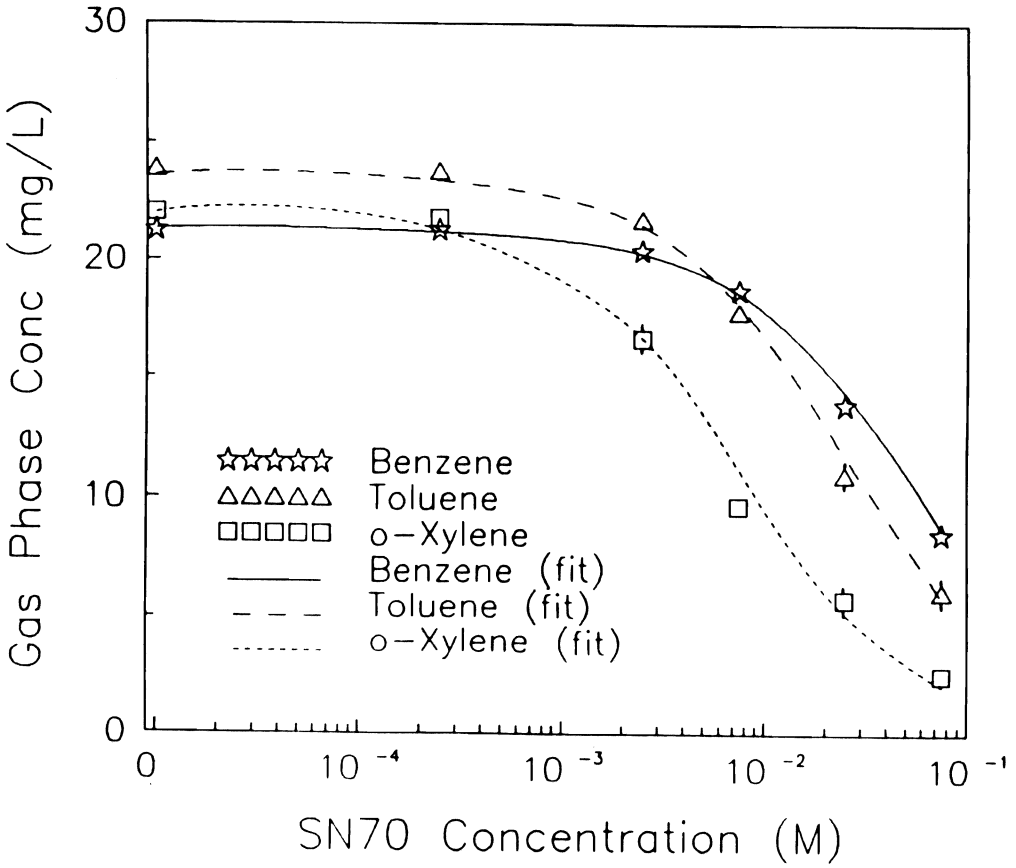

Figure 3. Observed and model-fitted edquilibrium gas phase concentrations of benzene, toluene, and o-xylene versus logarithm of SN70 concentration. Error bars provided when standard deviations exceed symbol size.

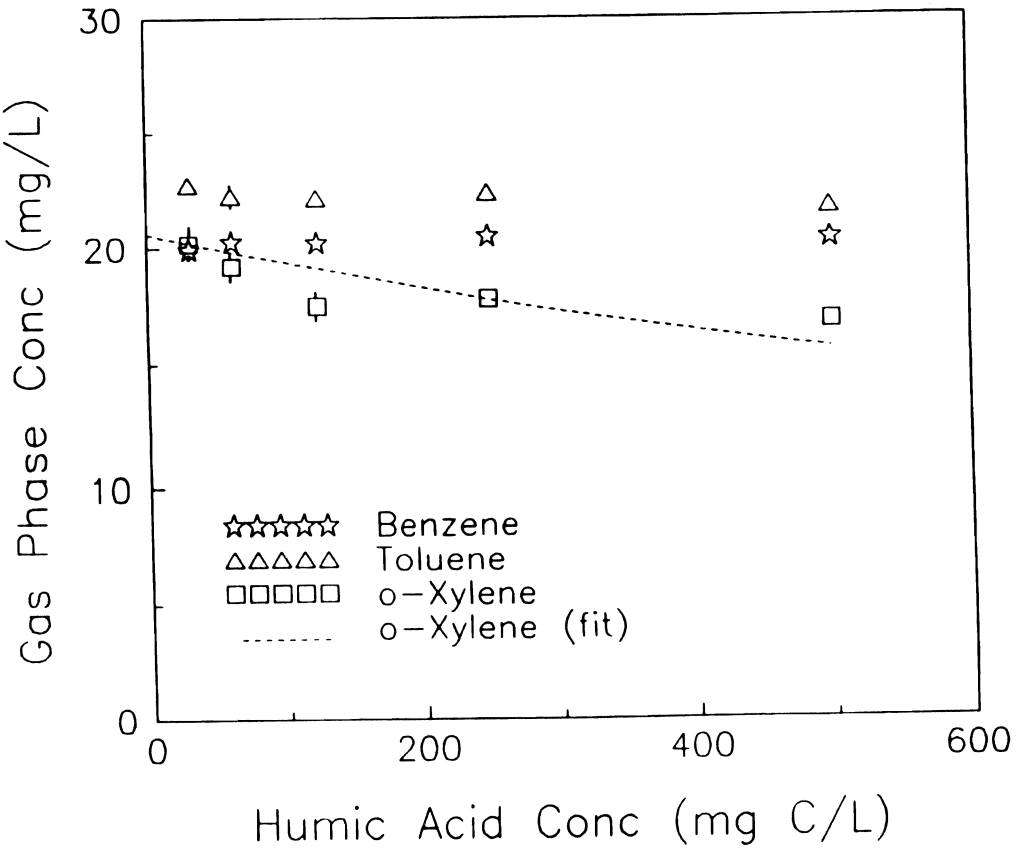

Figure 4. Observed and model-fitted edquilibrium gas phase concentrations of benzene, toluene, and o-xylene versus humic acid concentration. Error bars provided when standard deviations exceed symbol size.

Development of a Stochastic Model of Crack Structure and Flow in Cracking Soil

ZBIGNIEW J. KABALA AND HENRYK SOBCZUK
Department of Soil and Environmental Sciences, Riverside Campus

Summary

Efficient irrigation water management and control of groundwater contamination caused by agriculture activities on cracking vertic soils depend on reliable field-scale models of flow and transport in such soils. The models available currently are deterministic and do not allow for the virtually random nature of the crack distribution nor for the effects of small-scale spatial heterogeneities observed in parameters characterizing flow, transport, sorption, and degradation processes in all natural soils. This three-year research project is designed to develop a stochastic model of soil cracking processes and an associated field-scale water flow model which together, in the future, will form the basis for the development of a transport model for contaminants in cracking soils. The transport model will account for the small-scale heterogeneities of local parameters (via their auto- and cross-correlation functions) that characterize flow processes in natural cracking soils. A field experiment will be conducted to measure the spatial distribution of cracks, their size, and dimensions as a function of moisture content. These measurements will be used to estimate the parameters required by the field-scale water flow model developed in this project.

Key Words: Voronoi tessellation, crack distribution, crack network

Project Objectives Addressed in 1991-92

1. Develop a probabilistic model of the crack distribution in vertic soils that connects the crack structure with the bulk moisture content.

Research Plan and Procedures in 1991-92

1. Perform thorough literature review.

2. Analyze the suitability of parent-daughter model and the random tessellation model to describe the cracking structure of vertic soils.

3. Formulate a stochastic model of cracking structure of vertic soils capable of reproducing the main features of cracks observed in fields.

4. Simulate synthetic cracks for vertic soils.

5. Propose measurement methods for identifying model parameters.

Results

Literature Review

The crack structure of rocks, concrete, and other media is quite well-described in the literature. Presently, there is no complete description, however, of crack structure, cracking evolution, and conductivity of cracking vertic soils. Hallaire.(1981) observed the evolution of the crack network on the soil surface during drying. He found two stages of evolution: at the beginning, the uniform network of cracks emerged with small spacings; and after that, some of the cracks started to grow, and formed the network of bigger cracks with much bigger spacing. The rest of the cracks preserved their widths or even shrunk during the second stage. Panozzo (1986), Scott et al.(1986), and Scott et al. (1988 a,b) introduced crack density and orientation as parameters of crack structure. They used connectivity density and described appropriate measurement methods based on investigations of sample sections. To describe the network of cracks on a rock surface, Velde et al. (1990) investigated the probability of a cross section of cracks with the probe line. This type of measurement is easy to perform and gives reliable results in the case of many replications. Velde et al. (1990) observed the anisotropy of fracture network caused by the nonisotropic distribution of stress within the rock. Hestir et al. (1987) proposed a parent-daughter model to describe crack distribution in rock employing the Poisson probability distribution function for both parent and daughter cracks. Khaleel (1987) considered cracks in a rock as a regular hexagonal colonnade and performed two dimensional areal simulations using a porous continuum model (equivalent porous medium model). He presented the results of calculating crack network conductivity as a mean value from 100 computer simulations of the network.

Numerous authors have investigated water movement in swelling and cracking soils: Bronswijk (1991a,b) measured the vertical movement of soil vs. water content in cracking clayey soils and proposed methods to determine three dimensional volume changes of the soil; Perroux and Zegelin (1981) described laboratory observations of water flow in the clayey soil and observed a bypass flow for higher water flow ratio. Cracks and macropores were responsible for quick water movement within the soil sample.

Parent-daughter Model

Although the parent-daughter model has been used successfully in descriptions of the cracking structure for rocks, it does not generate the mosaic observed in vertic soils as naturally as does the tessellation model. We, therefore, chose to adopt the tessellation model.

Tessellation (mosaic) is a convenient model for describing properties of natural shapes, which show some regularity, like soap bubble froths (N. Rivier, 1983), crystal aggregates (Meijering, 1953), and crack shapes (Gray et al., 1976; Einstein and Herda, 1986). Zaninetti (1989) used it in astrophysics for modeling the distribution of matter in the Universe. Radecke (1980) described parameters that define geometry of tessellations. Bartlett (1975) and Stoyan et al.(1987) reviewed the methods for description and measurement of actual tessellations.

Description of Random Planar Tessellation

(a) Definition of the Voroni tessellation.

A planar Voroni tesselation is defined using a set α of generating points on a plane. The neighborhood $T(y)$ defined for each point y belonging to α forms a cell of the tessellation. Each cell of the tessellation (neighborhood $T(y)$ of a point $y \in \alpha$) consist of points $x \in R^2$ that follow the restriction:

$$T(y) = \{x \in R^2 \ : \ n(x) = y\} \qquad (1)$$

where $n(x)$ is a function that gives as a value the nearest to x neighbor point of α.

Following this definition $T(y)$ is a convex polygon with edges formed by perpendicular bisectors of segments connecting nearest neighboring points. The detailed structure of the tessellation depends on the distribution of generating points. Regularly distributed points generate a regular tesselation , while random points yield random tesselations (Okabe et al., 1992).

(b) Other structures considered with the tessellation and used for its description.

For the description of complicated tesselation structures, it is useful to define attached point processes and fiber processes. The structure of these constructions is simpler than that of tessellation and their description is more developed. Two additional planar point processes with the exception of generating point process α, can be associated with tesselation ϑ: the set of nodes α_o forms the point process of intensity λ_o, and the set of edge midpoints α_1 forms the point process of intensity λ_1 .

The intensity λ of the point process gives an expected number of α points per unit area. For planar stationary tessellation ϑ one can define the fiber process ψ given by the edge set of the tessellation. Intensity λ_ψ of fibers in ψ defined as the mean length of fibers per unit surface area may be estimated by

$$\lambda_\psi = \frac{1}{A(W)} E\psi(W) \qquad (2)$$

where

W is. the sampling window
A(W) is the sampling window surface area
$\psi(W)$ the total length of fibers within sampling window
E is a mean value operation

(c) First order characteristics of point processes

To provide a full description of a point process one should define an infinite series of distribution functions for one point, pair of points, triples of points, etc. Practically only first and second order characteristics are in use (Stoyan et al. 1987). The main characteristics of the point process α is the intensity λ that gives an expected number of α points per unit area. Thus the mean number of α points n_α that hit into the sampling window *W* is given by

$$n_A = E\alpha(W) = \lambda A(W) \qquad (3)$$

where

W is the sampling window
A(W) is the sampling window surface area
$\alpha(W)$ is number of process α points within sampling window *W*
E is a mean value operation

(d) Second order characteristics of point processes

An important characteristic of a point process is a second reduced moment function *K(r)* describing stochastic properties of pairs of points (Ripley, 1977).

The quantity $\lambda K(r)$ is an expected value of the number of process points that lie within a circle of radius r centered at a point that belongs to α (the central point itself is not counted). For a Poisson point process $K(r) = \pi r^2$, i.e., points are distributed independently with constant probability such that the mean number of points that hit into the circle of radius r depends only on its area. For this case, the probability of n points falling within the observation window W has the Poisson distribution with the mean value N_W:

$$N_W = A(W)\lambda \qquad (4)$$

where $A(W)$ is the surface area of the observation window W and λ is an intensity of a point process.

Non-Poisson point processes are characterized by different forms of function $K(r)$. As an example, consider hard core point process (Fraser, 1991) when points are not allowed to lie within a circle of radius $r > r_0$ in a neighborhood of another point. The function $K(r)$ vanishes then for $r < r_0$. The method of generation of point processes with various distribuiton functions is described by Ripley (1977) and Bartlett (1975) and bases on thinning of a Poisson point process following different rules (Paloheimo, 1971).

(e) The rose of directions

The rose of directions is defined as the distribution of directions of tessellation edges. The estimation of the rose of directions R is given by Stoyan et al. (1987):

$$F_R(\beta) = \frac{1}{2L_A}\left[\frac{d}{d\beta}P_I(\beta) + \int_o^\beta P_I(\alpha)d\alpha\right] \qquad (5)$$

where $\frac{d}{d\beta}P_I(\beta)$ is a numerical derivative of the rose of intersections $P_L(\beta)$.

The rose of intersections is defined as the intensity of intersections of ψ with a sampling line at angle β to the sampling line.

Voronoi Tessellation As A Crack-Network Model

We use Voronoi tessellations for the description of a network of cracks on the surface of vertic soils as do Weaire (1983) for cellular systems, Einstein and Herda (1986) for cracking rocks, and Vrettos et al. (1989) for a description of pores in porous media. For practical description, we use single and double point distributions, neglecting the higher order distributions as do Stoyan (1987) and Ripley (1977). We use the intensity λ that gives an expected number of

points representing cell centroids α per unit area, and a second order characteristic - a second reduced moment intensity function *K(r)* (Ripley, 1977). Both the intensity λ and second reduced moment intensity function *K(r)* are estimated from the measurement of cracked soil surface and used for further simulation of cracks.

The Model of Width of Cracks

Width of cracks depends on network geometry. Lachenbruch (1962) described the relationship between stress relief around cracks and the distance between cracks. He provided qualitative discussion to explain why cracks form networks and what factors influence the distance between surface cracks. Even qualitative description of interacting cracks is complicated, and due to their heterogeneity, needs to be described stochastically (Kachanow, 1986; Maekin, 1990). We examined three methods to generate widths of cracks on tessellations.

(a) Global correlation of cracks.

This method is based on the assumption that cracks are globally correlated. If the stress field forces the soil medium such that cracks are more likely in one direction than in another, then crack network and crack widths show strong anisotropy (Velde et al., 1990). In such a case, we model cracks using the assumption that the crack width depends on crack direction.

(b) Correlation with surrounding cracks.

In a second approach, we assume that each crack is strongly correlated just with the surrounding cracks. In this case, the geometry of surrounding cracks plays a major role. The main idea is based on the discussion provided by Lachenbruch, (1961, 1962) and Vallejo (1988). We tested various correlation functions that show physically acceptable properties, i.e.:a long parallel crack lying in the vicinity of a given crack suppresses growth (negative interaction due to stress release), cracks that form a linear sequence with the given crack allow its growth (positive interaction due to stress concentration near crack tips). cracks perpendicular to a given crack weakly influence its growth weak interaction).

(c) Hierarchical model of crack distribution.

We propose a hierarchical model of crack network. It is well known that cracks on the soil surface form networks (Hallaire, 1981). The spacing between cracks depends on their widths - small and narrow cracks form a fine network, while long and deep cracks form a coarse network which has bigger cells than the fine network. One can imagine a few overlapping networks that form complicated crack structures of differing widths. We generate each network separately as a Voronoi tessellation and then interpolate it by the finest network. We assume that each crack in a fine network that interpolates the crack of a coarse network has a width characteristic of the coarsest crack.

The crack surface ratio is defined as a ratio of crack surface area to the total area. Each class d crack is characterized by its own function $K_d(r)$ and the distribution of crack widths $P_d(w)$ within the class. The function $K_d(r)$ characterizes the distribution of cell centroids in class d. All parameters can be measured from a cracked field and used in computer simulation of the crack network.

Computer Simulations of Crack Structure

We perform the calculations in the following steps:

(a) Generation of point processes of cell centroids.

Each point process of cell centroids is generated first as the Poisson point process with the intensity λ_d and then the distribution function $K_d(r)$ is calculated from generated points. If the calculated value of $K_d(r)$ is greater than the assumed $K_d^0(r)$ within the range of radii $(r, r + \Delta r)$, then points that are within this distance are moved to random positions with probability proportional to a difference between the calculated and the assumed distribution functions. This procedure is applied to each generated point. Change of point positions is effective when calculation for all points is completed. After that, the distribution function $K_d(r)$ is calculated again and iteration is repeated until no point is moved in a next step or the assumed number of iterations is performed. This procedure preserves the intensity λ_d and simulated $K_d(r)$ is approximately equal to the given function $K_d^0(r)$.

(b) Generation of Voronoi tessellation.

We use the procedure proposed by Tipper (1991) to generate Voronoi tessellations. We modified the Tipper (1991) algorithm using a parametric rather than directional representation of lines. The modified version works properly even if calculated lines are vertical, as opposed to the original version.

We assume periodical boundary conditions for the network to avoid problems that can emerge on the network boundary. The networks are generated on the surface that is topologically equivalent to the surface of a torus, which has the advantage that each point can be treated equally, independent of its position. In a case for which specific network dimensions are much bigger than the mean length of network edges, the network periodicity is assumed not to disturb stationarity of the process significantly.

(c) Projection of coarse network onto the fine network.

Widths of cracks are generated according to the distribution functions Pd(w). To project an edge of a coarse crack onto the fine network we do the following:

(i) Find the nearest neighbors at tips of a big crack that belong to the fine network,

(ii) Starting from one of these points, find an edge that is closest to the coarse edge and take its free end as the starting point for the next search.

(iii) End at the second end of a coarse crack.Then, the resulting sequence of fine cracks that approximates a coarser crack is assigned a width according to the distribution Pd(w).

Results of Calculation

As an example, we present a series of graphs illustrating the procedures above. Figure 1 shows the Poisson's point process with the number of points per unit surface area $\lambda = 8$. Figure 2 presents a Voronoi tessellation generated by a Poisson point process. We show, in Fig. 3, crack widths generated using the global criterion with $w_i \sim \cos^2(\alpha_i - \alpha_0)$, where α_0 is the most likely angle and α_i the actual angle with OX. In Figs. 4, 5, and 6, we present generated networks for crack widths fully correlated with the geometry of cracks lying within a circle of radius ρ. The hierarchical model of crack widths is shown in Figs. 7 and 8. Fig. 7 presents two superimposed networks of cracks while Fig. 8 gives the projection of the coarse crack network on the fine crack network. The ratio of crack surface area to the total surface area is 10%. For simplicity, in the example, we assume that all cracks within the class have the same width.

Field Measurements of Parameters Describing the Model of Cracks

Parameters of the proposed models are estimated by measurements of a cracked soil surface. The intensity λ_d of point process characterizing cell centroids for crack class d is estimated as a mean number of separate crack cells per unit area. The distribution $K_d(r)$ is then estimated from the distribution of cell centroids. Ripley (1977) and Stoyan (1987) described relevant estimation procedures.

Discussion

The crack structure in vertic soils may be described by means of hierarchical Voronoi tessellations with random generating points. The cracking structure is divided into n width classes and each class is modeled by separate Voronoi tessellations. The hierarchical model will allow a relatively easy description of hydraulic conductivity of vertic soils. A number of issues still need to be resolved; in particular, the connection between (i) the crack structure and the soil moisture content, and (ii) the crack structure and the hydraulic conductivity of the cracked part of the porous media. A field experiment is being designed to address these issues.

References

Bartlett, M.S. 1975. The statistical analysis of spatial pattern. Monographs on applied probability and statistics. Chapman and Hall Ltd.

Bronswijk, J.J.B. 1991a. Relation between vertical soil movements and water-content changes in cracking clays, Soil Sci. Soc. Am. J. 55:1220-1226.

Bronswijk, J.J.B.1991b. Drying, cracking, and subsidence of clay soil in a lysimeter, Soil Sci. 152:92-99.

Einstein, H.H. and H.H. Herda. 1986. Discrete modeling of the geometry of rock joint systems, in Annals of Israel Phys. Soc. Vol. 8, Fragmentation and flow in fractured media.

Elbaz, M. and Jean-Claude Spehner. 1990. Construction of Voronoi diagrams in the plane by using maps, Theoretical Computer Science 77:331-343.

Fraser, D.P. 1991. Voronoi hard core systems, Materials Characterization 26:73-83.

Gray, N.H., J.B. Anderson, J.D. Devine, and J.M. Kwasnik. 1976. Topological properties of random crack networks. Math. Geol. 6:617-626.

Hallaire, V. 1984. Evolution of Crack networks during shrinkage of a Clay Soil Under Grass and Winter Wheat Crops. pp 49-54, Proceedings of the ISSS Symposium on Water and Solute Movement in Heavy Clay Soils, Wageningen, The Netherlands.

Hestir, K., j. P. Chiles, J. Long, D. Billaux. 1987. Three Dimensional modeling of fractures in rock: from data to a regionalized parent - daughter model, Flow and Transport Through Unsaturated Fractured Rock, Monograph 42:133-140.

Kachanov, M., On many crack problem in elastic solids. in Annals of Israel Phys Soc., Vol. 8, Fragmentation and flow in fractured media., 1986.

Khaleel, R. 1987. Porous continuum model for fractured basalts., Flow and Transport Through Unsaturated Fractured Rock, Geophysical Monograph 42:141-148.

Lachenbruch, A.H. 1961. Depth and spacing of tension cracks. J. Geophys. Res. 66:4273-4292.

Lachenbruch, A.H. 1962. Mechanics of thermal contraction cracks and ice-wedge polygons in permafrost. Special GSA paper no. 70.

Maekin, P., G. Li, L.M. Sander, H. Yan, F. Guinea, O. Pla, E. Louis. 1990. Simple stochastic models for material failure. Chapter 7 in Disorder and fracture, Ed. J. C. Charmet et al. (eds.) Plenum Press.

Meijering, J.L. 1953. Interface area, edge length, and number of vertices in crystal aggregates with random nucleation. Philips Res. Rep. 8:270-290.

Panozzo, R. 1986. Quantitative description of connected and unconnected surfaces in rock. In Annals of Israel Phys. Soc., Vol. 8, Fragmentation and flow in fractured media.

Perroux, K.M. and S. J. Zegelin. 1981. Constant Flux Infiltration in Swelling Soil, The Properties and Utilization of Cracking Clay Soils.

Radecke, W. 1980. Some mean value relations on stationary random mosaics in the space. Math. Nachr. 97:203-210.

Ripley, B.D. 1977. Modeling spatial patterns, Jour. Royal Statist. Soc. B., 39, no 1.

Rivier, N. 1983. On the structure of random tissues or froths, and their evolution. Philosophical Magazine B 47:L45-L49.
Scott, G.J.T., R. Webster, and N. Nortcliff. 1984a. The Topology of Pore Structure in Cracking Clay Soil: I. The Estimation of Numerical Density. In Proceedings of the ISSS Symposium on Water and Solute Movement in Heavy Clay Soils Wageningen, The Netherlands.
Scott, G.J.T., R. Webster, and N. Nortcliff. 1984b. The Topology of Pore Structure in Cracking Clay Soil: II. Connectivity density and its Estimation, Proceedings of the ISSS Symposium on Water and Solute Movement in Heavy Clay Soils Wageningen, The Netherlands.
Scott, G.J.T., R. Webster and N. Nortcliff. 1986. An Analysis of Crack Pattern in Clay Soil: its Density and Orientation. J. Soil Sci. 37:653-668, 1986.
Stoyan, D., W.S. Kendall, J. Mecke. 1987. Stochastic geometry and its applications, Wiley series in probability and mathematical statistics. John Wiley & Sons Ltd.
Tipper, J.C. 1991. Fortran programs to construct the planar Voronoi diagrams. Computers & Geosciences, 17:597-632.
Vallejo, L.E. 1988. The brittle and ductile behavior of clay samples containing a crack under mixed mode loading, Theoretical and Applied Fracture Mechanics 10:73-78.
Velde, B., J. Dubois, G. Touchard, A. Badri. 1990. Fractal Analysis of Fractures in Rock: the Cantor Dust Method, Tectonophysics 179:345-352.
Vrettos, N.A. 1989. Transport properties of porous media from the microgeometry of a three dimensional Voronoi network, Chem. Eng. Process 26:237-246.
Weaire, D. 1983. Random two dimensional cellular systems, in Topological disorder in condensed matter, F. Yonezawa, T. Ninomiya (eds.), Springer series in solid state series.
Yule, D.F. 1981. Volumetric Calculation in Cracking Clay Soils. The Properties and Utilization of Cracking Clay Soils, 1981, 1.
Zaninetti, L. 1989. Dynamical Voronoi tessellation, Astron. Astrophys 224:345-350.

Publications and Reports

Sobczuk, H. and Z. J. Kabala. 1992. Hierarchical model of surface cracks in cracking clay soil. (In preparation).

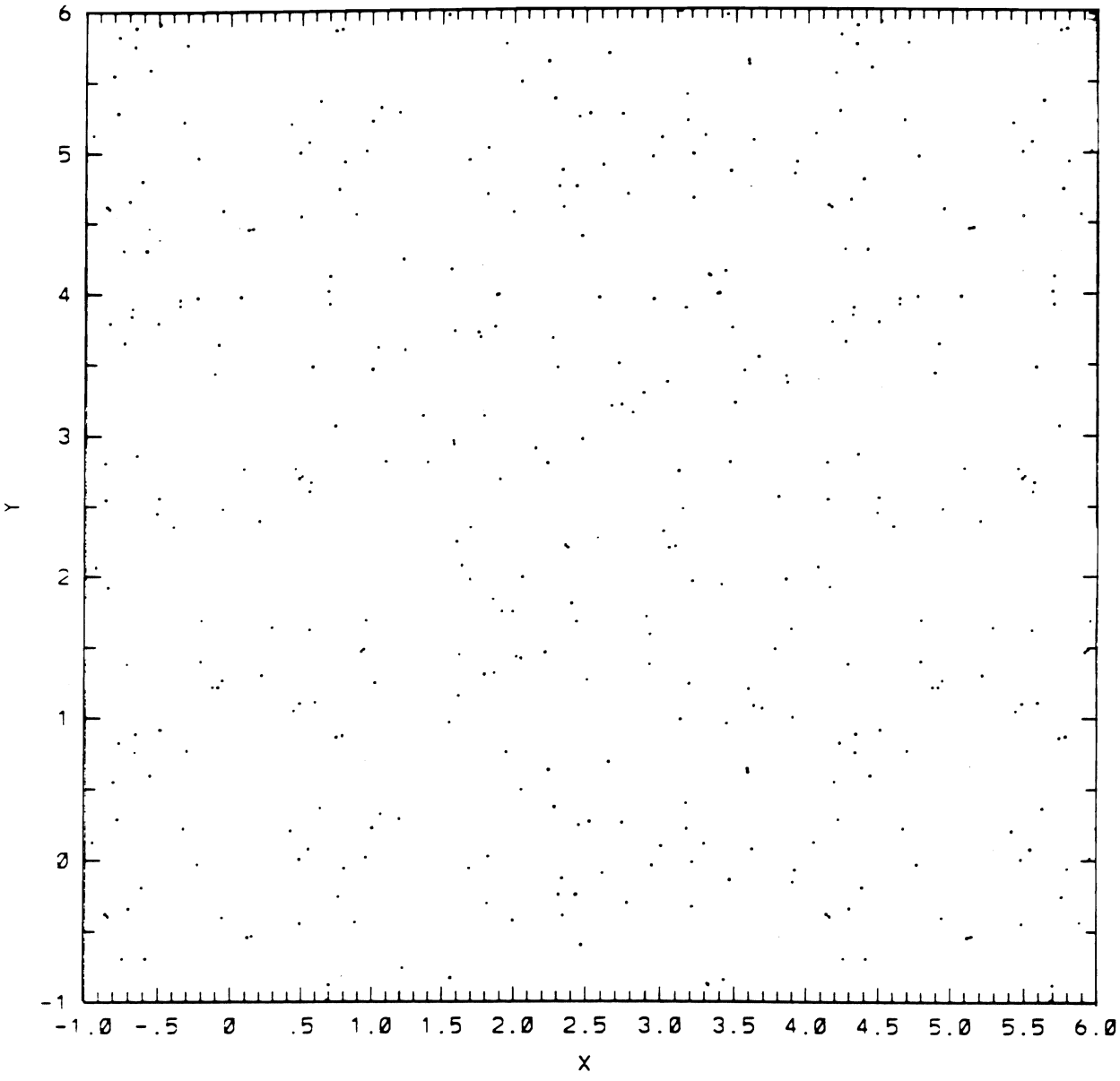

Figure 1. The Poisson point process in two dimensions. The mean number of points that belong to the point process per unit surface area is λ_2=8.

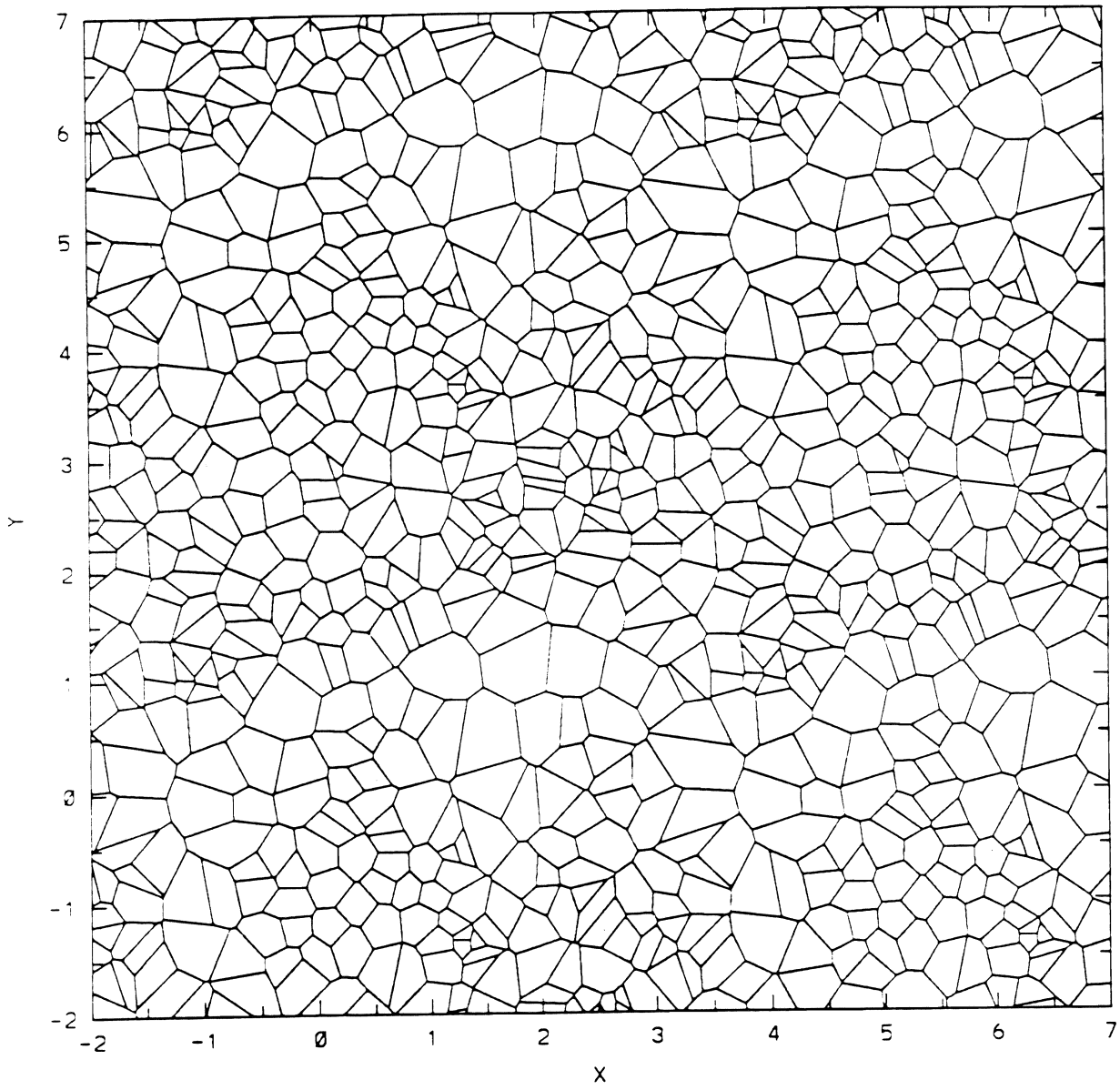

Figure 2. An example of Poisson-Voroni tessellation with periodical boundary conditions. The primary region of interest is a square (0.0;5.0)x(0.0;5.0) with the rest of the picture being the periodical repetition of this square.

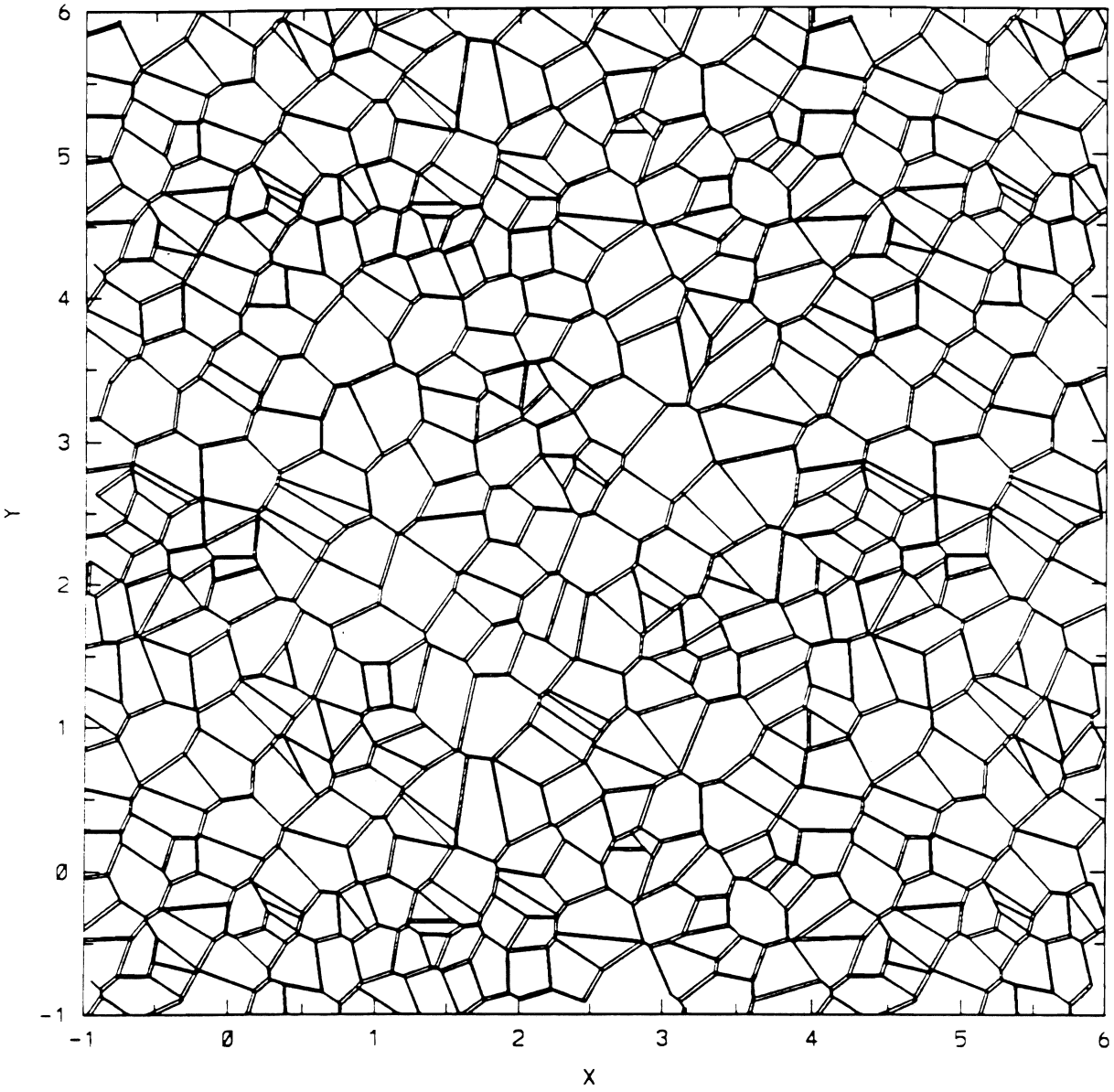

Figure 3. The network of cracks with their width dependent on the crack direction. The width of each crack is proportional to the value:

$$[b] \qquad w_i \sim \cos(\alpha_i - \alpha_o)^2$$

where:

α_O - most likely angle between crack and X-axis,

α_i - angle of actual crack.

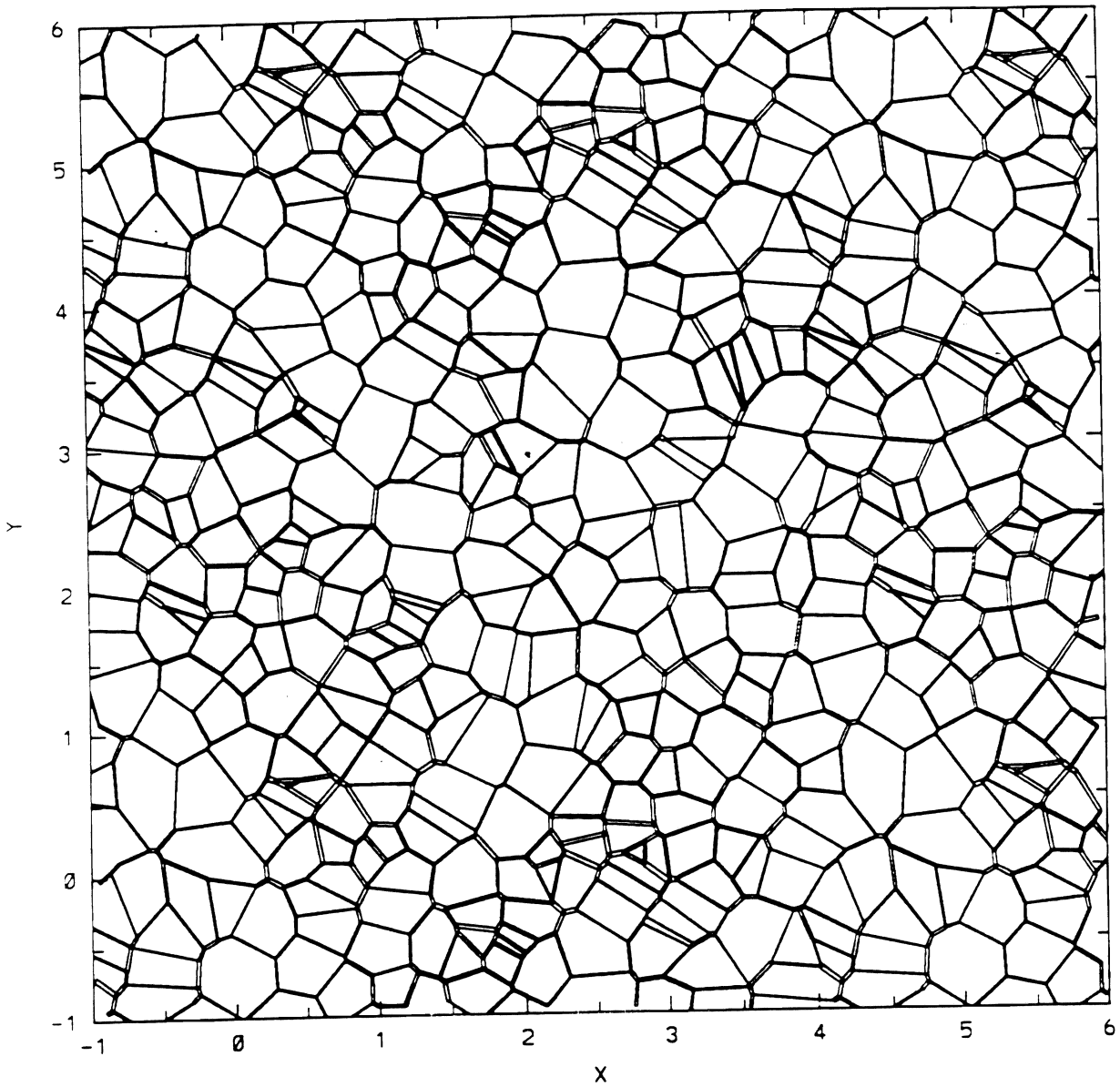

Figure 4. A network of cracks with their width dependent on the neighboring cracks. Width is proportional to the sum of interactions given by:

$$[a] \quad w_i \sim \sum_{\substack{j_i r_{i,j} < \rho \\ i \neq j}} l_j \sin(\gamma_{i,j}) \sin(\gamma_{j,i}) |\cos(\alpha_j - \alpha_i)|$$

where:

$r_{i,j}$ - distance between centers of cracks i and j,

$\gamma_{i,j}, \gamma_{j,i}$ - angles between normal to the crack and vector $r_{i,j}$ connecting centers of cracks,

α_i, α_j - angles between cracks and X-axis

l_j - length of the neighboring crack.

Radius of corfrelation, $\rho = 0.4$.

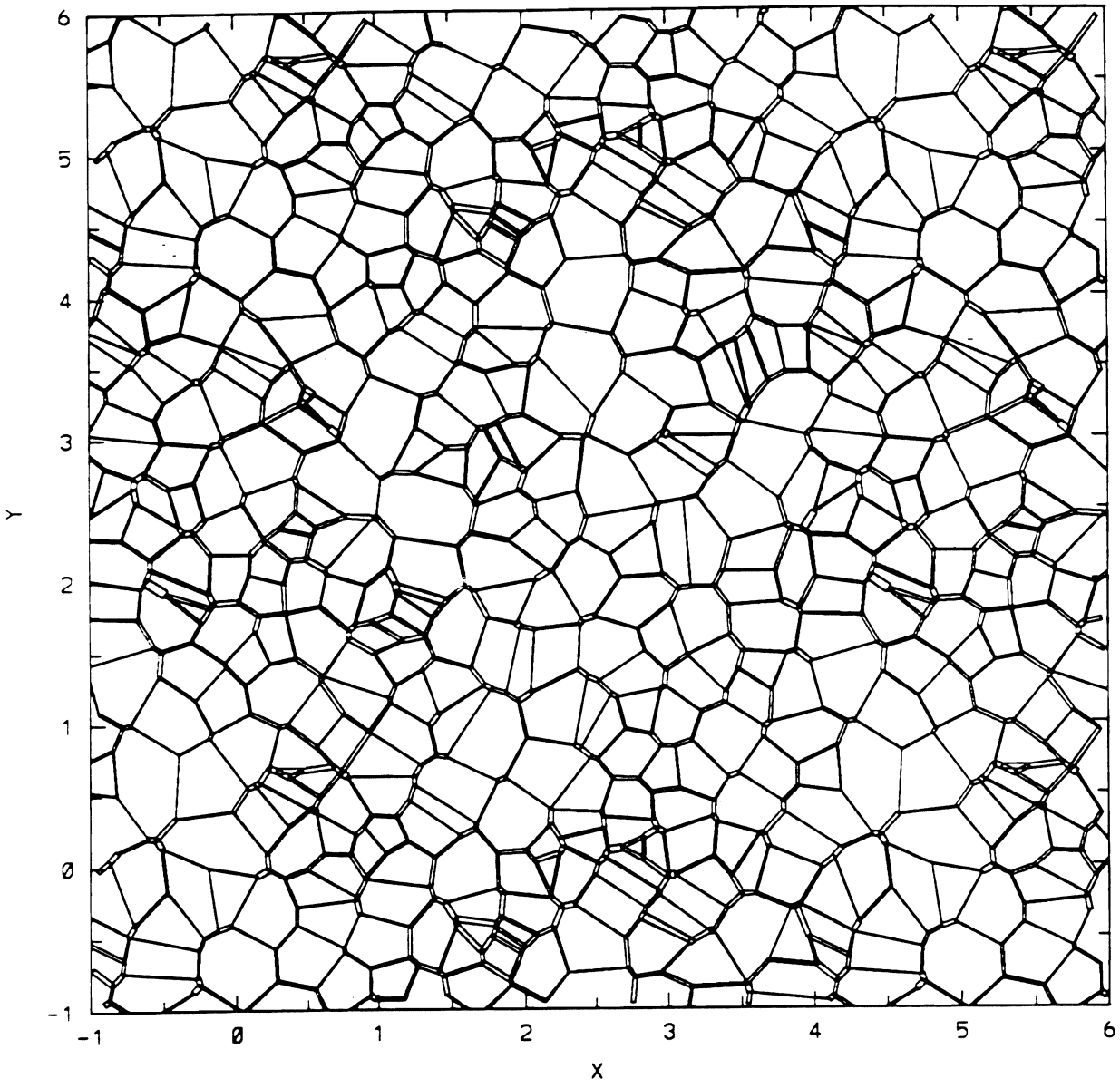

Figure 5. The same as Fig. 4, but with $\rho = 0.3$.

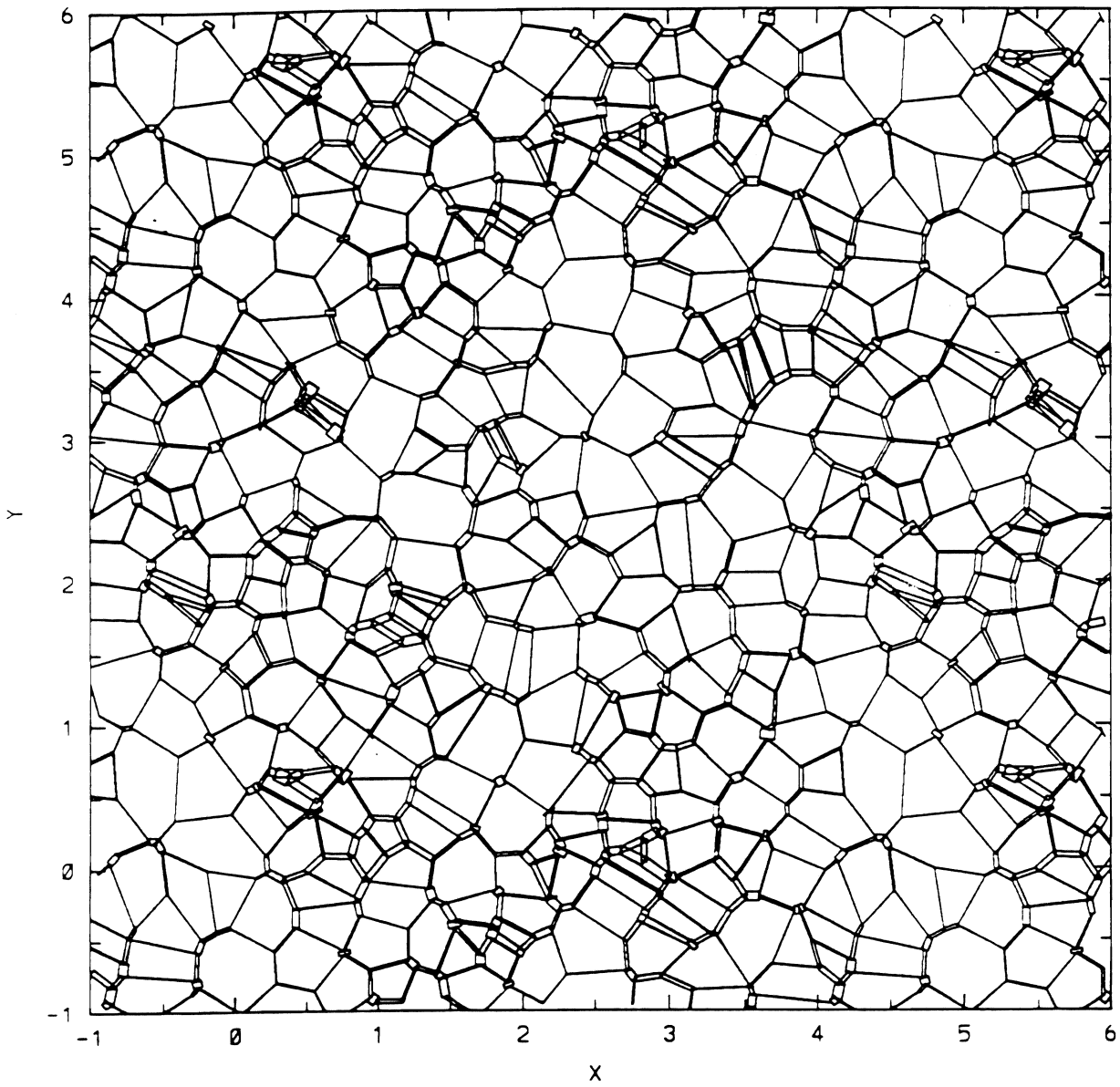

Figure 6. The same as Fig. 4, but with $\rho = 0.2$.

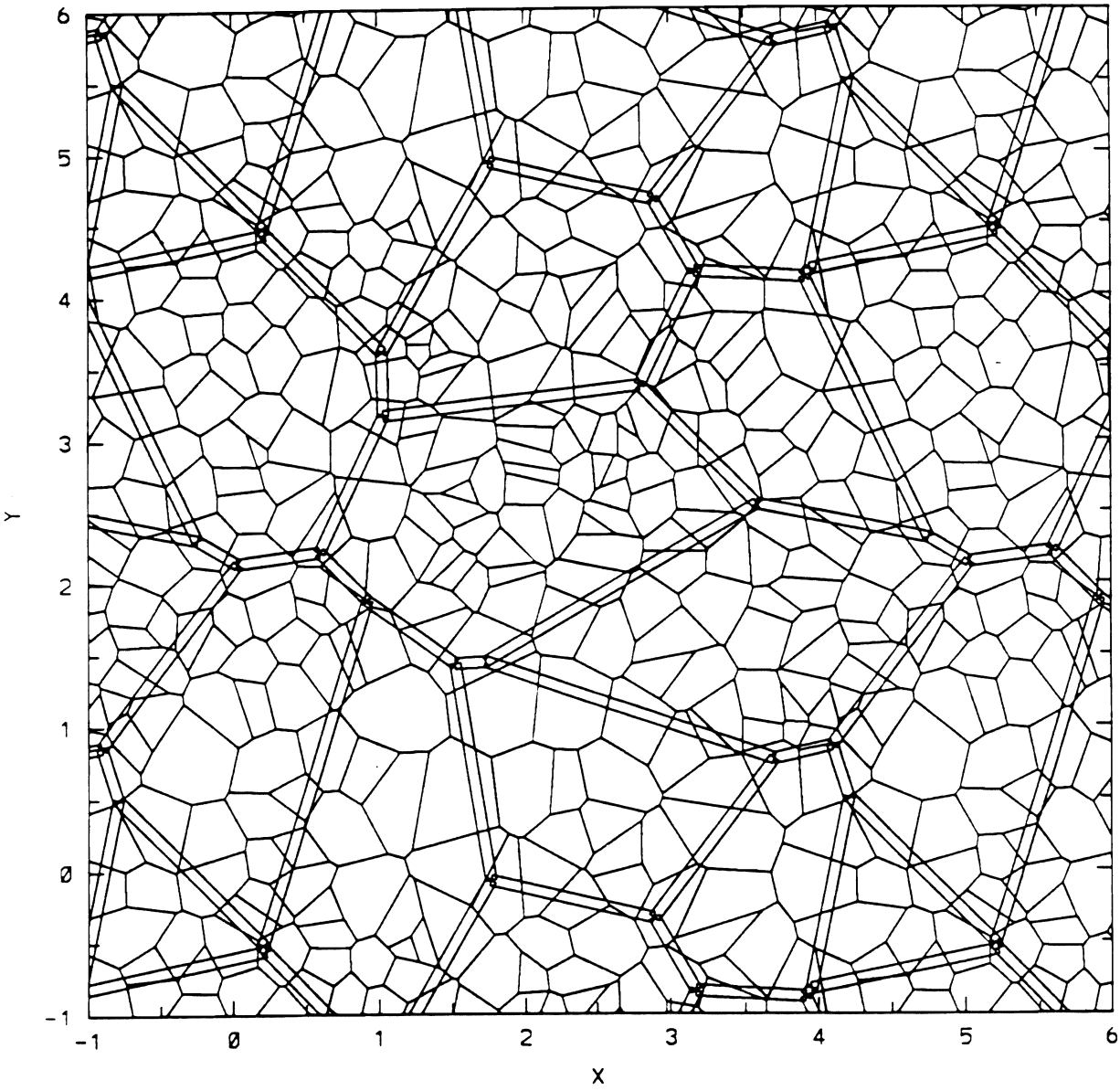

Figure 7. Two networks of cracks overlapped on the same picture. Coarser network represents bigger cracks.

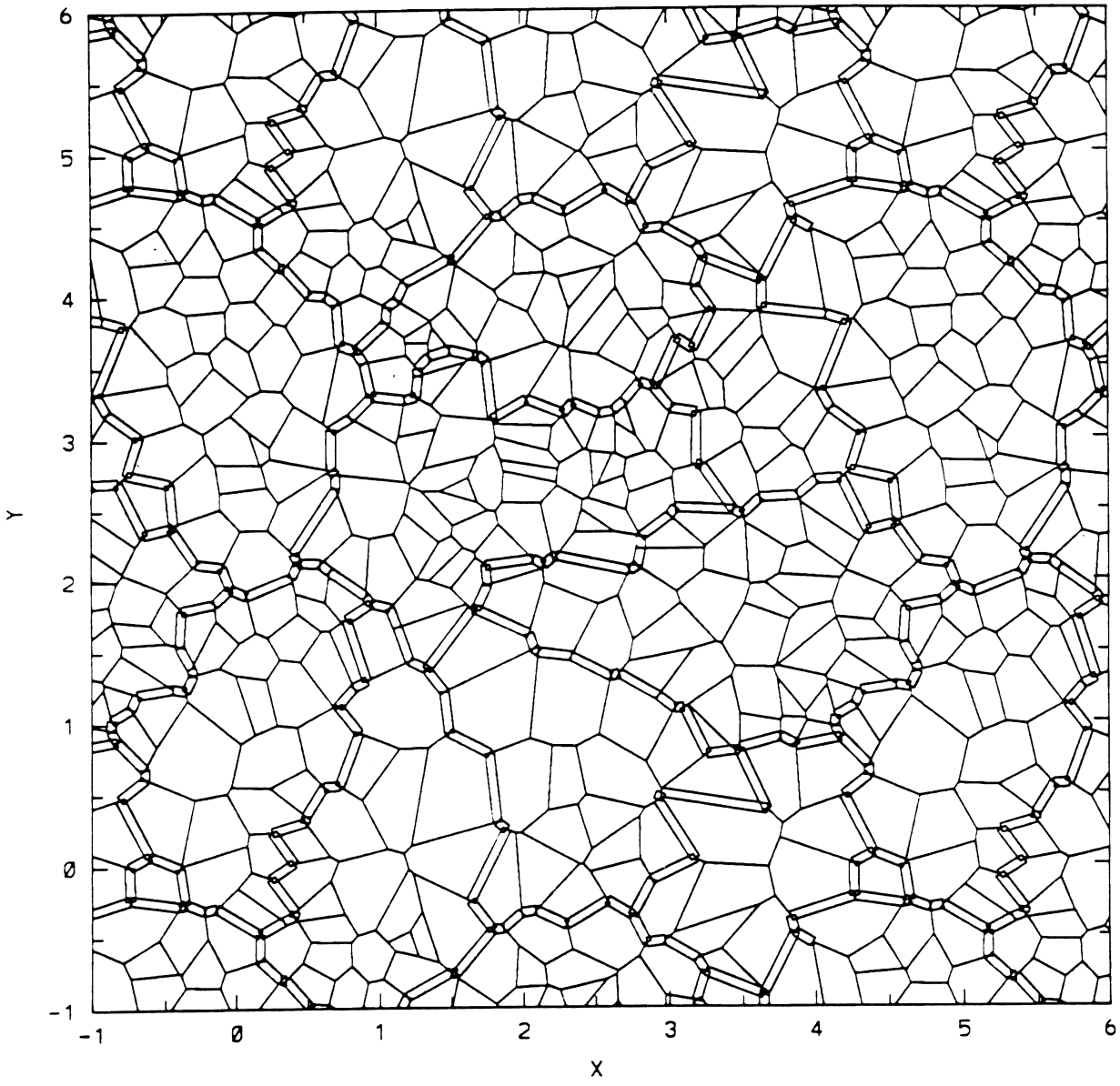

Figure 8. Projection of the coarse crack network on the fine crack network. Cracks interpolating coarser network are wider than cracks that represent finer network. The networks are the same as in Fig. 7.

Deterministic Fractal Modeling of the Spatial Patterns of Soil Contaminants

CARLOS E. PUENTE
Department of Land, Air and Water Resources, Davis Campus

Summary

Knowing the fate of contaminants in our groundwater resources is clearly one of the most important environmental questions today. In spite of the progress that has been made throughout the years, even the most advanced approaches to the problem still possess undesirable limitations (Sposito et al., 1986; Gelhar, 1986). Although sophisticated stochastic techniques may provide adequate predictions, (Gelhar and Axness, 1983; Dagan, 1984; Sudicky, 1986), it is also common to encounter situations in which this approach is unsatisfactory (Black and Freybert, 1987). Problems arise due to the underlying assumptions that are essential to the analytical development of relevant equations. Although natural conditions provide only a single soil matrix, the resulting data are considered a plausible realization of an underlying ergodic stochastic mechanism. Other convenient working assumptions, not always physically observed, include some type of spatial homogeneity and Gaussian-related probability distributions.

This research project deals with the geometric quantification of the concentration patterns that are observed when a pollutant migrates within the soil, in particular, focusing on snapshot contours of such patterns. This work represents an attempt to capture explicitly the geometrical features observed in pollution studies, i.e. the "shades of concentrations" observed. Given the intricate and rough appearance of most of the observed patterns, techniques based on deterministic fractal geometry appear ideally suited for the task of describing them (Mandelbrot, 1983). Because the observed physical shapes are mere reflections of ongoing physical mechanisms, capturing them may provide a clearer picture of how such patterns evolve in space-time.

The objective of this research is to test whether these contours, the two-dimensional geometrical features observed in pollutant concentration fields, e.g., vertically-averaged concentrations, can be described properly via iterations of appropriate sets of transformations. Given a particular contour section at a given time, the investigator is developing an appropriate set of transformations such that they reproduce, via iterations, the original contour concentrations in question. These transformations are being sought for the purpose of capturing the geometrical features of the contours with the least possible number of parameters. If such quantification may be obtained, it is conceivable that few surrogate parameters could have captured the essence of pollution migration. Consequently, future studies on the time evolution of concentration patterns may be carried out in terms of these surrogate parameters.

Figure 5 explains graphically how to generate measures that may be used to describe concentration patterns. As with the case explained in Figures 1 and 2, again there are two components needed: a multiplicative multifractal measure (the same as before) and a fractal function from one to two dimensions, "a convoluted wire." Weighing this wire by the multifractal and projecting it over the Y - Z plane yields the desired object: a bivariate multifractal measure, as seen in Figure 6.

Listed below are some of the cataloging qualifiers that are being computed for alternative bi-dimensional multifractal measures.

Results

The following statistical and fractal attributes are being computed to quantify generated measures and actual data, appropriately normalized so that they become probability measures themselves:

- Distribution, $F_{Y,Z}$
- Autocorrelation function, $\rho_{Y,Z}(\tau_1\tau_2)$
- Spectral density function, $S_{Y,Z}(\omega_1\omega_2)$
- Isotropic autocorrelation function, $\rho_{Y,Z}(r)$
- Radial spectral density function, $S_Y^R, Z(\omega)$
- Mass exponents, $\tau(q)$
- Multifractal Spectrum, $f(\alpha)$
- Multifractal moments function, $\kappa(q)$
- Co-dimension function, $c(\gamma)$
- Bivariate multifractal spectrum, $f(a,a')$

Figure 7 shows some of these qualifiers for the bivariate graph of Figure 6. Given that the cataloging exercise is being carried out at the moment, there are no general trends to indicate which sets of parameters to use at this time. Such work will be accomplished during the second year of this research project.

Figure 8 is included to illustrate that one can generate shapes that appear to describe familiar features on contamination plumes. All of these patterns, which could be thought of as evolving clockwise, are parameterized by only 5 numbers that play the role of the *p's* and *z's* above.

References

Barnsley, M.F.1988. Fractals Everywhere, Academic Press.

Black, T. C. and D. L. Freyberg. 1987. Stochastic Modeling of Vertically Averaged Concentration Uncertainty in a Perfectly Stratified Aquifer, Water Resources Research 23(6):997-1004.

Dagan, G. 1984. Solute Transport in Heterogeneous Porous Formations, Journal of Fluid Mechanics 145:151-177.

Dagan, G. 1984. Solute Transport in Heterogeneous Porous Formations, Journal of Fluid Mechanics 145:151-177.

Gelhar, L. W. 1986. Stochastic Subsurface Hydrology: From Theory to Applications, Water Resources Research 22(9):135S-145S.

Gelhar, L. W. and C. L. Axness. 1983. Three Dimensional Stochastic Analysis of Microdispersion in Aquifers, Water Resources Research 19(1):161-180.

Mandelbrot, B. B. 1983. The Fractal Geometry of Nature, Freeman.

Puente, C. E. 1992. Multinomial multifractals, fractal interpolators, and the Gaussian distribution, Physics Letters A, 161:441-447.

Sposito, G., W. A. Jury and V. K. Gupta. 1986. Fundamental Problems in the Stochastic Convection-Dispersion Model of Solute Transport in Aquifers and Field Soils, Water Resources Research 22(1):77-88.

Sudicky, E. A. 1986. A Natural Gradient Experiment on Solute Transport in a Sand Aquifer: Spacial Variability of Hydraulic Conductivity and Its Role in the Dispersion Process, Water Resources Research 22(13):2069-2082.

Presentations

Puente, C. E. and J. E. Pinzón. Bivariate multifractal measures and the geometry of correlation, American Geophysical Union Spring Meeting, Montreal, Canada, May 12-16, 1992.

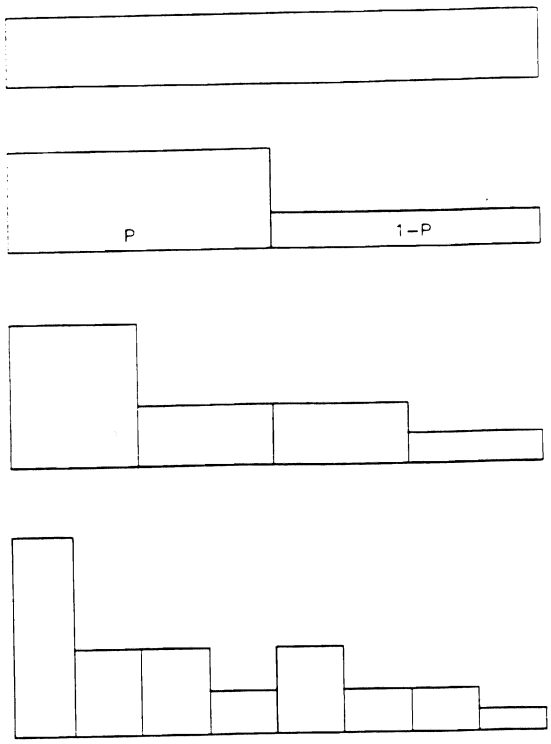

Figure 1. Construction of multifractal measure

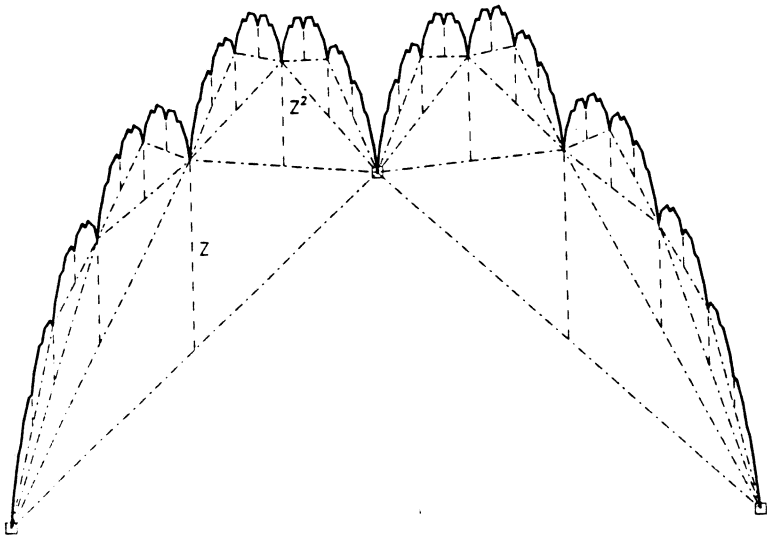

Figure 2. Construction of fractal interpolator

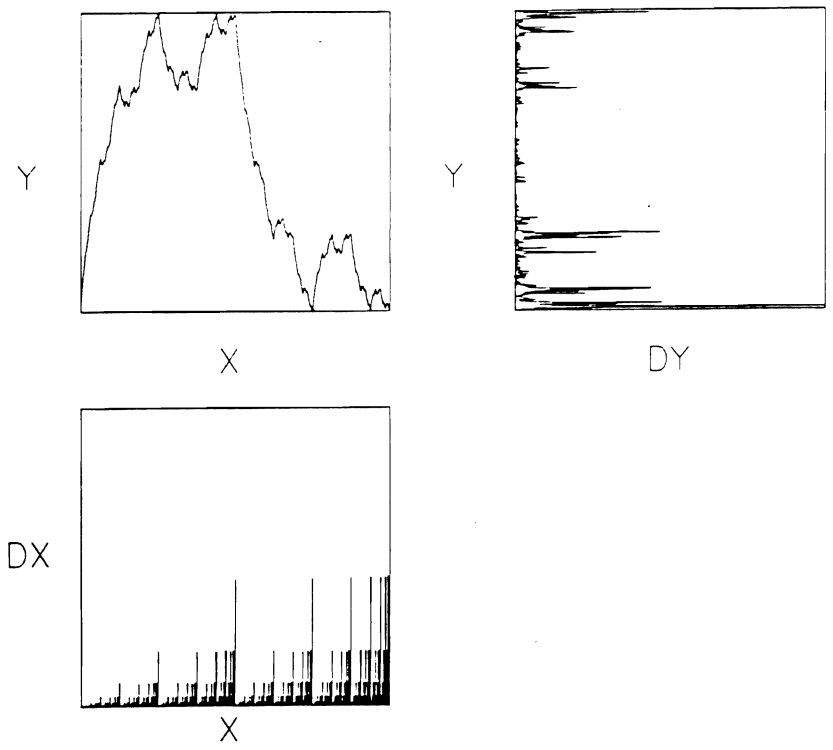

Figure 3. Fractal transformation and measures, $z = 0.51$, $p = 0.7$.

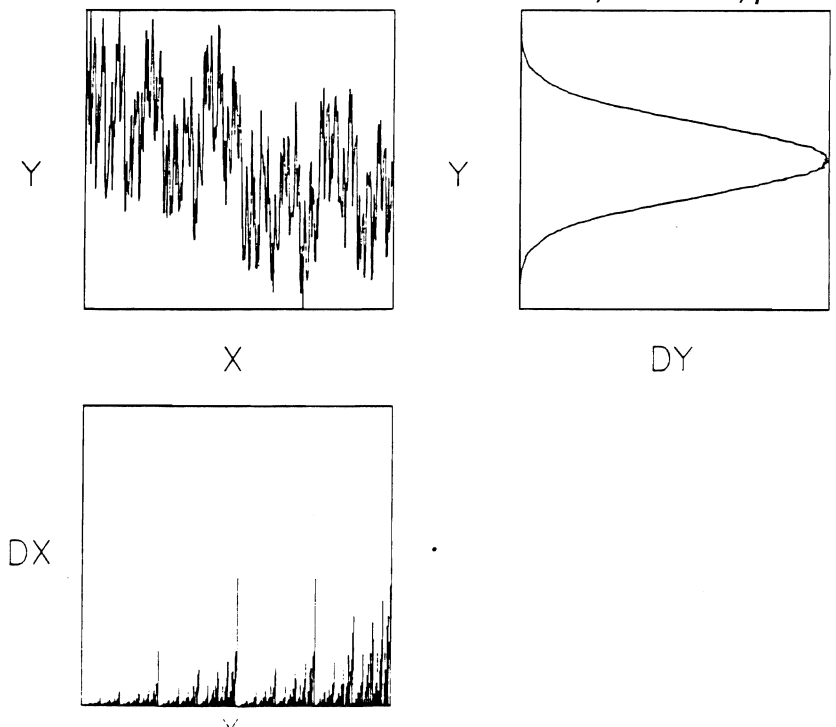

Figure 4. Fractal transformation and measures, $z = 0.995$, $p = 0.7$.

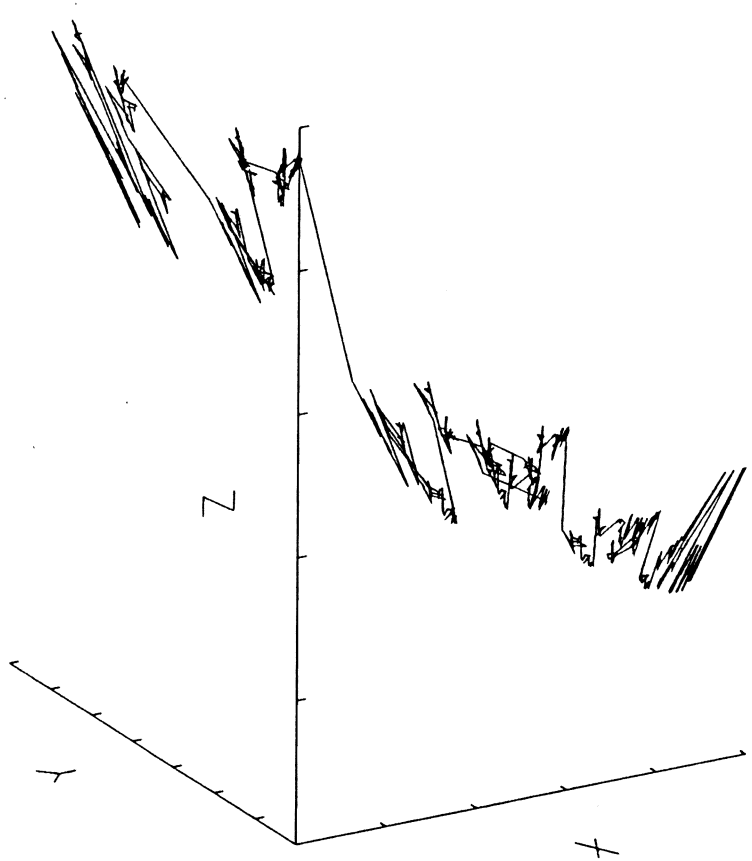

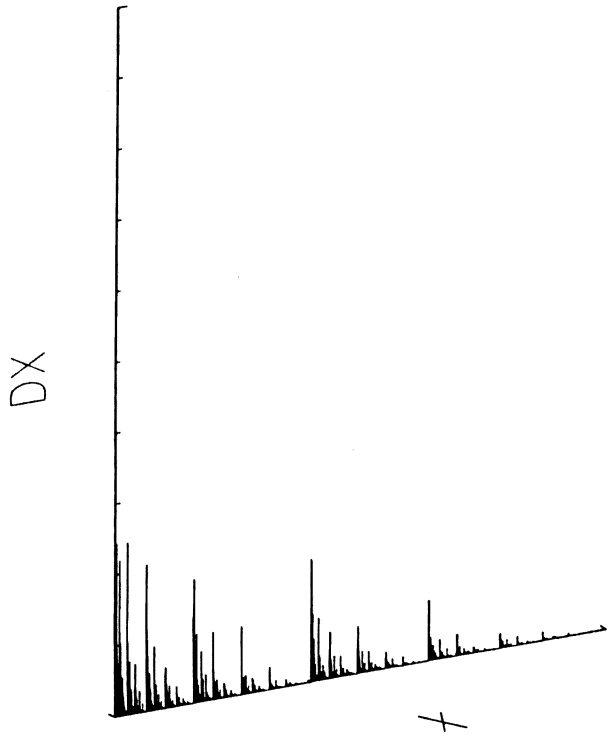

Figure 5. Construction of bivariate measure

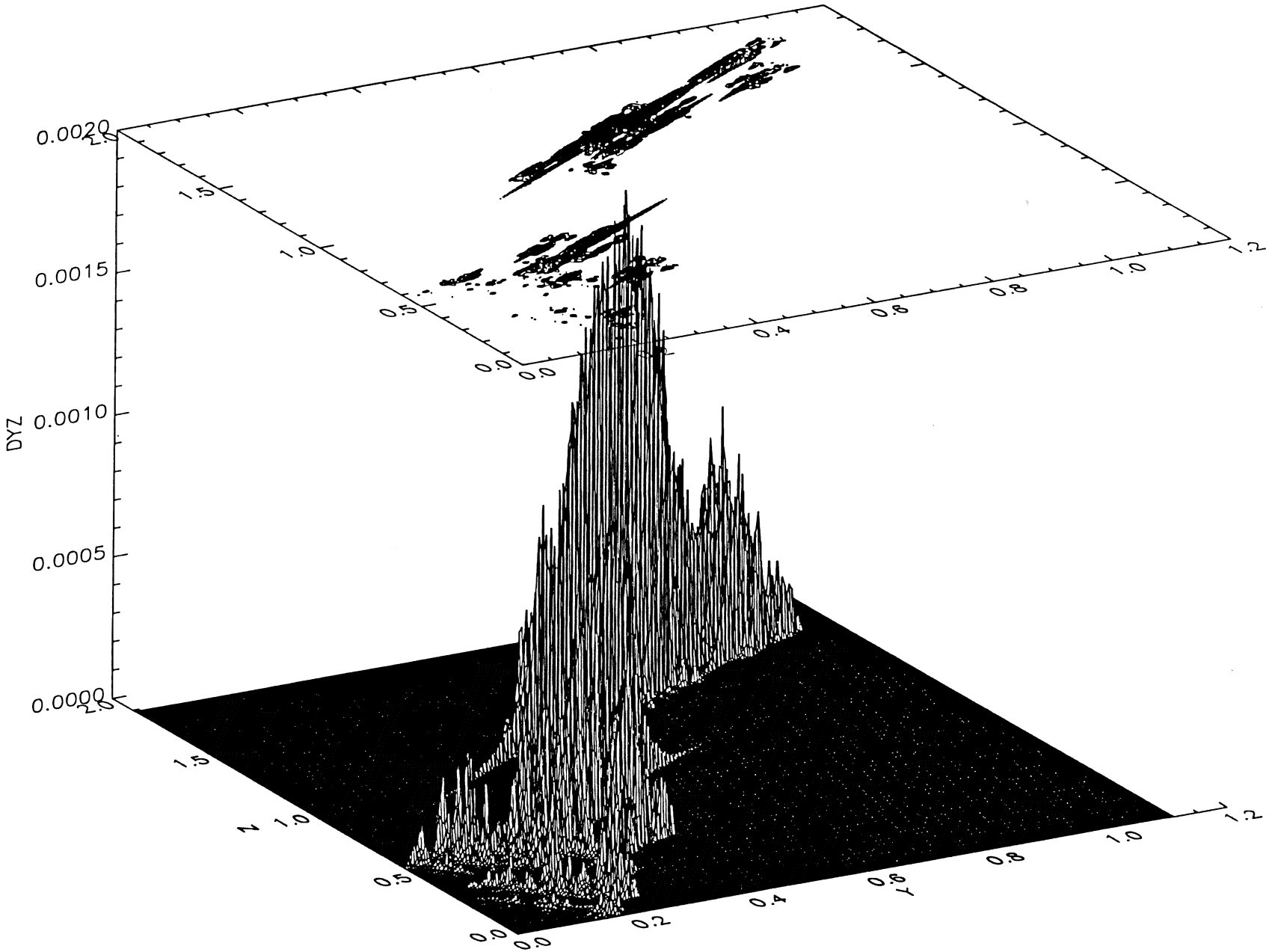

Figure 6. Derived bivariate multifractal measure.

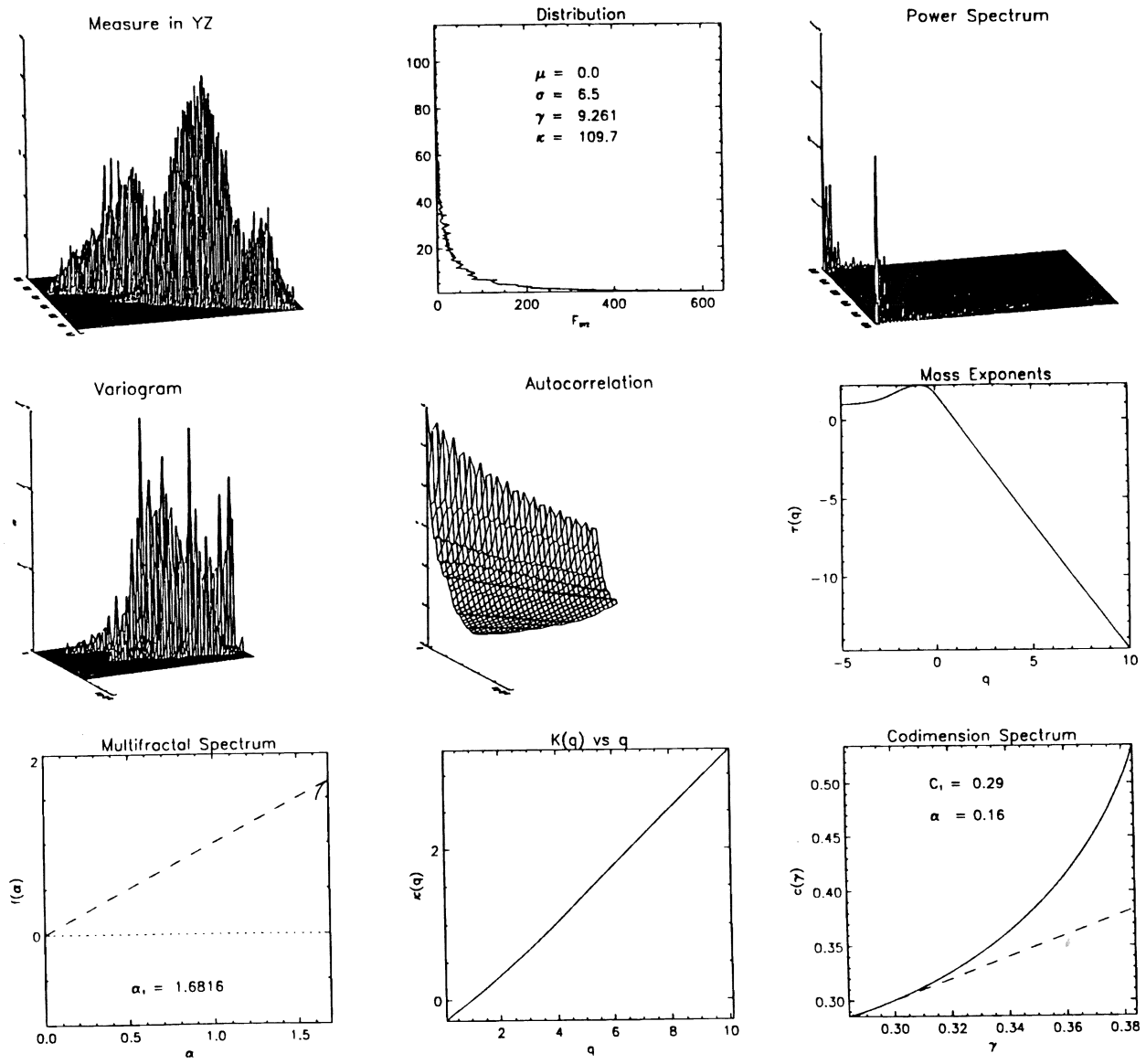

Figure 7. Statistics of derived bivariate multifractal measure.

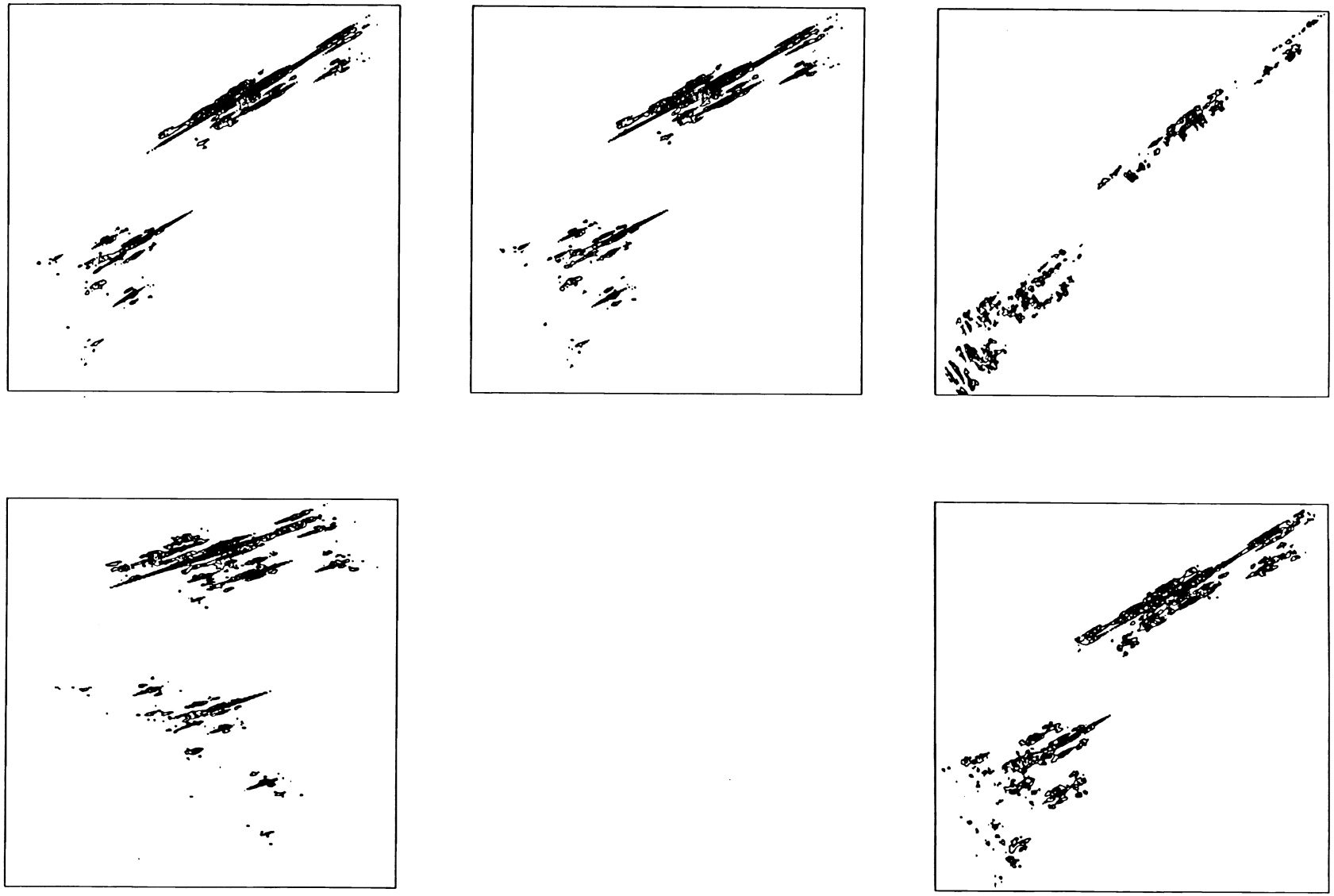

Figure 8. A plausible soil contaminant evolution.

Preferential Transport of Microbial Contaminants in Soil

MARYLYNN V. YATES
Department of Soil and Environmental Sciences, Riverside Campus

Summary

It has been well-documented that disease-causing microorganisms can travel considerable distances in soils and contaminate underlying ground water. In many instances, the contamination results in a waterborne disease outbreak. However, available models of contaminant transport in soil generally underestimate the extent and velocity of microbial movement. The purpose of this project is to examine several possible mechanisms for the preferential transport of microorganisms in soil and to establish a relationship that will allow more accurate prediction of microbial transport in soil and ground water. This will be accomplished by conducting column studies using several well-characterized soils and particles of different sizes and properties. The relationship established between soil properties and microbial transport will be validated by conducting additional column studies using new soils. The results obtained will have important implications for public water utilities that apply for a variance from the mandatory groundwater disinfection requirement to be finalized in the near future. In addition, application of the results will lead to minimizing the potential for ground water contamination by disease-causing microorganisms by elucidating appropriate practices for land application of sludge, for irrigation with treated sewage effluent, and for siting of septic tanks.

To fulfill the objectives of this research project, viruses have been used as a model to identify and quantify the factor(s) responsible for the rapid transport of human pathogenic microorganisms in soil-water systems. The rapid movement of viruses through soil has been observed in laboratory and field studies. In the experiments conducted to date, viruses and a conservative tracer were found to move at the same rate in the sand used. This was not surprising, as the pores in the soil were approximately 1000 times the size of a virus particle. Attempts to explain the low recovery of viruses (<50%) after transport through soil columns have resulted in observing a heretofore undescribed phenomenon: It appears that virus aggregates may influence transport as well as the interpretation of results of column studies. A series of experiments to define further the role of virus aggregates in the observed transport behavior is being planned. Results of these studies will be necessary in order to be able to predict accurately virus transport in the subsurface.

Key Words: virus, groundwater pollution, pathogens

Project Objectives Addressed in 1991-92

1. Determine important processes affecting the transport of viruses in well-characterized soils under carefully controlled conditions.
2. Compare the movement of virus particles with that of conservative solute tracers.
3. Establish a relationship between soil properties and the preferential transport of the virus particles relative to the conservative solute tracers.
4 Validate the relationship established in (3) by predicting viral behavior in different soils.

Research Plan and Procedures

Column Experiments The column experiments were conducted in a 30-cm-long plastic column. Soil was packed in the column to achieve a bulk density of 1.47 g cm^{-3}. All column experiments were performed using the same soil type, sand that had been sieved to a size that passed through a #20 sieve, but was retained in a #35 sieve. Each experiment was performed using a freshly packed column. Prior to tracer addition, the soil in the column was saturated by adding water from the bottom of the column to decrease the possibility of forming air bubbles. Carbon dioxide was applied to the column to increase the degree of water saturation.

After steady-state flow conditions were achieved, the tracers were added as a pulse to water ponded on the soil surface. Column effluent samples were collected for 2-8 pore volumes and stored until analysis, as described below.

Determination of Soil Pore Size Distribution The distribution of pores in the experimental soils was determined using a modification of the water desorption method (Danielson and Sutherland, 1986). The apparatus necessary to determine the pore size distribution had to be constructed, as none was available in the department. To determine the pore size distribution, a saturated soil sample was placed on a ceramic plate, and tension was applied to the plate. The amount of water released from the soil was measured at several increasing levels of tension, until water was no longer released from the soil. A moisture-characteristic curve was determined, and the effective pore-size distribution calculated from capillary theory.

Virus Analyses MS2 coliphage analyses were performed using the double-agar overlay technique of Adams (1959) with *E. coli* ATCC strain 15597 as the host bacterium. One ml of the appropriate dilution of sample and one ml of a log- phase culture of *E. coli* were added to a tube of molten tryptic soy agar (TSA). The tube was mixed, then the contents poured onto plates of TSA. The plates were incubated overnight at 37° C. Viruses in the sample infected the *E. coli*, causing lysis of the cell and spread to surrounding cells. After approximately 9 h, a sufficient number of bacterial cells were lysed to form a clear area, or plaque, in the lawn of bacteria on the agar surface. In this method, each plaque is assumed to be the result of one infective virus particle.

Nitrate Analyses All nitrate analyses were performed using the Alpkem flow-through analyzer.

Results

Soil Characterization The pore size distribution of the sand used in the column experiments is given in Table 1, and the moisture characteristic curve is shown in Figure 1. The largest fraction (41%) of soil pores had a radius of 0.0059 cm, and the smallest pores measured 0.0033 cm.

Column Experiments To date, four column tracer experiments have been performed. A summary of these experiments is given in Table 2. Peak virus concentrations were measured at 1.02-1.25 pore volumes, while the nitrate peaks occurred at 1.08 and 1.14 pore volumes. A typical breakthrough (from Experiment 2) is shown in Figure 2.

Discussion

The efforts during the first year of this project have focused on constructing the apparatus required to determine the pore-size distribution and perfecting the column experiment protocol. Now that this has been accomplished, the rate at which experiments can be performed has increased substantially.

In all experiments performed to date, the peak virus and nitrate concentrations occurred at approximately one pore volume. The similarity between the tracers is not unexpected, as even the smallest pores (0.0033 cm = 33,000 nm) in the soil used are 1000 times the size of a single virus particle (27 nm). One would predict that all pores in this soil would be equally capable of transporting viruse; thus, no early arrival or shift in mean travel time should occur. Observations made in a related study of virus and bromide movement in a field soil demonstrated that a small fraction of viruses arrived much earlier than the conservative tracer. The mechanism responsible for this observation has not yet been elucidated. Experiments to be conducted during the second year of this research project will test the transport behavior of viruses in soils with pores small enough that preferential transport should be observed.

The low recovery percentage of viruses in the column experiments (21-44%) prompted a number of peripheral experiments to determine the cause of this observation. Experiments to quantify the loss of viruses due to physical inactivation during the time course of the experiments revealed that only approximately 2% of the input number of viruses could be expected to be inactivated during the 5-8 h of an experiment. After experiments 1-3 were conducted, the columns were destructively sampled and the soil analyzed for viruses adsorbed to the soil surface. In all cases, less than 1% of the input viruses could be recovered. Therefore, further investigations were conducted to determine the fate of the remaining 50% or more of the viruses.

As stated previously, the method used to enumerate the viruses assumes that each plaque represents one infective virus particle. If, however, the viruses are present as aggregates, each aggregate would result in the formation of one plaque, and thus be counted as one virus particle. A series of experiments has been initiated to determine the role of aggregation in virus transport through soil columns.

In experiment 3, the column effluent samples obtained during the peak of the breakthrough curve were split and analyzed using two methods. The first method was the standard method in which the samples are diluted in 1% peptone to the appropriate level and then analyzed. The second method consisted of diluting the samples in a solution of 6% beef extract, pH 9. Beef extract is used extensively to desorb viruses from soil and is believed to work by disrupting hydrophobic interactions between the virus and soil surface. The motivation for using beef extract to analyze effluent samples was that if aggregates were present, the beef extract could cause the viruses to de-aggregate by disrupting hydrophobic interactions. The results of this experiment are shown in Table 3. The samples analyzed using beef extract had higher virus concentrations than did those analyzed using the standard method. In fact, the total difference in the number measured using the beef extract method comprised 26.6% of the input concentration. In a second experiment, experiment 4, all samples were split and analyzed using both the standard method and the beef extract method. The virus recovery using the beef extract method was 57% of the input concentration, compared with 38% using the standard method.

There are several implications of this finding. In most environmental situations (i.e., water and wastewater), viruses are present in the aggregated or solid-associated state (Sobsey et al., 1991). If virus aggregates become de-aggregated during the transport process, it will be important to determine the conditions under which this occurs, so that this phenomenon can be considered, if not quantified, for public health applications. Another implication is of more interest academically than practically and is related to the use of beef extract to desorb viruses during column experiments. If, in fact, as we have shown, beef extract is capable of not only desorbing viruses from soil particles but also of breaking up virus aggregates, then investigators (e.g., Bales et al., 1991) reporting high virus recoveries after application of beef extract to soil columns may have reported inaccurately high numbers. This has real implications for modeling accurately virus survival and transport in the subsurface. A series of experiments is being planned to examine further this observation. A manuscript describing this observation will be prepared as soon as all necessary supporting evidence is obtained.

References

Adams, M.H. 1959. Bacteriophage. Interscience Publishers, New York Bales, R.C., S.R. Hinkle, T.W. Kroeger, K. Stocking, and C.P. Gerba. 1991.Bacteriophage adsorption during transport through porous media: chemical perturbations and reversibility. Environ. Sci. Technol. 25:2088-2095.

Danielson, R.E. and P.L. Sutherland. 1986. Porosity. In: Methods of Soil Analysis. A. Klute, Ed. American Society of Agronomy, Inc., Madison, Wisconsin.

Sobsey, M.D., T. Fuji, and R.M. Hall. 1991. Inactivation of cell-associated and dispersed hepatitis A virus in water. J. Amer. Water Works Assoc. 83: 64-67.

Table 1. Soil pore size distribution

Tension (cm)	Pore Radius (cm)	% Total Pore Space
0		
2	0.0734	1.3
4	0.0367	2
7	0.021	3.4
10	0.0147	7.2
15	0.01	13.3
20	0.0073	16.9
25	0.0059	41.3
30	0.0049	3.3
35	0.0042	1.7
40	0.0037	1.2
45	$\leq$0.0033	2.1

Table 2. Summary of column experiments.

Experiment	Tracer Input		Peak Time (pore volumes)		% Recovered	
	MS-2[1]	Nitrate[2]	MS-2	Nitrate	MS-2	Nitrate
1	1 E07		1.25		39	
2	6.9 E06	10	1.14	1.14	21	90
3	6.4 E08	25	1.14	1.08	44	110
4	4.3 E08		1.02		38	

[1] PFU (plaque-forming units)
[2] mg

Table 3. Effect of beef extract on virus enumeration

Sample No.	PFU* (std. assay)	PFU (beef extract)	Difference
12	1.379 E07	4.165 E07	2.786 E07
13	3.8115 E07	5.676 E07	1.8645 E07
14	5.274 E07	8.172 E07	2.898 E07
15	6.771 E07	8.177 E07	1.406 E07
16	2.145 E07	6.000 E07	3.855 E07
17	1.8725 E07	4.165 E07	2.2925 E07
18	1.3125 E07	2.80 E07	1.4875 E07
22	1.445 E06	5.95 E06	4.505 E06
TOTAL	2.271 E08	3.975 E08	1.704 E08

* PFU = plaque-forming unit

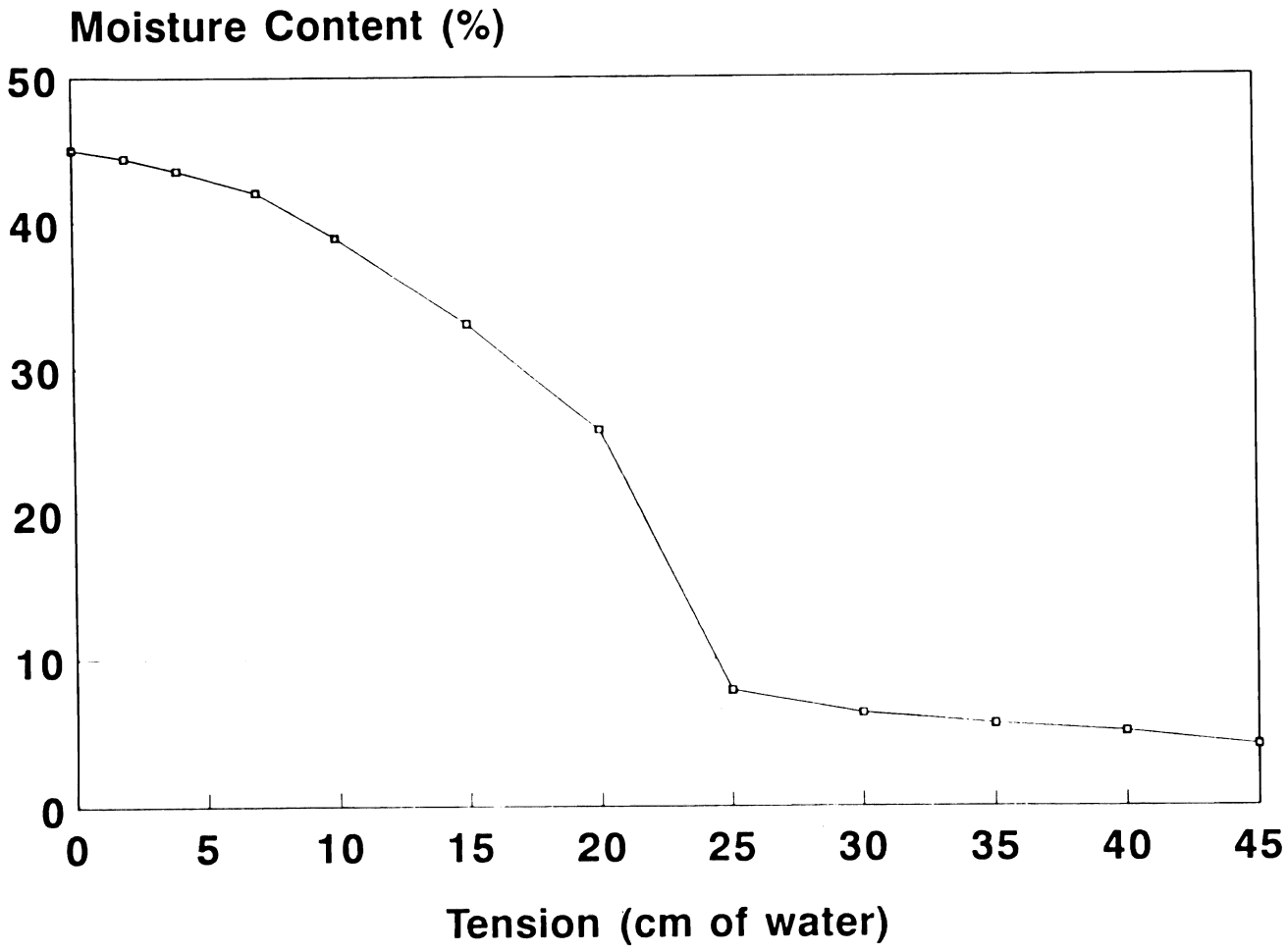

Figure 1. Soil moisture characteristic curve

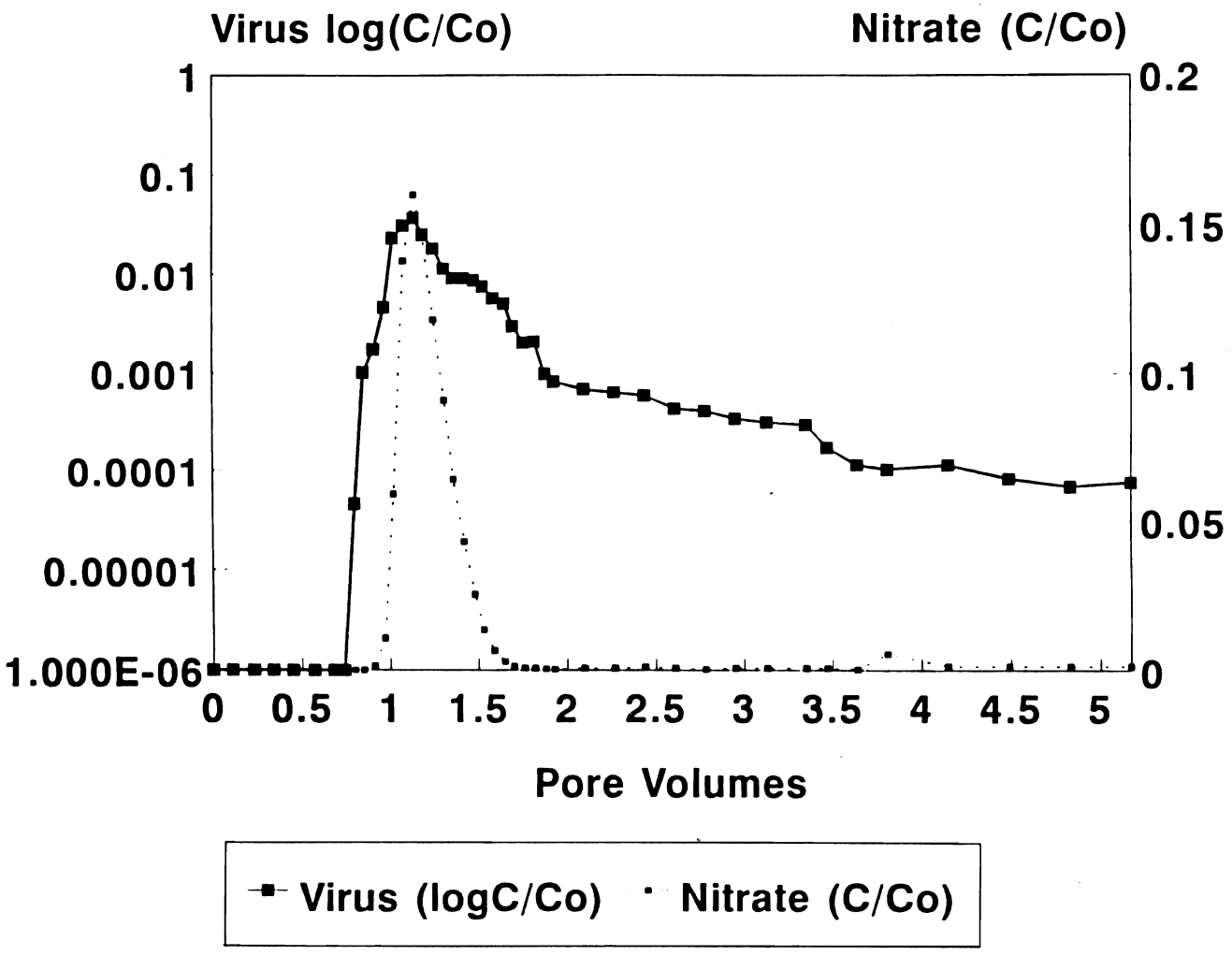

Figure 2. Virus/nitrate breakthrough curve

Density-Driven Flow and Multinary Diffusion of Volatile Organic Chemicals in the Unsaturated Zone

DENNIS E. ROLSTON
Department of Land, Air and Water Resources, Davis Campus

Summary

Volatile organic chemical (VOC) liquid mixtures contaminating many underground sites give rise to multi-component mixtures of their vapors. Fick's first law is inherently not suitable to track the simultaneous diffusion of more than one gas in soils; thus, the more rigorous multi-component formulations arising from the kinetic theory of gases are utilized to approximate fluxes within a multinary mixture of non-uniform gases. Previous investigators have shown that in an isobaric, isothermal multi-component vapor system, when the effective binary diffusion coefficients D_{ij} for any species i with the other species j are sufficiently different (a factor of 2 reported), Fick's estimate of the flux for each species should not be used. Our theoretical investigation of a multi- component semi-hypothetical "gasoline" mixture, containing relatively volatile aromatic constituents plus carbon tetrachloride as an additional component, shows that the multi-component effect can also be observed when the D_{ij} are not substantially different, which occurs when the total mole fraction of the diffusing species is sufficiently high.

During this two-year investigation, differential equations for multinary diffusion and density-driven flow of VOCs are being derived from general kinetic equations of non-uniform gases. Solutions to these equations are being determined by analytical and numerical techniques. Using the derived solutions, sensitivity analyses are being conducted in order to provide insight into which soil conditions and for what VOCs the effects of multinary diffusion and density-driven flow will be important. Laboratory column experiments are being conducted for VOCs with a range of densities and vapor pressures and for an air-dry soil. Soil and environmental conditions are being identified for which simplifications of the more rigorous theory can be used. This research project will result in improved mathematical solutions and models for density-driven flow and multinary diffusion of toxic VOCs in the unsaturated zone.

Key Words: multi-component diffusion, pressure diffusion, volatile organics, gas phase flow, gasoline.

Project Objectives Addressed in 1991-92

1. Derive the differential equations for multinary diffusion and density-driven flow of volatile organic chemicals (VOCs) from general equations developed from the kinetic theory of gases.

2. Determine solutions to these differential equations. For the simple binary cases, analytical solutions may be possible. For systems with more than two vapor species, numerical techniques need to be employed to solve the n simultaneous equations for n different VOCs existing in the soil.

Research Plan and Procedures

Theory: For a binary system, the number-averaged velocities (cm/sec) of the two gases v_i and v_j with respect to the mean velocity of the mixture in one dimension are related to each other by (Chapman and Cowling, 1970, pp257)

$$v_i - v_j = -\frac{n^2}{n_i n_j} D_{ij} \left\{ \frac{\partial n_i / n}{\partial r} + \frac{n_i n_j (m_j - m_i)}{n \rho p} \frac{\partial p}{\partial r} - \frac{\rho_i \rho_j}{p \rho} (F_i - F_j) + K_T \frac{1}{T} \frac{\partial T}{\partial r} \right\} \quad (1)$$

where n and n_i are the number densities (molecules/cm^3) for the mixture and species i, respectively; r is the spatial vector (cm); m_i is the mass of one molecule of species i (g);ρ and ρ_i are the mass densities (g/cm^3) of the mixture and of gas i, respectively; p is the total gas pressure (Pa) in the volume element of thickness ∂r; F_i is the external force vector per unit mass of species i; $K_T=D_T/D_{ij}$ is the thermal diffusion ratio, where D_T is the thermal diffusion coefficient; T is temperature (K); D_{ij} is the effective binary diffusion coefficient (cm^2/sec) in soil for species i and j. D_{ij} is related by the Millington-Quirk tortuosity model (Millington and Quirk, 1961) to the binary diffusion coefficient in the absence of a porous medium D^b_{ij} where

$$D_{ij} = D^b_{ij} \frac{\theta_a^{10/3}}{\phi^2} \quad (2)$$

θ_a is the soil air content, and ϕ is the soil porosity.

In (1) F_i s are due to external forces which impart different accelerations to different species of molecules. For VOC vapor transport in soils, gravity is the only external force assumed. Gravity imparts equal acceleration (force per unit mass) to all molecules, hence the term involving (F_i-F_j) becomes zero. Thermal diffusion appears to be minimal (Grew and Ibbs, 1952). It requires high temperature gradients which are not experienced under the normal diurnal conditions. Equation (1) is then written as

$$v_i - v_j = -\frac{n^2}{n_i n_j} D_{ij} \left\{ \frac{\partial (n_i/n)}{\partial r} + \frac{n_i n_j (m_j - m_i)}{n \rho p} \frac{\partial p}{\partial r} \right\} \tag{3}$$

The first term in brackets in (3) represents the driving force for the ordinary or molecular diffusion in response to a concentration gradient. The second term describes the contribution to the total diffusive flux in response to a pressure gradient. A pressure gradient causes the heavier (lighter) molecules to diffuse towards the regions of greater (lower) pressure. Therefore, under the natural atmospheric pressure gradient, the heavier molecules tend to diffuse downward along the direction of gravity. The atmospheric pressure gradient is small but is expected to become more significant in the VOC vapor diffusion as profile depth increases. Even though many contaminated sites are situated in profiles with maximum depth to water table of only tens of meters, new repositories are chosen on sites with maximum distance to the water table. Therefore, we would like to retain this flow component to investigate its significance to the total diffusive flux.

Curtiss and Hirschfelder (1949) present the following equation for a multi-component mixture of species 1 through s,

$$\sum_{j=i, i \neq j}^{s} \frac{y_j J_i - y_i J_j}{D_{ij}} = -\frac{p}{RT} \left\{ \frac{dy_i}{dx} + \left(y_i - \frac{\rho_i}{\rho} \right) \frac{1}{p} \frac{dp}{dz} \right\} \tag{4}$$

This form in one dimension z reduces exactly to equation (3) for a binary system when we note the following relationships

$$J_i = \frac{n_i v_i}{M_o}, \quad y_i = \frac{n_i}{n}, \quad \frac{n}{M_o} = \frac{p}{RT}, \quad \rho = \sum_{i=1}^{s} \rho_i = \sum_{i=1}^{s} n_i m_i$$

where M_o is Avogadro's number; J_i, the molar flux of i; y_i, the mole fraction of i; p, the atmospheric pressure; R, the universal gas constant; and r has been replaced by z, which represents the vertical direction. Writing the diffusion flux in terms of the gradient of mole fraction, not molar concentration, is preferable since mass or molar concentrations vary strongly with temperature, but the mole fraction is much more nearly constant, independent of temperature (Cussler, 1984, pp 463). Air will be designated as species s henceforth. When the horizontal direction x is considered, dp/dx=0 and equation (4) reduces to the well-known Stefan-Maxwell equation,

$$\sum_{j=i, i \neq j}^{s} \frac{y_j J_i - y_i J_j}{D_{ij}} = -\frac{p}{RT} \frac{dy_i}{dx} \tag{5}$$

The Stefan-Maxwell fluxes calculated from equation (5) when subtracted from the total fluxes given by equation (4) will furnish the pressure diffusion fluxes. In

(4) and (5), since $\sum_{i=1}^{s} y_i = 1$, they comprise *s-1* equations for s unknowns and are indeterminate. However, at steady-state, soil air is stagnant so that its flux can be set equal to zero. This enables a solution of (4) and (5) to be determined.Equations (4) and (5) are written in a form where they involve y_i as the only dependent variable and are solved by a numerical simulation procedure.

Results and Discussion

The fluxes simulated for several binary cases were virtually the same as the predictions using Fick's law. For multinary cases, the outputs of our program were compared to the simulation results of Leffelaar (1987) and the experimental data (Table 1) of Baehr and Bruell (1990). Simulations of vapor transport for a representative gasoline mixture (Cline et al., 1991) were performed to gain insights into the effect of multinary vapor mixtures on single species transport and the vapor plume at steady-state.

The system studied and modelled by Baehr and Bruell (1990) is a more simplified system than what is under study here. Their study involved two stagnant gases in a ternary system. The two stagnant gases O_2 and N_2 acted very similarly with respect to the diffusion of the third gas in their ternary mixture. Effectively, the third gas behaved as in a binary system consist of itself and one other gas - "air". When more complex, albeit hypothetical, systems involving the same ternary systems with only one stagnant gas are studied, the results show different behaviors for the moving species than when two species are stagnant. In these hypothetical cases, the concentration gradient of O_2 gas is opposite to the VOC vapor. In a vapor mixture arising from a multi-component liquid VOC mixture, all moving species have gradients in the same direction. Therefore, the results of these hypothetical cases are not directly applicable to a mixture of VOC vapors diffusing in a stagnant soil air. The systems studied by Leffelaar (1987) are either similar to those in Baehr and Bruell (1990), with two stagnant species, or correspond to equimolar counter-current diffusion. What still needs to be investigated is the co-current diffusion of gases in a mixture when one species is stagnant.

In order to investigate the magnitude of the multinary effect on vapor diffusion, we used the liquid gasoline composition reported in Table 2 of Cline et al. (1991). They give weight percentages in the fuel for a few gasoline components which were identified in the aqueous extract of their mixture. For the purposes of our analysis, we assumed our "gasoline" to be composed only of these species with their average weight ratio as reported in Cline et al. (1991). We replaced n-propylbenzene and 3-, 4-ethyltoluene with carbon tetrachloride (CCl_4), a solvent, which may accompany organic contaminant mixtures at spill or dump sites. The choice of CCl_4 was also influenced by its high vapor pressure and high molecular weight relative to other components in the system. In this way, a wider range of vapor pressures than was in the original mixture could be investigated. The weight ratio of CCl_4 was set equal to

the sum of the ratios of n-propylbenzene and 3-, 4-ethyltoluene in the original mixture. In this way, the relationship between the other species and the mixture as a whole was not disturbed. Table 2 contains some properties of these substances. The soil column for the following simulations was assumed to have r_b=1.325 g/cm^3, q_w=0.06, and length=1.0 m. All the binary diffusion coefficients needed as input to the program were calculated using the method of Fuller et al. (1966) and are given in Table 3. The effective binary diffusion coefficients are calculated using Equation 2.

Table 4 contains the percentage departures from Fick's fluxes obtained for various amounts of the VOC species in the gas phase. In run 1, all the constituents have their liquid weight fractions as reported in Cline et al. (1991) with the changes discussed above. In runs 2 and 3, the more volatile species, CCl_4, benzene, and toluene, have ten times more and less weight in the liquid mixture than in run 1, respectively. The former corresponds to a mixture of highly volatile species and the latter to a liquid mixture in which less volatile species are predominant. Or they could correspond to mixtures in which the more volatile species leave the liquid phase more quickly than the less volatile ones. The liquid composition then would change to a less volatile one than what was initially present. Run 4 corresponds to a situation in which species with similar binary diffusion coefficients are grouped together to form a representative species.

The percentage departures for runs 1 and 3 reported in Table 4 indicate that when total VOC vapor mole fraction is low, Fick's law is adequate to model fluxes of each species independently from the other species. In run 3, the total vapor phase mole fraction occupied by VOCs is 0.0176 and the percentage departures are relatively very small. When VOCs occupy 0.0428 of the total gas volume in run 1, the presence of the other VOC molecules in the system begins to exert a minimal effect. This effect increases to rather significant levels for many of the species when the total volume of air occupied by VOC vapors increases to 0.0615 (run 2). Thibodeaux et al. (1988) stated a limit of 5% by volume (0.05 mole fraction) concentration in air was sufficient to cause deviations from Fick's law estimates of single species diffusion through landfill covers. The values of D_{ij} reported in Table 3 show less than a twofold difference between the species but more between each species and air. This means that in addition to the observation of Leffelaar (1987), the multi-component effects can become significant above a certain total mole fraction of diffusing species. This total mole fraction as indicated by simulations for our "gasoline" mixture seems to be about 0.05 mole fraction or 5% concentration by volume. Below this level, the gases diffuse effectively as though in a binary system of each with the bulk soil air. Needless to say, the increasing importance of flux inter-dependence in a multi-component mixture at higher total mole fractions is irrespective of the presence of any particular porous medium.

The percent differences in Table 4 provide other observations. First, they are all positive, indicating overprediction by Fick's law compared to the multi-component predictions. The binary diffusion coefficients of each VOC species with others given in Table 3 are all less than with air. Therefore, the binary

encounters between the VOC molecules cause slower fluxes than if all the encounters were with the "air" molecules. Furthermore, the flux of 1,2,3-trimethylbenzene, which has the smallest diffusion coefficient, is reduced the most, and benzene, with the largest diffusion coefficient, is reduced the least. Finally, the magnitude of the multi-component fluxes and Fick's estimated fluxes change with the air content and porosity of the medium (data not shown) but the percent difference between them does not depend on the properties of the soil medium.

The three species, ethylbenzene, p-xylene, and o-xylene, have similar diffusion coefficients in all other species. Even though this may be an artifact of using the Fuller et al. (1966) method, their binary diffusion coefficients with other components of the system are expected to be very similar due to their similar molecular geometry and equal molecular weight. Hence they were grouped together as one component in the multinary "gasoline" system investigated. The diffusion coefficients and equilibrium single species vapor pressure of the grouped component are molar averaged from the species comprising the group. The total VOC mole fraction is then similar to run 1 whose liquid weight fractions were used. The percent differences indicate that combining similar species in a group leads to virtually the same system as in run 1.

Conclusions

Steady-state fluxes of vapors in a multi-component volatile organic hydrocarbon mixture were calculated based on equations from gas kinetic theory for soil columns with constant boundary conditions. These fluxes were then compared to Fick's estimates using the same boundary conditions. The comparisons indicate that when the total mole fraction of the VOC vapors in air exceeds about 0.05, Fick's law may overpredict the vapor flux for each species significantly. The overprediction is higher (lower) for the species with lower (higher) diffusion coefficients in bulk gas (e.g. air). Below a total mole fraction of 0.05, Fick's law can be used adequately to describe diffusion for each species independent of others. This condition for applicability of Fick's law to isobaric multi-component diffusion needs to be added to the requirement that the binary diffusion coefficients of the diffusing species have to be sufficiently different for multi-component effects to be observed (Leffelaar, 1987). When gas species are similar in terms of their vapor diffusion coefficients with other species, they can be grouped together as one species. For this reason, O_2 and N_2 can be combined to form "air", and various similar VOC species can be grouped likewise to form one representative gas. This reduces greatly the number of equations to be solved numerically.

Various sinks reduce the concentration of species in the gas phase which reduces the interdependence of VOC vapor fluxes and reduces the magnitude of the pressure diffusion flux. The effect of the various mass-exchange processes and density-induced convective flow upon the total transport of VOC vapors in a multi-component mixture will be investigated during the second year of this project.

References

Baehr, A.L. and C.J. Bruell. 1990. Application of the Stefan-Maxwell equations to determine limitations of Fick's law when modeling organic vapor transport in sand columns. Wat. Res. Res. 26(6):1155-1163.

Chapman, S. and T.G. Cowling. 1970. The Mathematical Theory of Non-Uniform Gases. 3rd edition. Cambridge University Press.

Cline, P.V., J.J. Delfino, and P.S.C. Rao. 1991. Partitioning of aromatic constituents into water from gasoline and other complex selvent mixtures. Env. Sci. Tech. 25:914-920.

Corapcioglu, M.Y. and A.L. Baehr. 1987. A compositional multiphase model for groundwater contamination by petroleum products 1. Theoretical considerations. Wat. Res. Res. 23(1):191-200.

Curtiss, C.F., and J.O. Hirschfelder. 1949. Transport properties of multi-component gas mixtures. The J. of Chem. Phys. 17(6):550-555.

Cussler, E.L. 1984. Diffusion:Mass Transfer in Fluid Systems. Camb. Univ. Press.

Duncan, J.B. and H.L. Toor. 1962. An experimental study of three component gas diffusion. AIChE J. 8(1):38-41.

Falta, R.W., I. Javandel, K. Pruess, and P.A. Witherspoon. 1989. Density-driven flow of gas in the unsaturated zone due to the evaporation of volatile organic compounds. Wat. Res. Res. 25(10):2159-2169.

Grew, K.E. and T. L. Ibbs. 1952. Thermal Diffusion in Gases. Cambridge University Press, Cambridge, MA.

Hirschfelder, J.O., C.F. Curtiss, R.B. Bird. 1964. Molecular Theory of Gases and Liquids. Wiley, New York.

Leffelaar, P.A. 1987. Dynamic simulation of multinary diffusion problems related to soil. Soil Sci. 143(2):79-91.

Mendoza, C.A. and E.O. Frind. 1990. Advective-dispersive transport of dense organic vapors in the unsaturated zone 1. Model development. Wat. Res. Res. 26(3):379-387.

Millington, R.J. and J.M. Quirk. 1961. Permeability of porous solids. Trans. Faraday Soc. 57:1200-1207.

Thibodeaux, L.J., K.T. Valsaraj, C. Springer, and G. Hildebrand. 1988. Mathematical models for predicting chemical vapor emissions from landfills. J. Haz. Mat. 19:101-118.

Table 1. Mass fluxes (g/cm^2/sec) from Baehr and Bruell (1990), from our simulations, and from Fick's law.

Species	Baehr and Bruell (1990)	our simulations*	Fick's Law†	% diff.**	Δy_i‡
Benzene	1.14e-7	1.28e-7	1.23e-7	4	0.1136
Hexane	2.02e-7	2.18e-7	2.00e-7	18	0.196
Isooctane	6.64e-8	6.91e-8	6.77e-8	2	0.0583

* Simulated with only the flux of N_2 set equal to zero with O_2 being free to attain a flux.

** (Fick's flux - multi-component flux)*100/Fick's flux.

†Calculated assuming the bulk gas was all nitrogen and using the binary diffusion coefficient of nitrogen for each VOC species.

‡ $\Sigma(y_i^L - y_i^o)$.

Table 2. Relevant physical properties of the "gasoline" species and carbon tetrachloride.

Species	Average Weight ratio relative to 1,2,3-tri methylbenzene	Molar weight gr/mole	Pure liquid vapor pressure, KPa
Carbon Tetrachloride	3.46	153.84	15.18
Benzene	2.16	78.11	12.7
Toluene	11.89	92.14	3.8
Ethylbenzene	2.01	106.16	1.28
p-Xylene	7.44	106.16	1.19
o-Xylene	2.91	106.16	0.88
1,2,3-trimethylbenzene	1.00	120.19	0.3

Table 3. The effective binary diffusion coefficients ($m^2/sec * 10^4$) for the "gasoline" components and CCl_4. $D_{ij}/D^b=\theta_a^{10/3}/\phi^2$ where D^b was calculated based on the method of Fuller et al. (1966) and $\theta_a=0.44$ and $\phi=0.50$.

	CCl_4	Benzene	Toluene	Ethyl benzene	p-Xylene	o-Xylene	1,2,3-tri methylbenzene
Benzene	0.0095	-	-	-	-	-	-
Toluene	0.0084	0.0101	-	-	-	-	-
Ethyl benzene	0.0076	0.0093	0.0083	-	-	-	-
p-Xylene	0.0076	0.0092	0.0083	0.0075	-	-	-
o-Xylene	0.0076	0.0092	0.0083	0.0075	0.0075	-	-
1,2,3-tri methyl benzene	0.0070	0.0086	0.0076	0.0070	0.0070	0.0070	-
air	0.0220	0.0245	0.0220	0.0202	0.0202	0.0202	0.0187

Table 4. Simulations performed for various combinations of the volatile species. Percent differences are as in Table 1.

Species	Run 1 (1)	(2)	Run 2 (3)	(4)	Run 3 (5)	(6)	Run 4 (7)	(8)
Carbon Tatrachloride	0.0111	+2.4	0.0176	+3.5	0.0024	+0.8	0.0111	+2.4
Benzene	0.0114	+1.8	0.0181	+2.7	0.0024	+0.6	0.0114	+1.8
Toluene	0.0159	+2.2	0.0252	+3.4	0.0034	+0.8	0.0159	+2.3
Ethyl benzene	0.0008	+2.8	0.0001	+4.2	0.0017	+1.1		
p-Xylene	0.0027	+2.8	0.0004	+4.2	0.0058	+1.0	0.0043	+2.8
o-Xylene	0.0008	+2.8	0.0001	+4.2	0.0017	+1.1		
1,2,3-Tri methylbenzene	0.0001	+3.3	1.283e-5	+4.8	0.0002	+1.2	0.0001	+3.3
Totals	0.0428		0.0615		0.0176		0.0428	

* Columns 1, 3, 5, and 7 are vapor mole fractions.

** Columns 2, 4, 6, and 8 are the percent differences from Fick's law estimates of fluxes

Liquid-Vapor Transport of Organic Chemicals in Relatively Dry Soils

MARK E. GRISMER
Department of Land, Air and Water Resources, Davis Campus

Summary

In arid and semi-arid regions where net infiltration and soil moisture are relatively low, movement of volatile organic compounds (VOC) in the vadose zone may be dominated by vapor transport and adsorption mechanisms. These compounds may enter the vadose zone through direct application, spills, or seepage from waste or storage sites. Previous research has considered chemical movement in either the liquid or vapor phases, assuming equilibrium adsorption reactions; however, rate of vapor adsorption to soils may be important for correct characterization of VOC concentrations in the liquid and gas phases during slow seepage/infiltration events. Through laboratory experiments, this investigation examines simultaneous liquid-vapor transport and adsorption of VOCs to bridge the current gap in research between liquid transport and vapor adsorption studies. Results from these experiments will then be used in numerical simulation studies to evaluate the effects of liquid-vapor transport on displacement of VOCs from the vadose zone over a broader range of conditions than those considered in the laboratory.

Specific objectives of this two-year study include: (1) determination of the rate and maximum adsorption capacity of selected VOCs on dry and moist clay minerals; (2) determination of liquid-vapor diffusivities of these VOCs as a function of initial soil moisture and VOC liquid saturation; (3) determination of the efficacy of VOC displacement by water at low saturations; and (4) evaluation of the effects of temperature on enhancement of liquid-vapor transport or evaporation from soils.

In this first year of the study, we have developed the nondestructive laboratory methods to monitor the simultaneous movement of organic liquids, water, and vapor in soils and their relative displacement during infiltration. Herein, we evaluate the problems of determining the resolving time and the machine dead time for gamma attenuation-based measurements, and the probable error in liquid saturations associated with such measurements. From this evaluation, a procedure was established to correct Gamma count rates to achieve the least probable error in measurements of liquid saturations for multiphase flow systems.

Key Words: multiphase flow in soils, vadose zone processes, dual gamma attenuation systems, probable error analysis

Project Objectives Addressed in 1991-92

Of the original four project objectives stated in the summary, the work reported here focuses on the second and third objectives, to establish the basic experimental procedures and methods required to determine liquid-vapor diffusivities and efficacy of liquid displacement processes. The specific objectives of this first year of the overall project were to

1. Evaluate the probable error associated with the simultaneous measurement of water saturation and hydrocarbon fluid saturation in porous media using a dual gamma attenuation system.
2. Develop a computer model to determine the optimal resolving and dead times of a dual-gamma energy system and to predict the probable error in the saturation of two fluids in porous media.

Research Plan and Procedures

Accurate simultaneous measurements of oil and water saturation in soil columns is difficult, leading researchers to consider use of non-destructive experimental methods. Lenhard et al. (1988) and others have used the dual gamma radiation system for simultaneous determination of volumetric contents of oil and water in soil. Errors associated with these measurements are due to the random nature of gamma ray emission and the sorption characteristics of these rays in soil (Gardner, 1972). The degree of significance of these errors depends on the counting time and the absorption characteristics of the scanned material. We conducted an error analysis associated with calibration of the measurement devices and of the measurements themselves when using a dual-source gamma system.

Beginning with the fundamental attenuation equations for a water, oil, and gas system in soil for ^{241}Am and ^{137}Cs sources, we developed solutions for the saturation of water, S_w, oil, S_o, and gas, S_g, shown below.

$$S_w = \frac{(\beta_{oc}\ln[I_a / I_{ea}] - \beta_{oa}\ln(I_c / I_{ec}))}{\phi X(\beta_{oa}\beta_{wc} - \beta_{oc}\beta_{wa})} + \frac{(\beta_{oc}\mu_{sa} - \beta_{oa}\mu_{sc})\rho_b}{\phi(\beta_{oa}\beta_{wc} - \beta_{oc}\beta_{wa})} \quad (1)$$

$$S_o = \frac{(\beta_{WC}\ln[I_a / I_{ea}] - \beta_{wa}\ln(I_c / I_{ec}))}{\phi X(\beta_{wa}\beta_{oc} - \beta_{WC}\beta_{oa})} + \frac{(\beta_{WC}\mu_{sa} - \beta_{wa}\mu_{sc})\rho_b}{\phi(\beta_{wa}\beta_{oc} - \beta_{WC}\beta_{oa})} \quad (2)$$

$$S_g = 1 - S_w - S_o \quad (3)$$

I is the count rate, b is the attenuation coefficient (cm^{-1}), m is the mass absorption coefficient (cm^2/gm), f is the porosity, X is the radiation path length (cm) and r_b is the soil bulk density (gm/cm^3). The subscripts "*oa*" and "*oc*" refer

to the coefficients for oil for the americium and cesium sources, respectively. Similarly, "*wa*" and "*wc*" apply to the coefficients for water for each radiation source, respectively. I_a and I_c are the actual count rates through the soil column from the americium and cesium sources, respectively, and I_{ea} and I_{ec} are the "empty" column concentrates from each source, respectively.

A dual gamma source containing ^{241}Am and ^{137}Cs was used in this research. The measurements were taken with a collimated beam, 2.54 cm in height and 0.31 cm in width, of 59.6 Kev gamma photons (Am source) and 662 Kev gamma photons (Cs source). The sources contained 100 mCi of ^{241}Am and 30 mci of ^{137}Cs. Determination of the attenuation coefficients of the porous media, oil (soltrol 130 and ethanol), and water were carried out first. The porous media in these experiments consisted of Yolo clay loam and sand. The attenuation coefficients were determined using a cubical Plexiglas cell that had five compartments. Each compartment had a constant thickness of 1.185 cm. Gamma count rates for the Am source were obtained first on an empty cell to obtain the empty count rate, then on a cell which had one compartment filled with water. The second compartment was then filled with water, and the count rates were also taken. Count rates were also taken when the third, fourth, and fifth compartments were filled with water. The same procedure was employed for oil, soil, and sand. Three 1-min. counts were taken for each thickness of every material. The same procedure was performed for the Cs source. The basic attenuation equation can be written

$$LnI = Ln\, I_o + \mu_i \rho_i \chi \qquad (4)$$

where i = water, oil, soil, or sand. The slope $m_i r_i$ *of* Eq. (4) was calculated using linear regression, after correcting for resolving time (discussed below). This slope represents the attenuation coefficient, b, for a given material i.

Correcting for Errors in Observed Count Rate

The measured count rate does not always reflect the actual number of gamma-ray photons which encountered the scintillation crystal due to resolving time, scattering of gamma rays, the gamma rays' absorption process (Fritton, 1969), and due to drift in the counting system (Gardner et al., 1972). The resolving time or the system dead time of a gamma-ray counting system is defined as the minimum time that separates two consecutive recorded gamma-ray photons or the minimum time necessary to process a pulse (Stillwater, 1988). Any photon that arrives at the scintillation crystal before the minimum time has elapsed is not counted; therefore, correction for the observed count is required to adjust for the missing photons.

Correction for the electronic drift in the measuring system was performed on all observed counts prior to any other correction. Electronic drift occurs mainly due to fluctuation in voltage and temperature in the counting system. All counts were taken at constant room temperature (25°C ± 0.2°C). To account for electronic drift, counts were taken on a standard absorber before and after each

set of measurements. Correction was based on a linear interpolation with time (Grismer, 1984) using the following equation

$$R_{tc} = \left(\frac{R_s(0)}{R_s(t)} \right) R_t \tag{5}$$

where R_{tc} is the corrected Gamma count rate at time *t*, $R_s(0)$ and $R_s(t)$ are the standard absorber count rates at time *0* and *t*, respectively, and R_t is the count rate at time *t*. $R_s(t)$ was found from the linear interpolation between the standard absorber count before and after each of the measurements.

In this research, count rates were corrected using two independent methods: the resolving time method described by Fritton (1969) and the system dead time method which will be called from now on the machine dead time (MDT) method. The measured count rate can be corrected for the resolving time using the following equation (Fritton, 1969)

$$I = R/(1 - TR) \tag{6}$$

where *I* is the true count rate in counts per minute (cpm), *R* is the observed count rate (cpm), and *T* is the resolving time (min/count). All counts were corrected using the above equation. The weighted variance equation (Fritton, 1969) was used to calculate the weighted variance of Plexiglas cells of different thicknesses

$$\text{weighted variance} = \sum_{i=1}^{n} (\textit{deviation from regression})_i^2 / I_i \tag{7}$$

where *n* is the number of cells used to determine the regression equation and *I* is the true count rate. Three 1-min. counts were taken for each of the 12 Plexiglas plates using the Am source. Each of the 12 Plexiglas plates had a constant thickness of 0.315 cm. Three 1-min. counts were also taken for each of the five thicknesses of water, oil (soltrol 130 and ethanol), soil, and sand, as described earlier. The same procedure was performed using the Cs source. The weighted variance was calculated for resolving times ranging from 0 to 50 msec/count at 0.5 msec/count intervals. The resolving time, which resulted in a minimum weighted variance (Fritton, 1969), was used to determine the mass absorption coefficient of water, oil (soltrol 130 and ethanol), soil, and sand. The relative weighted variance was also calculated using the following equation

$$\text{relative weighted variance (RWV)} = \frac{\text{weighted variance}}{\frac{1}{n}\sum_{i=1}^{n} I_i} \tag{8}$$

where *n* and I are as defined earlier. The principle of relative weighted variance was introduced to account for the variability in counting time and the number of

compartments (or thicknesses) used to calculate attenuation coefficients. The resolving time was determined for both Am and Cs sources. A computer program was used to determine the resolving time that corresponds to the minimum RWV.

Error Analysis of Liquid Saturations

Here, we are interested in the measurement precision of both water and oil saturations. Assuming that the variances of all components of Eqs. (1) and (2) are independent, variances of the various components of these two equations can be summed to give the variance in water or oil saturation using the standard error propagation formula (Young, 1962; Knoll, 1979). The standard error propagation analysis was used by Gardner et al. (1972) to examine the magnitude of the experimental error in the measurements of water content and soil bulk density. The error propagation formula can be used to find the variances of S_w and S_o. The probable error for any measured value of S_w can be calculated from the following equation

$$\sigma S_w^2 = \left(\frac{\partial S_w}{\partial \beta_{oa}}\sigma\beta_{oa}\right)^2 + \left(\frac{\partial S_w}{\partial \beta_{oa}}\sigma\beta_{oc}\right)^2 + \left(\frac{\partial S_w}{\partial \beta_{wa}}\sigma\beta_{wa}\right)^2 + \left(\frac{\partial S_w}{\partial \beta_{wc}}\sigma\beta_{wc}\right)^2$$
$$+ \left(\frac{\partial S_w}{\partial I_a}\sigma I_a\right)^2 + \left(\frac{\partial S_w}{\partial I_{ea}}\sigma I_{ea}\right)^2 + \left(\frac{\partial S_w}{\partial I_c}\sigma I_c\right)^2 + \left(\frac{\partial S_w}{\partial I_{ec}}\sigma I_{ec}\right)^2 + \left(\frac{\partial S_w}{\partial \mu_{sa}}\sigma\mu_{sa}\right)^2 \quad (9)$$
$$+ \left(\frac{\partial S_w}{\partial \mu_{sc}}\sigma\mu_{sc}\right)^2 + \left(\frac{\partial S_w}{\partial X}\sigma_X\right)^2 + \left(\frac{\partial S_w}{\partial \phi}\sigma_\phi\right)^2 + \left(\frac{\partial S_w}{\partial \rho_b}\sigma\rho_b\right)^2$$

where s is the standard deviation in the mean value of the component indicated by the subscript. An analogous equation can be written for the probable error of *So*.

The count rate over a specific time has a Poisson distribution (Gardener, 1972), thus s_I can be replaced by $\sqrt{I}$. Evaluation of sS_w^2 and sS_o^2 requires knowledge of the probable variance of the mass absorption coefficients (m_{sa}, m_{sc}), the attenuation coefficients (b_{wa}, b_{wc}, b_{oa}, b_{oc}), the porosity, the path length, and the bulk density of the soil. The value of the probable variance of the attenuation coefficient can be estimated from the maximum range about the arithmetic average of several values (Grismer, 1984). The probable variances of f, *X*, and r_b can be found similarly. However, the errors in the measurements of the attenuation coefficients, the mass absorption coefficients, porosity, *X*, and bulk density can be eliminated by taking a large number of measurements for each component (Grismer, 1984). Attainable precision of S_w and S_o is limited by the random emission of the radioactive sources (Gardner et al., 1972), and

therefore the limit of the absolute precision can be obtained from the terms of Eq. (9), which contains the Gamma count rates (I_a, I_{ea}, I_c, I_{ec}). Carrying out the partial differentiation of Eq. (1) with respect to I_a, I_{ea}, I_c, I_{ec}, and replacing s_I by $\sqrt{I}$ yields

$$\sigma S_w^2 = \frac{1}{\left[\phi X\left(\beta_{oa}\beta_{wc} - \beta_{oc}\beta_{wa}\right)\right]^2}\left(\frac{\beta_{oc}^2}{I_a} + \frac{\beta_{oc}^2}{I_{ea}} + \frac{\beta_{oc}^2}{I_{ec}} + \frac{\beta_{oc}^2}{I_c}\right) \qquad (10)$$

where I_a and I_c should be replaced by their equivalents from the basic attenuation equations. The variances in S_W and S_O due to random emission of radioactive sources are inversely proportional to the count rate or count time. Variances in S_W and S_O are also a function of water and oil saturations, column thickness, and porosity. The above equation was used to find the probable error in the measurement of S_W and analogous equations were used to calculate the probable error in the measurement of S_O.

Results and Discussion

Experimentally determined mass absorption coefficients of water and oil depend on correction of the observed count data for resolving time. Determining the correction for resolving time was performed by using two independent methods: the resolving time method of Fritton (1969), described earlier, and the observed machine dead time method (MDT). Each of the above two methods was used with and without considering 0 thickness, resulting in four different cases for determining the attenuation coefficients:

Case 1: 0 thickness included without the observed MDT correction.
Case 2: 0 thickness included with the observed MDT correction.
Case 3: 0 thickness excluded without the observed MDT correction.
Case 4: 0 thickness excluded with the observed MDT correction.

The attenuation coefficients of Plexiglas, water, soltrol 130, ethanol, soil, and sand were calculated for resolving times ranging from 0 to 50 msec/count. Figure 1 shows the attenuation coefficient of water (Am source) and the relative weighted variance (RWV) as a function of resolving time. The RWV is relatively small for all cases up to 20 msec/count. The RWV significantly increases after 40, 20, and 30 msec/count for cases 1, 2, and 4, respectively. The RWV of case 3 remains nearly constant. The curve slope for case 2 approaches infinity after a resolving time of 40 msec/count which indicates severe deviation from the regression equation. The deviation of corrected data at resolving times of more than 40 msec/count from the general attenuation equation of water indicates that the actual resolving time is less than 40 msec/count. However, it does not identify the exact resolving time.

Fritton's method is accurate in determining the maximum value of resolving time. However, determining the exact value of resolving time is not

possible when the weighted variance or the RWV is very small or almost constant. The RWV of the four cases shown in Figure 1 is almost constant for resolving times of less than 20 μsec/count. However, variability in the water attenuation coefficient is almost 50% for any particular case for resolving times ranging from 0 to 20 μsec/count. Such variability is problematic in determining the resolving time as described by Fritton (1969).

Weighted variance, RWV, and the attenuation coefficients of soltrol 130, ethanol, soil, sand, and plexiglas were also determined (but not shown) for all four cases of correction. All results were similar to water with some variability in resolving times. Comparing the four cases for determining resolving time, when the attenuation material was water, case 2 (Figure 1b) yielded the lowest RWV and the maximum correlation coefficient (R). Similar results were also found for soltrol 130, ethanol, soil, sand, and Plexiglas. Resolving times which yielded the lowest RWVs were not the same for all materials.

The attenuation coefficient of water is directly affected by resolving time regardless of the shape of the RWV curve. The attenuation coefficient of water increases linearly with resolving time when the RWV is relatively constant. Deviation from linearity becomes evident when the RWV increases. Increases in attenuation coefficient due to increases in resolving time are due to the fact that count rates for all thicknesses of water (0, 1.185, 2.370, 3.555, 4.740, and 5.925) were all corrected by a constant ratio for a given resolving time. The intensity of photons which encountered the scintillation crystal was the highest for 0 cm thickness and the lowest for 5.925 cm thickness. The resolving time may need to be adjusted to account for the thicknesses of the material of interest. In future studies, resolving time should be considered as a function of the count rate and the thickness of the material of interest. The effect of resolving time on the attenuation coefficient should be studied for different material thicknesses and different numbers of compartments.

Similar results to those shown in Figure 1 were obtained using the ^{137}Cs source. Except for case 3, the RWV increased with resolving time. The optimum resolving time was 0 for all cases, the RWV of case 2 for ^{137}Cs was very similar to case 2 for ^{241}Am. The RWVs for all cases were significantly smaller than the RWVs when the Am source was used due to the lower Cs count rate. The increase in the attenuation coefficient or the RWV in case 2 had the highest increase per unit increase in resolving time. The same increase was also observed in case 2 when Am was the radiation source (Figure 1). This is due to the fact that counts were corrected for MDT first, then for resolving time.

These results indicated that case 2 was the optimal combination of time corrections. Thus, we identified resolving times, RWVs, attenuation coefficients, and correlation coefficients (R) for all media and each radiation source for case 2. For the ^{241}Am source, there were significant differences between the RWV and the attenuation coefficient at resolving times of 0 and the optimal time (resolving time which yields the lowest RWV) for all media except Plexiglas. Correlation coefficients all improved marginally when the optimal resolving time was used. The optimal resolving time was not the same for all media, which

may indicate that the optimal resolving time for a particular gamma system is dependent on the media used to determine the resolving time. When the Cs source was used, the optimal resolving time was 0 for all cases, except sand and soil. It is evident that the optimal resolving time when soil or sand were used did not influence greatly the RWVs and the attenuation coefficients, as was the case when Am was used. This suggests that a resolving time of 0 for all media is adequate to predict the saturation of water and oil in porous media.

Several researchers have determined different resolving times for the same media. Fritton (1969) determined a value of 5.2 micro sec/count for the resolving time associated with Cs radiation through Plexiglas, the values for soil and water were 4.9 and 5.0 micro sec/count, respectively. Hopmans and Dane (1986) reported a value of 2.5 msec/count for both Am and Cs. Stroosnijder and de Swart (1974) reported a value of 4.75 and 6.50 msec/count for Am and Cs, respectively. Goit et al. (1978) reported a value of 15 msec/count for the Am and 3.6 msec/count for the Cs. Except for the values reported by Hopmans and Dane (1986), the above values show there is a large variability between the Am and the Cs resolving times. Variability in the equipment used to determine the count rate explains most of the differences in the resolving time (Stillwater, 1988). We found that a resolving time of 0 yielded the least errors in saturation measurements.

From the results discussed above, we determined the optimal combination of resolving time and MDT to be used for quantitative determination of the attenuation coefficients of all media for both radiation sources from which it was possible to calculate the probable error of the liquid saturations measurements.

Tables 1 and 2 summarize the probable error (PE) in water/soltrol 130 and water/ethanol saturations for a 4-min. counting time for a relatively dry sand column. The PE in liquid saturation could be reduced significantly to achieve acceptable precision by increasing the attenuation coefficient for the liquid of interest or increasing the counting time. Increasing counting time is not always practical during transient flow experiments; therefore, we have chosen to increase the attenuation coefficient of water. The attenuation coefficient of any fluid can be increased by dissolving a solute of relatively large ionic cloud in the liquid (e.g., Pb, Sr, Ur or I). Iodine attenuates gamma radiation significantly and is readily added to water in the form of KI or NaI salts (Grismer, 1984). Tables 3 and 4 summarize the effects of different concentrations of KI on the attenuation coefficient of water for both sources. The same procedure can be used to increase the attenuation of soltrol 130 or ethanol by the addition of a large ion. For multi-phase systems, the solute should be soluble in one liquid but not in both in order to differentiate between the two fluids.

Conclusion

Experimentally determined attenuation coefficients of water, soltrol 130, ethanol, soil, sand, and Plexiglas depend on correction of data for resolving time and MDT. The resolving time method and MDT method can be used to correct observed count rates for photons which are missed, due to arrival at the scintillation crystal before the minimum time has elapsed for recording another event. Am and Cs counts need to be corrected for MDT without any further correction for resolving time to achieve the lowest PE in the saturation of water and oil (soltrol 130 or ethanol). The PE in liquid saturation could be reduced significantly to achieve acceptable precision by increasing the attenuation coefficient of the liquid of interest.

References

Corey, A. T. 1985. Mechanics of immiscible fluids in porous media. Water Resources Publications. Littleton, Colorado. 225 p.

Cory, J. C., S. F. Peterson, and M. A. Wakat. 1971. Measurement of attenuation of ^{137}Cs and ^{241}Am gamma rays for soil density and water content determinations. Soil Sci. Soc. Am. J. 35:215-219.

Davidson, J. M., J. W. Biggar, and D. R. Nielsen. 1963. Gamma-radiation attenuation for measuring bulk density and transient water flow in porous materials. J. Geophys. Res. 68:4777-4783.

Fritton, D. D. 1969. Resolving time, mass absorption coefficient and water content with gamma-ray attenuation. Soil Sci. Soc. Am. J. 33:651-655.

Gardner, W. H., G. S. Campbell, and C. Callissendroff. 1972. Systematic and random errors in dual gamma energy soil bulk density and water content measurements. Soil Sci. Soc. Am. Proc. 36:393-398.

Goit, J. B., P. H. Groenevelt, B. D. Kay, and J. G. P. Loch. 1978. The application of dual gamma scanning to freezing soils and the problem of stratification. Soil Sci. Soc. Am. J. 42:858-863.

Grismer, M. E. 1984. Water and salt movement in relatively dry soils. Ph.D. Dissertation, Colorado State University, Fort Collins, Colorado.

Gurr, C. G. 1962. Use of gamma rays in measuring water content and permeability in unsaturated columns of soil. Soil Sci. 94:224-229.

Hopmans, J. W. and J. H. Dane. 1986. Calibration of a dual-energy gamma radiation system for multiple point measurements in a soil. Water Resour. Res. 22:1109-1114.

Knoll, G. F. 1979. Radiation Detection and Measurement. John Wiley and Sons, Inc.

Lenhard, R. J., J. H. Dane, J. C. Parker, and J. J. Kaluarachchi. 1988. Measurement and simulation of one-dimensional transient three-phase flow for monotonic liquid drainage. Water Resour. Res. 24:853-863.

Reginato, R. J. and C. H. M van Bavel. 1964. Soil water measurements with gamma attenuation. Soil Sci. Soc. Am. Proc. 28:721-724.

Shalhevet, J. and B. Yaron. 1967. Ion distribution, moisture content and density of soil columns measured with gamma radiation. Soil Sci. Soc. Amer. Proc. 31:153-156.

Stillwater, R. 1988. Improved methodology for a collinear dual-energy gamma radiation system. Water Resour. Res. (24)8:1411-1422.
Stroosnijder, L. and J. G. de Swart. 1974. Column scanning with simultaneous use of Am and Cs gamma radiation. Soil Sci. 118:61-66.
Young, H. D. 1962. Statistical Treatment of Experimental Data. McGraw-Hill, New York.

Reports and Publications

Poster presented at the 1992 Annual Meeting of American Society of Agronomy, Minneapolis, MN.

Table 1. Probable error in the saturation of water and soltrol 130 for the sand column for a 4-min. counting time (water/soltrol 130).

Corrected for MDT	Resolving time (μ sec)		Probable Error	
	Am	Cs	Water	Ethanol
No	0.0	0.0	0.0142	0.0277
Yes	0.0	0.0	0.0110	0.0207
No	30.0	0.0	0.0411	0.0750
Yes	14.0	0.0	0.0189	0.0343

Table 2. Probable error in the saturation of water and ethanol for the sand column for a 4-min. counting time (water/ethanol).

Corrected for MDT	Resolving time (μ sec)		Probable Error	
	Am	Cs	Water	Ethanol
No	0.0	0.0	0.0062	0.0100
Yes	0.0	0.0	0.0051	0.0082
No	30.0	0.0	0.0089	0.0141
Yes	14.0	0.0	0.0066	0.0103

Table 3. Attenuation coefficients of water at different KI concentrations for the Am source.

Corrected for MDT	Res. time (μ sec)	Attenuation coefficient (β_{wa}) KI concentration (g/L)					
		0	10	20	30	slope	R^2
No	0.0	0.16004	0.21671	0.27450	0.33147	0.03575	0.99999
Yes	0.0	0.18330	0.24152	0.30088	0.35997	0.03215	0.99998
No	30.0	0.21284	0.27839	0.34159	0.40114	0.02951	0.99954
Yes	14.0	0.21368	0.27467	0.33667	0.39698	0.02864	0.99997

Slope: The ratio of increase in the attenuation coefficient per 1 g/L increase in KI concentration.

Table 4. Attenuation coefficients of water at different KI concentrations for the Cs source.

Corrected for MDT	Res. time (μ sec)	Attenuation coefficient (β_{wa}) KI concentration (g/L)					
		0	10	20	30	slope	R^2
No	0.0	0.07067	0.06934	0.07257	0.07193	0.00099	0.39973
Yes	14.0	0.08249	0.08048	0.08371	0.08312	0.00062	0.22089

Slope: The ratio of increase in the attenuation coefficient per 1 g/L increase in KI concentration.

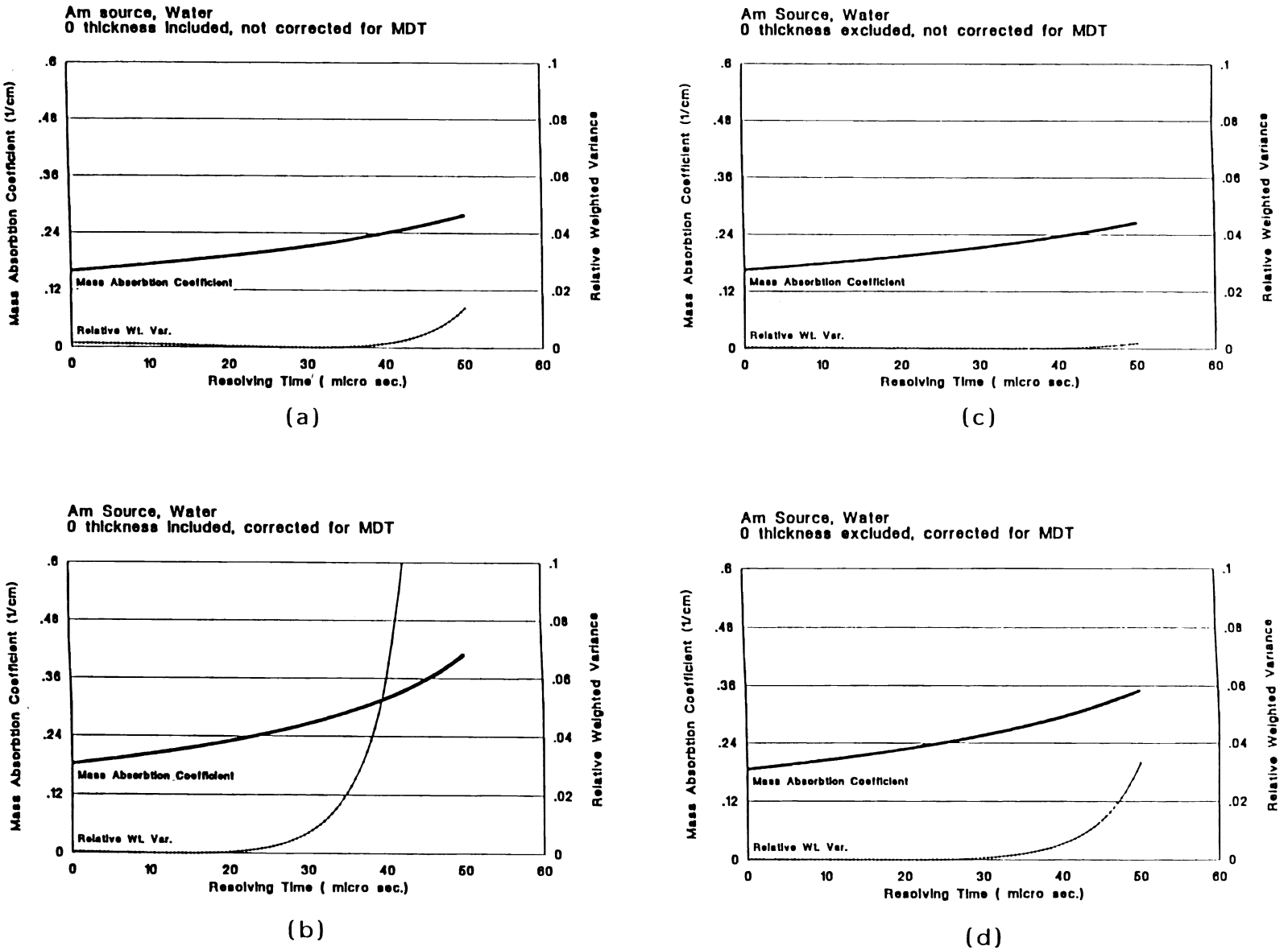

Figure 1. Relative weighted variance (RWV) and mass absorption coefficients (μ) for water using the Am source as function of resolving time and machine dead time (MDT) correction.

Lidar Measurement of Field Scale Volatilization Physics

MARC B. PARLANGE
Department of Land, Air and Water Resources, Davis Campus

Summary

An understanding of atmospheric turbulence phenomena, which control the volatilization of agricultural chemicals between the land surface and the atmosphere, is essential to describe the volatilized chemical losses at field-scales. The vapor loss is dependent on the atmospheric turbulent removal and transfer into the surface layer of the atmosphere. Mathematically, similarity theory can be used to describe such field scale volatilization into the atmospheric surface layer, but field scale volatilization had never been measured before. Remote sensing technology to view these highly intermittent processes and the three-dimensional turbulent motion which control the vapor removal is relatively recent. Light detection and ranging (Lidar) will now allow rapid, high precision observation of local and field-scale scalar transport.

A Lidar experiment was carried out during August-September 1991 over vegetated and nonvegetated surfaces at the UC Davis Campbell Tract to measure scalar transport from the land surface. The objective of the research was to measure and analyze lower atmospheric scalar transport with the Lidar to understand implications for measurement of field-scale volatilization. The Lidar observations are described in the context of Monin-Obukhov universal similarity theory. The results obtained are generalized so that the theory can be applied for any chemical vapor flux and land surface properties at the field scale.

The description of turbulent transport processes in the lower atmosphere, including volatilized scalar transport, relies on the theory of random fields for proper formulation of time and space averaging and integral time and length scale determination. Practical approaches for atmospheric modeling of turbulent heat and momentum transfer in the lower part of the atmosphere generally assume that statistics of the fluid field exhibit homogeneity in direction, stationarity in time, and ergodicity so that point measurements can be used to infer ensemble statistics. The validity of these idealized states of turbulence were investigated using a Raman Lidar system to measure scalar transport in the lower atmospheric boundary layer. Experiments and analysis have been carried out using the Los Alamos Lidar to examine the stationarity, homogeneity, isotropy and ergotic assumptions used in scalar transport studies. Examination of the existence and values of turbulent integral scales was also performed and consequences for point measurements are being developed.

Key words: volatilization, Raman Lidar, scalar transport, turbulence

Project Objectives Addressed in 1991-92

1. To determine with great precision and resolution atmospheric profiles of vapor with Raman Lidar remote sensing over an agricultural field.

2. To describe the transport of chemical species from the land surface with improved description of lower atmosphere characteristics in both space and time.

Research Plan and Procedures

Field Experiments The experimental data used in this analysis were collected at the Campbell Tract at the University of California, Davis in August 1991. The field is a bare soil field which extends some 400 m by 400 m. A solar-blind water-Raman Lidar was used in the experiment (Eichinger et al., 1992). A pulse of high energy light is emitted by the Lidar, and the Raman-shifted return light from both atmospheric nitrogen and water vapor is collected using a telescope and then digitized. Because nitrogen is the dominant atmospheric gas, dividing the water Raman return signal by that of the nitrogen normalizes each pulse. The divided return signals are directly proportional to the absolute water vapor content of the air and require only a correction for differential ozone absorption at the two return wavelengths. The data set used is referred to as a time-dimensional (TD) scan because the observations were sampled at the same points in space over a period of time. This type of data set is generated by firing the laser along a single line-of-site parallel to the ground oriented along the mean wind direction. The rate at which data collection frequencies varied was 0.11 s to 2.0 s with the total length of the time series varying from three to twenty minutes.

Results

Data Figure 1 shows an example of six (out of 545) independent experiments of the spatial stochastic process. For each point in the field away from the Lidar source, the probability distribution from these ensemble experiments can be computed, and the spatial evolution of the probability density function can be studied. Figure 2 displays the evolution of the probability density function (pdf) in space. The specific humidity random field can be considered homogeneous (in the strict sense) if the probability density function is invariant in space. This was examined by computing the Chi-squared probability function (Katul et al., 1992). It was found that the pdf's are essentially equal for at most a 3 m lag distance. The probability of distribution equality is no longer valid beyond 3 m. Homogeneity was investigated in the weak sense by establishing whether the mean is invariant in space and the covariance is origin independent. It should be added that to apply a t-test the distributions at each point should be gaussian, which they were, based on the skewness and kurtosis. The means were not found to be statistically different (95%). The covariance function for various origins and space lags is shown in Figure 3. The covariance function was origin-independent and only a function of lag distance. The statistics of the turbulent fluid field may be approximated by

a weakly homogeneous random field, though, in the strict sense, not for distances greater than 3 m.

Stationarity was analyzed from a Time-Domain scan sampled at 8 Hz. In this analysis, we assumed that at each instant in time, an ensemble of similar experiments was carried out in space under the same average external conditions. The covariance function computed is shown for one example in Figure 4 for various time origins and time lags. The covariance functions appeared to be origin-invariant and time lag dependent only. Further analysis on both isotropy and ergodicity was carried out and presented in Katul et al. (1992).

Discussion

A stochastic analysis of solar-blind Raman-Lidar specific humidity measurements was performed to investigate the structure of the atmosphere. This analysis is critical for the future development of stochastic models of scalar transport. The random specific humidity field was first analyzed in space with time increments generating various realizations of the spatial stochasticity. Then specific humidity was treated as a random function in time only with spatial observations generating the ensemble experiments.

Chi-Square statistical analysis indicated that the specific humidity field was homogeneous in the strict sense for distances not exceeding 3 m along the mean horizontal wind speed, while second order homogeneity was valid for up to 6 m. Higher order moment coefficients, namely skewness and kurtosis, indicated that the gaussian distribution was a reasonable approximation for the probability distribution at each location.

First order and second order isotropic conditions were not found to exist in this study, indicating that the axisymmetric flow assumption may not be very accurate in the surface layer. The partial autocorrelation function indicated that the spatial relative turbulent intensities exhibit a Markovian "memory" structure with directional lag. This can provide a workable stochastic differential equation to incorporate anisotropy, especially in lagrangian particle release stochastic models used to describe volatilization at the liquid-air interface..

Ergodicity in space was investigated in the strict sense and in the weak sense. The Chi-Square probability function at various spatial origins and spatial lags indicated that the specific humidity field was not ergodic, in the strict sense, and indicated that a single realization in space could not yield all the ensemble statistics. Nevertheless, the covariance as a function of spatial origin and lag indicated that the specific humidity field was ergodic in the mean.

At any instant in time, spatial observations were not dense enough to justify a probability density function and the ensemble statistical analysis; hence only second order stationarity was investigated. Second order stationarity may be a workable hypothesis due to the nature of the covariance behavior as a function of temporal origin and temporal lag.

Publications and Reports

Katul, G.G., M.B. Parlange, W.E. Eichinger, D. Holtkamp and D. Cooper. 1992. The structure of the atmospheric surface layer from Lidar measurements of humidity. (Submitted to Journal of Atmospheric Sciences).

Eichinger, W.E., D. Cooper, M.B. Parlange, and G.G. Katul. 1992. The application of a scanning, water raman-Lidar as a probe of the atmospheric boundary layer. (Submitted to I.E.E.E. Geoscience -Remote Sensing)

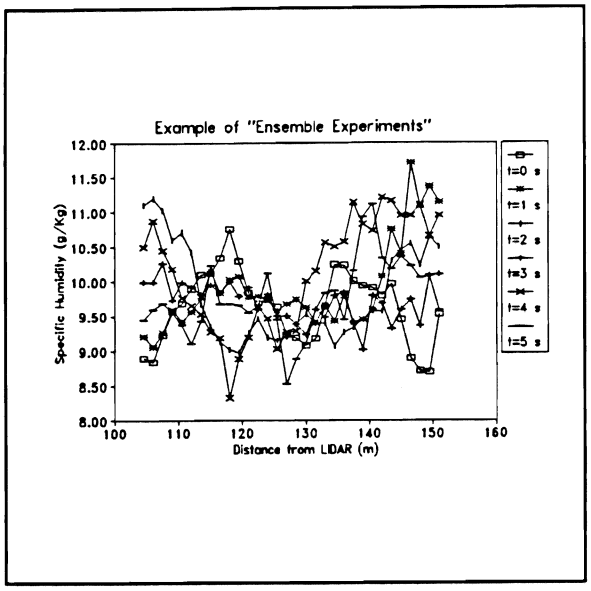

Figure 1. Example of an "Ensemble Experiments" of a random process in space under similar external conditions.

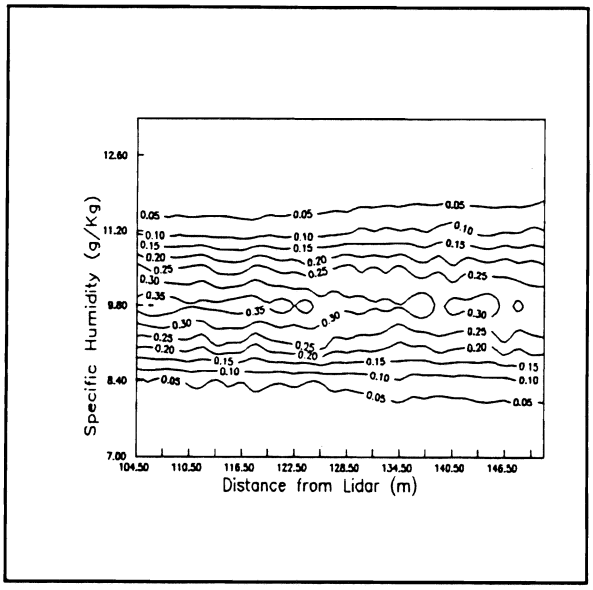

Figure 2. Variation of the specific humidity spatial probability density function from a series of 1 Hz scans on 08-23-91 at 17:04.

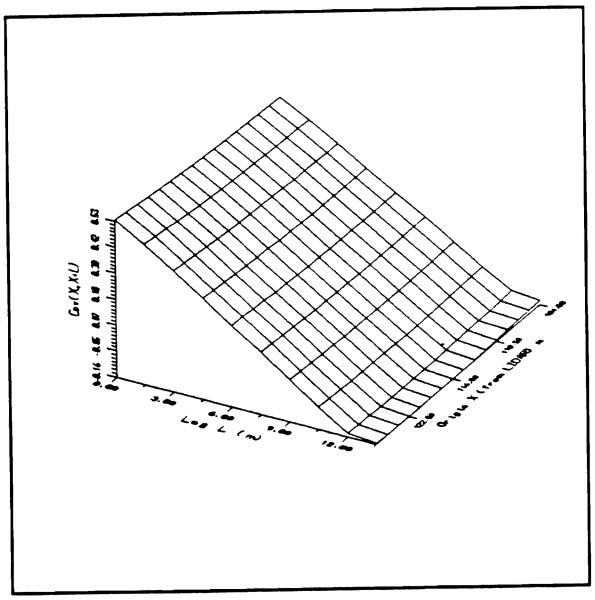

Figure 3. The covariance (g^2Kg^{-2}) as a function of spatial lag (L) and origin X.

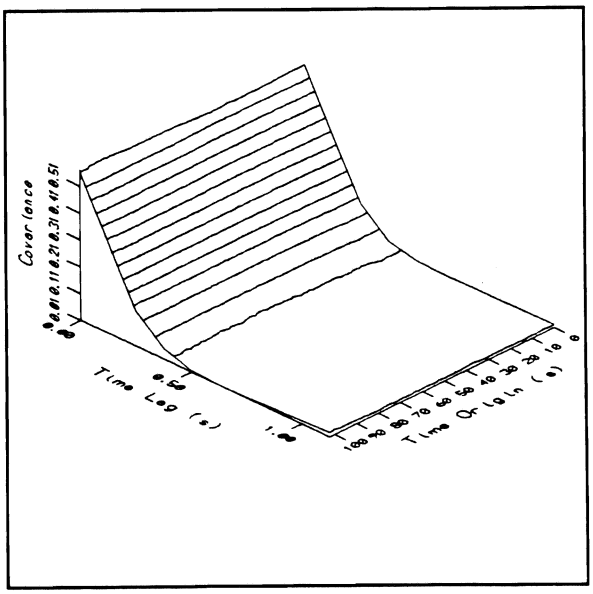

Figure 4. The covariance (g^2Kg^{-2}) as a function of time lag (s) and origin.

Objective, Organization and Function of
The University of California
Kearney Foundation of Soil Science

Adopted August 4, 1969
Revised June 30, 1982

Objective

The Kearney Foundation of Soil Science shall focus its program and support research in definitive missions in the fields of soils, plant nutrition, and water science.

Organization

A. The Kearney Foundation of Soil Science is administratively responsible to the Vice President-Agricultural and University Services (A&US) through the Director of the Agricultural Experiment Station and the Associate Director of the Agricultural Experiment Station located on the campus on which the Director of the Foundation is resident.

B. The Kearney Foundation of Soil Science is administered for the Division of Agricultural Sciences by a Director with policy guidance by an Advisory Committee and assistance from a Technical Committee.

1. The Director is appointed by the Vice President-A&US, after approval by the Dean and Associate Director of the Agricultural Experiment Station and the Chancellor of the campus on which the Director is to be resident. The Advisory Committee will propose a slate of candidates for the position of Director to the Vice President-A&US for his consideration.

2. The Advisory Committee of the Kearney Foundation is appointed by the Vice-President-A&US and is responsible to him through the Director of the Agricultural Experiment Station for guidance of the Foundation. The Chairman of the Committee is the Associate Director of the Agricultural Experiment Station at the location where the Director of the Foundation resides. The remaining members are the chairmen, or designees, of the Departments of Land, Air and Water Resources at Davis, Plant and Soil Biology at Berkeley, Soil and Environmental Sciences at Riverside, and one representative from a crop production department, one representative from Agricultural Economics and one representative from Agricultural Extension.

3. The Technical Committee of the Kearney Foundation is appointed by the Vice President-A&US. The Technical Committee shall consist of the Foundation Director as Chairman and four to seven other individuals. Individuals will be selected for the Technical Committee on the basis of their expertise on the Kearney Foundation mission subject matter with consideration for appropriate campus, cooperative extension and possibly non-university representation.

4. The Foundation Director may employ necessary administrative, technical or clerical staff to accomplish the Kearney Foundation goals, but there shall be no permanent staff for the Foundation. The Foundation Director will submit an annual report as prescribed by the University for Multi-campus Research Units.

Functions

A. The function of the Kearney Foundation is to encourage and support research and information dissemination on a specific definitive mission approved by the Vice President-A&US upon the recommendation of the Advisory Committee for a period of five years. The mission shall be one of public concern on which useful contributions are likely to be made in a five-year period. Successive missions will be selected each five years with a new Director for each mission.

B. The Foundation Director shall (1) keep faculty and cooperative extension individuals on various campuses informed on the Foundation goals and objectives and on funding opportunity from the Foundation, (2) solicit research proposals from UC investigators and with help from the Technical Committee develop a proposal funding priority list for review by the Advisory Committee, (3) allocate funds, after review by the Advisory Committee, to accomplish the Foundation mission, (4) be responsible for administrative details including preparation of appropriate reports, (5) assist faculty members to seek funds from sources other than Kearney Foundation that will contribute to the Foundation mission, (6) encourage information dissemination on the mission subject matter to appropriate segments of society, and (7) prepare "wrap-up" document(s) which synthesize the information gained during the five year mission.

C. The Advisory Committee shall (2) advise the Foundation Director when needed, (2) recommend research policy, (3) evaluate progress on the mission research, (4) review recommended allocation of funds by Foundation Director, (5) encourage inter-campus coordination and cooperation to make optimum use of resources and facilities, (6) select a definitive five year research mission to succeed an existing mission, and (7) nominate qualified candidates for a succeeding Director of the Foundation.

D. The Technical Committee shall (2) assist the Director in defining research priorities, (2) evaluate and develop a priority rating on research proposals, and (3) provide advice as requested by the Foundation Director on matters related to technical subject matter.

General Operational Guidelines

A. Recommended missions and Foundation Director candidates are to be submitted to the Director of the Agricultural Experiment Station and the Vice President-A&US by July 1 preceding the final year of an existing research mission. The new mission and Director-designate are to be selected as soon thereafter as possible to enable the Director-designate to plan the program for activation the following July 1.

B. The Director will manage and authorize expenditures of all funds transferred to the Kearney Foundation as of July 1 of the last year of the mission. Any funds transferred into the Kearney Foundation after that time will be used to accomplish the goals of the succeeding mission.

C. The Director normally will use the year after the five year mission period to "wrap up" the mission by holding symposia, preparing publications, etc. Funds to accomplish this task must be reserved from the budget specifically assigned tot he mission during the preceding five years. The immediate past Kearney Foundation Director will report to the Vice President-A&US through the appropriate Dean and Advisory Committee on progress and budgetary expenditures in achieving wrap up of the mission. At the appropriate time, the mission will be considered complete, the Director formally released from responsibility and any unexpended funds will revert back to the Kearney Foundation for use in subsequent missions.

D. The Director and members of the Advisory and Technical Committees are eligible to submit proposals for funding. They must, however, be excluded from discussion or action related to the particular project.

E. Normally extramural contracts or grants supporting activities consistent with the Kearney Foundation mission will be assigned directly to the Department of the scientist serving as PI rather than to the Kearney Foundation. When an outside agency makes an offer or solicits a proposal from the Foundation Director, the Director will make that information known to the Advisory Committee.

F. Kearney Foundation resources are to supplement Agricultural Experiment Station budgets and provide incentives for research redirection. Because of the temporary nature of the funds, funding of non-career employees such as post-doctoral appointments, research assistantships and part time laboratory helpers is strongly encouraged and routinely approved. Justified funding for career employees with supplemental employee benefit costs must be approved by the Advisory Committee.

Kearney Foundation of Soil Science Advisory Committee

Dr. Lanny J. Lund
Chair, Kearney Foundation of Soil Science Advisory Committee
Associate Dean, Agricultural Experiment Station,
College of Natural and Agricultural Sciences
Professor of Soil Science and Soil Scientist
Department of Soil & Environmental Sciences
University of California
Riverside, CA 92521
(909) 787-7291 or (909) 787-3859

Dr. Harvey E. Doner
Chair, Department of Soil Science
Professor of Soil Chemistry
University of California
Berkeley, CA 94720
(510) 642-4148, (510) 642-8051 or (510) 643-6908

Dr. John M. Duniway
Chair, Department of Plant Pathology
Professor of Plant Pathology and Plant Pathologist
University of California
Davis, CA 95616
(916) 752-0324 or (916) 752-4269

Dr. Steven Grattan
Cooperative Extension Water Relations Specialist
Department of Land, Air, & Water Resources, Hydrologic Science Section
University of California
Davis, CA 95616
(916) 752-1130

Dr. William A. Jury
Chair, Department of Soil & Environmental Sciences
Professor of Soil Physics and Soil Physicist
University of California
Riverside, CA 92521
(909) 787-5134 or (909) 787-5116

Dr. Andre Lauchli
Associate Dean for Research, College of Agricultural and Environmental Sciences
Professor of Plant Nutrition and Plant Physiologist
Department of Land, Air, & Water Resources, Soils & Biogeochemistry Section
University of California
Davis, CA 95616
(916) 752-0819, (916) 752-7270 or (916) 752-1406

Dr. Henry J. Vaux, Jr.
Associate Vice President -- Programs
Associate Director, Agricultural Experiment Station and
Associate Director, Cooperative Extension
Office of the Vice President, Division of Agriculture and Natural Resources
Director, Water Resources Center
Professor of Resource Economics and Resource Economist
University of California
Oakland, CA 94612
(510) 987-0026, (909) 787-4327 or (909) 787-4657

Kearney Foundation of Soil Science Technical Committee

Dr. Andrew C. Chang
Chair, Kearney Foundation of Soil Science Technical Committee
Director, Kearney Foundation of Soil Science
Professor of Agricultural Engineering and Agricultural Engineer
Department of Soil & Environmental Sciences
University of California
Riverside, CA 92521
(909) 787-5325

Dr. John W. Biggar
Professor of Water Science and Water Scientist
Department of Land, Air, & Water Resources, Hydrologic Science Section
University of California
Davis, CA 95616
(916) 752-0681 or (916) 752-0453

Dr. Arthur L. Craigmill
Cooperative Extension Toxicology Specialist
Department of Environmental Toxicology
University of California
Davis, CA 95616
(916) 752-2936

Dr. Dennis D. Focht
Professor of Soil Microbiology and Soil Microbiologist
Department of Soil & Environmental Sciences
University of California
Riverside, CA 92521
(909) 787-3446

Dr. John G. McColl
Professor of Forest Soils
Department of Soil Science
University of California
Berkeley, CA 94720
(510) 642-1028 or (510) 643-6088

Dr. T. Ishwar Murarka
Senior Program Manager, Land and Water Quality Studies
Electrical Power Research Institute
P. O. Box 10412
Palo Alto, CA 94303
(415) 855-2150

Dr. Albert L. Page
Professor of Soil Science and Chemist
Department of Soil & Environmental Sciences
University of California
Riverside, CA 92521
(909) 787-3654

Dr. Martinus Th. Van Genuchten
Adjunct Professor of Soil Physics
Department of Soil and Environmental Sciences
United States Salinity Laboratory
University of California
Riverside, CA 92521
(909) 369-4847

Index of Principal Investigators

Dr. Michael A. Anderson
Assistant Professor of Soil Chemistry and Assistant Soil Chemist
Department of Soil & Environmental Sciences
University of California
Riverside, CA 92521
(909) 787-3757

Dr. Richard G. Burau
Professor of Soil Science and Environmental Toxicology and Soil Chemist
Department of Land, Air, & Water Resources, Soils & Biogeochemistry Section
University of California
Davis, CA 95616
(916) 752-0194 or (916) 752-1406

Dr. David E. Crowley
Assistant Professor of Soil Science and Assistant Soil Chemist
Department of Soil & Environmental Sciences
University of California
Riverside, CA 92521
(909) 787-3785

Dr. Walter J. Farmer
Professor of Soil Science and Chemist
Department of Soil & Environmental Sciences
University of California
Riverside, CA 92521
(909) 787-3756

Dr. Robert C. Graham
Associate Professor of Soil Mineralogy
Department of Soil & Environmental Sciences
University of California
Riverside, CA 92521
(909) 787-3751

Dr. Mark E. Grismer
Associate Professor of Water Science and Associate Agricultural Drainage Engineer
Department of Land, Air, & Water Resources, Hydrologic Science Section
University of California
Davis, CA 95616
(916) 752-3243 or (916) 752-0453

Dr. William A. Jury
Chair, Department of Soil & Environmental Sciences
Professor of Soil Physics and Soil Physicist
University of California
Riverside, CA 92521
(909) 787-5134 or (909) 787-5116

Dr. Zbigniew J. Kabala
Assistant Professor of Hydrology and Assistant Hydrologist
Department of Soil & Environmental Sciences
University of California
Riverside, CA 92521
(909) 787-4289

Dr. John Letey
Professor of Soil Physics and Soil Physicist
Department of Soil & Environmental Sciences
University of California
Riverside, CA 92521
(909) 787-5105

Dr. John G. McColl
Professor of Forest Soils
Department of Soil Science
University of California
Berkeley, CA 94720
(510) 642-1028 or (510) 643-6088

Dr. Marc B. Parlange
Assistant Professor of Water Science and
Assistant Environmental Physicist/Water Scientist
Department of Land, Air, & Water Resources, Hydrologic Science Section
University of California
Davis, CA 95616
(916) 752-4953 or (916) 752-0453

Dr. Carlos E. Puente
Assistant Professor of Hydrologic Science and Assistant Hydrologist
Department of Land, Air, and Water Resources
University of California
Davis, CA 95616
(916) 752-0689 or (916) 752-0453

Dr. Dennis E. Rolston
Assoc. Chair, Department of Land, Air, & Water Resources,
Soils & Biogeochemistry Section
Professor of Soil Science and Soil Physicist
University of California
Davis, CA 95616
(916) 752-5028 or (916) 752-2113

Dr. Kate M. Scow
Assistant Professor of Soil Science and Assistant Soil Microbial Ecologist
Department of Land, Air, & Water Resources, Soils & Biogeochemistry Section
University of California
Davis, CA 95616
(916) 752-4632 or (916) 752-1406

Dr. Henryk Sobczuk
Postdoctoral Scientist
Department of Soil & Environmental Sciences
University of California
Riverside, CA 92521
(909) 787-4289

Dr. Garrison Sposito
Professor of Soil Physical Chemistry
Department of Soil Science
University of California
Berkeley, CA 94720
(510) 643-8297 or (510) 643-9171

Dr. Marylynn V. Yates
Associate Professor of Environmental Microbiology and
Associate Cooperative Extension Agronomist -- Groundwater Quality
Department of Soil & Environmental Sciences
University of California
Riverside, CA 92521
(909) 787-5488

Dr. Robert J. Zasoski
Associate Professor of Soil Science and Associate Soil Scientist/Plant Nutritionist
Department of Land, Air, & Water Resources, Soils & Biogeochemistry Section
University of California
Davis, CA 95616
(916) 752-2210 or (916) 752-1406

THIS BOOK IS DUE ON THE LAST DATE
STAMPED BELOW

BOOKS REQUESTED BY ANOTHER BORROWER
ARE SUBJECT TO IMMEDIATE RECALL

UCD LIBRARY

DUE JUN 3 0 2010

LIBRARY, UNIVERSITY OF CALIFORNIA, DAVIS

D4613-1 (5/02)M

OFFICE OF THE DIRECTOR
KEARNEY FOUNDATION OF SOIL SCIENCE
UNIVERSITY OF CALIFORNIA
RIVERSIDE, CA 92521
(909) 787-5325

Printed on recycled paper